INTERACTION OF SUPERCRITICAL CARBON DIOXIDE WITH QUATERNARY-AMMONIUM ORGANOCLAYS IN THE PROCESSING OF THERMOPLASTIC ELASTOMER NANOCOMPOSITES

INTERACTION OF SUPERCRITICAL CARBON DIOXIDE WITH QUATERNARY-AMMONIUM ORGANOCLAYS IN THE PROCESSING OF THERMOPLASTIC ELASTOMER NANOCOMPOSITES

by

JINLING LIU

A Thesis

Submitted to the School of Graduate Studies

in Partial Fulfillment of the Requirements

for the Degree of

Masters of Applied Science

McMaster University

MASTERS OF APPLIED SCIENCE (2008) McMaster University

(Chemical Engineering) Hamilton, Ontario, Canada

TITTLE:	Interaction of Supercritical Carbon Dioxide with Quaternary-Ammonium Organoclays in the Processing of Thermoplastic Elastomer Nanocomposites
AUTHOR:	Jinling Liu
	B. Eng. (Dalian Institute of Light Industry, China)
SUPERVISOR:	Dr. Michael R. Thompson
NUMBER OF PAGES:	xvii, 132

ABSTRACT

Organically modified montmorillonite has been extensively used as nanofiller in studies of polymer layered silicate nanocomposites, promising materials for today's automotive industry because the nano-materials reduce the overall weight of vehicle. However, industrial applications have not followed suit primarily due to cost/performance issues. Supercritical carbon dioxide is promising as an aid in the production of a fully exfoliated polymer layered silicate nanocomposite but has not been fundamentally studied in this regard at present.

As the first stage in studies of using supercritical carbon dioxide for aiding the production of thermoplastic elastomer nanocomposites, this thesis investigates the influence of this unique supercritical fluid on the microstructure and surface chemistry of five organically modified clays. Four alkyl-based quaternary ammonium surfactants with different number and length of chains attached and one aromatic quaternary ammonium surfactant were chosen to vary the degree of CO_2-philicity exhibited by the organoclay. In a high pressure batch vessel, the different organoclays were suspended in the supercritical solvent at temperatures of 50°C and 200°C and pressures of 7.6 MPa and 9.7 MPa for a fixed time and then removed after depressurization at 0.2 MPa/s or 4.8 MPa/s. The structures of these treated clays were characterized by XRD, TEM, DSC, TGA, FT-IR, and SEM, and their chemical properties were analyzed by various methods including atomic absorption spectroscopy, and contact angle measurement. The potential role of water to favor the interaction between $scCO_2$ and an organoclay was also investigated.

Solute-solvent interactions plasticized the organic modifier while suspended in the supercritical fluid, which resulted in greater chain mobility and further cation exchange. The results indicate that surfactants exhibiting a paraffin-type conformation within the galleries of the clay were most likely to experience significant basal expansion, provided

the tilt angle was not already close to being perpendicular to the silicate surface. For those organoclays demonstrating basal expansion, it was noted that the resulting particle size was increased due to enhanced porosity. Water proved useful in clay expansion in certain cases and primarily while operating conditions allowed the co-solvent to remain adsorbed to the clay surface.

ACKNOWLEDGEMENTS

My most sincere Thank You goes to my supervisor, Dr. Michael Thompson, for his excellent and patient guidance. His insight and dedication in research and supervision are impressive.

Many thanks go to Dr. Heinrich Krump for his instruction at the early stage of my studies, General Motors for the financial support, and, specifically, Dr. William Rodgers and Paula Fasulo for their helpful advice and analysis.

I would like to express my appreciation to Dr. Elizabeth Takacs for sharing her expertise on instrument and equipment operations, Mr. Paul Gatt for his help in apparatus manufacturing and technical support, Dr. James Britten, Mr. Graham Pearson, Mr. Frank Gibbs, Mr. Fred Pearson, Dr. Steve Kornic, and Mr. Steve Koprich for their kind assistance with XRD, TGA, TEM, FT-IR, and SEM.

I would also like to thank Kathy Goodram, Lynn Falkiner and Andrea Vickers at our main office, Dr. Ghodratollah Hashemi, Karen Rodgers and Abdullah Al Otaibi in our group, and other friends in the Department of Chemical Engineering for their support over the past two years.

Finally, I want to thank my husband and my daughter and dedicate this thesis to them.

TABLE OF CONTENTS

LIST OF FIGURES

LIST OF TABLES

NOMENCLATURE

Abbreviations

TPO	Thermoplastic polyolefin elastomer
MMT	Montmorillonite
MA	Maleic anhydride
MA-PP	Maleic anhydride grafted polypropylene
$scCO_2$	Supercritical carbon dioxide
PMMA	Poly(methyl methacrylate)
PS	Polystyrene
SCF	Supercritical fluid
PP	Polypropylene
SCP	Southern Clay Products
C20A	Cloisite 20A
NaMMT	Sodium montmorillonite
HPV	High pressure vessel for batch processing
HPC	High pressure cell for in-situ XRD observations
PEEK	Polyetheretherketone
XRD	X-ray diffraction
DOE	Design of experiment
wt	Weigh
DSC	Differential Scanning Calorimetry

FT-IR	Fourier Transform Infrared Spectrometry
TGA	Thermogravimetric Analysis
CEC	Cation exchange capacity

Symbols

T_c	Critical temperature
P_c	Critical pressure
γ^d	Dispersive component of surface energy
γ^p	Polar component of surface energy
γ^t	Total surface energy
θ	Contact angle of a liquid droplet on the flat surface of a material
2θ	X-ray diffraction angle in Bragg's Law
γ_s^d	Dispersive component of surface energy of solid phase
γ_s^p	Polar component of surface energy of solid phase
γ_l^d	Dispersive component of surface energy of liquid phase
γ_l^p	Polar component of surface energy of liquid phase
Δ	Difference of two figures

CHAPTER 1 INTRODUCTION

1.1 Background

Polymer/layered silicate nanocomposites are a new class of materials where nanoscale particles are uniformly dispersed into a polymer matrix. The large aspect ratio and the high surface area of the nanofiller provide potentially maximized specific mechanical properties at a lower filler loading. Such a characteristic material meets the urgent need for new materials in the modern automotive industry and therefore, the field of polymer nanocomposites has grown quite rapidly in publication and patent literature. However, the industrial application of this material class has not followed suit. Reasons for this may be related to multiple aspects, but the key factor goes to the cost/performance of the nano-material.

A multi-fold increase in mechanical properties is afforded by the uniform dispersion of the nano-scale filler in a polymer matrix, and the process of obtaining such an exfoliated structure in the matrix of a polymer is a mechanism strongly dependent upon thermodynamics [Alexandre and Dubois 2000, Dennis et al. 2001]. The mechanism is referred to as *intercalation* where polymer chains diffuse into the interlayer region of a clay tactoid, a bundle of clay platelets (sheets) held together by van der Waals and electrostatic forces. Intercalation of a polymer causes the spacing between adjacent platelets to increase and eventually the individual sheets are delaminated. During the diffusion of polymer chains into the interspace of clay tactoids, the entropy of the system decreases due to the severe confinement being imposed on the polymer chain, and

favorable enthalpic interactions must be present to minimize free energy. The surface of clay platelets, due to the hydroxyl group and oxygen atoms, is hydrophilic. In order to increase the lipophilicity of the clay, an organophilic modification must be applied to the clay, but the modified clay is presently costly due to the lengthy preparation process. For polymers with hydrophilic functionalities, the modification is sufficient for favorable polymer-clay interaction to be present in many cases [Fornes et al. 2003]. Even in these cases where the free energy of the process favors the intercalation, the rate limiting step of intercalation can make production of polymer/clay nanocomposites prohibitively expensive due to the low production rate. For polyolefins, the favorable enthalpic interaction required to overcome the entropic penalty of confining such large molecules in the nano-scale space between platelets does not exist due to their apolar nature and thus the free energy of the process does not favor intercalation, even for organically modified clays [Vaia and Giannelis 1997]. With compatibilizing agents added to such polyolefin systems some degree of intercalation is observed, but a fully exfoliated structure is extremely difficult to develop. Annealing times in the order of hours may be necessary to acquire an exfoliated clay structure in a polyolefin-compatibilizer system. Both the required addition of compatibilizer and the limiting production rate restrain scientists and engineers from satisfactorily developing a nanocomposite with sufficient value-added properties which would justify the expense of the material.

To solve the problem of limiting production rate, disruptive technologies have been proposed to advance the rate and extent of exfoliation. These technologies include high energy ultrasound [Lim et al., 2003], electrical fields [Lu et al., 2006], and the use of supercritical fluids [Mielewski et al. 2004, Horsch et al. 2006, Yang and Ozisik 2006, Nguyen and Baird 2007, Treece and Oberhauser 2007, Litchfield et al. 2007, Zhao and Huang 2008]. Among the three methods stated, the use of supercritical fluids can be seen as the most applicable to current industrial processing practices and the least damaging to equipment and the polymer structure. Supercritical carbon dioxide ($scCO_2$) is proposed as a means of aiding the production of a polymer (specifically in the case of this study, a

thermoplastic polyolefin elastomer, TPO) nanocomposite with a higher degree of exfoliation and an improved production rate. It is well known that carbon dioxide above its critical state has both gaseous properties, such as being able to penetrate through many materials, and liquid properties, such as being able to dissolve materials. Due to its basic non-polar nature, supercritical carbon dioxide is seen as a potential medium for improving miscibility of the different hydrocarbon-like species in a nanocomposite system. Development of a processing method upon supercritical carbon dioxide presents two major challenges. One is how the supercritical carbon dioxide participates in the intercalation of polymer chains into the clay interlayer region, which involves in the interactions of supercritical carbon dioxide with organoclays, compatibilizers and polymer matrices. The other challenge is if the developed intercalated or exfoliated morphology is thermodynamically stable or how to preserve the acquired morphology once the gas is withdrawn. The research in the present work will try to answer part of the first question, i.e. how supercritical carbon dioxide influences structures of organoclays.

1.2 Objectives

The goal of the entire project is to develop a processing strategy for the manufacture of a thermodynamically stable, exfoliated TPO nanocomposite. The basic idea of the processing route is: i) pre-treat an organoclay with supercritical carbon dioxide to make it more ready for the intercalation of polymer chains during the subsequent processing; ii) mix the clay-scCO_2 suspension with the melt-blend of a matrix polymer and compatibilizer all the while maintaining the system above the supercritical state; and iii) release the gas after compounding and pelletize the nanocomposite material. Based on this idea, as the first part of the project, the research carried out in this thesis covered:

a) Evaluation of pristine and several commercial versions of organically modified montmorillonite mixed with supercritical carbon dioxide under different conditions applicable to TPO extrusion, i.e. temperature, pressure, residence time

and pressure release rate. The clay will be mainly analyzed by X-ray diffraction and transmission electron microscopy for changes in structure. Other techniques such as thermogravimetry, differential scanning calorimetry, scanning electron microscopy, and other analyses will assist in characterizing the clay structure. This work is expected to allow us to understand the interaction mechanism of organoclay, especially its surfactant component, with the supercritical fluid. Additionally, the work will allow selection of ideal clay candidates for the next step in the research, and establish important parameter values related to operating conditions for clay pretreatment with the supercritical fluid.

b) Characterization of surface energy of the clays. Contact angle technique will be applied for this work. This evaluation will provide basic data on the clay surface for the next step of this project to examine their compatibility with selected compatibilizers and confirm the decision of organoclay candidates made based on the above step.

c) Considering the existence of moisture in clays and extra cost of removing it, whether water can become as a co-solvent favoring the interaction between supercritical carbon dioxide and an organoclay was also evaluated.

In general, the research in this thesis is anticipated to answer a question of scientific and industrial significance: if the supercritical fluid interacts with the nanofillers in a manner that may lead to increase interlayer spacing of the clay sheets. The manner is thought to facilitate the intercalation.

CHAPTER 2 LITERATURE REVIEW

2.1 Introduction

Nanocomposite materials have aroused attention, imagination and research interests of scientists and engineers for decades. This stimulation comes from the idea that new materials with unprecedentedly improved physical properties can be designed and created simply using nano-dimension building blocks. The building block may be nanometer scale in one dimensional, two dimensional and/or in all three dimensions. Layered silicates are inorganic fillers with one dimensional nanometer size, which were first introduced to the research field of polymer composites for the automotive industry in the early 1990s [Usuki et al. 1993, Kojima et al. 1993 (1, 2, 3)]. This introduction initiated the modern polymer nanocomposite field. The polymer composites with multiple fold increase in mechanical properties afforded by the nano-scale filler with almost negligible increase in weight are well suited to the automotive industry where lightweight of vehicles is urgently expected due to the issues of petroleum cost and emission limitation. From then on, studies on polymer-layered silicate (PLS) nanocomposites have become more and more prosperous. As polymer matrices have been varied from the partially polar Nylons to totally non-polar polyolefins, layered silicates have been developed with different surfactant modifications. Melt compounding has become one of the two dominant ways of preparing polymer/clay nanocomposites and is recognized as a promising approach due to its ease by employing conventional polymer mixing or extrusion processes and its low environmental impact and cost effectiveness. Thermoplastic polyolefin elastomer, organically modified montmorillonite and the melting compounding are the concerns of this project.

2.2 Components and Structures of PLS Nanocomposites

2.2.1 Structures and Surface Properties of Organoclays

Montmorillonite (MMT) is a 2:1 phyllosilicates clay mineral with a general formula given as

$$M_x(Al_{4-x}Mg_x)Si_8O_{20}(OH)_4 \qquad (2.1)$$

where M is referred to as monovalent metal cation and x is the degree of isomorphous substitution [Giannelis et al. 1999]. In literature, most of the relevant research studies are based on this clay. Montmorillonite is a layered silicate in which each layer consists of an octahedral sheet of alumina or magnesia sandwiched by two silica tetrahedrons by the tip, the oxygen ions belonging to both of the octahedral sheet and the tetrahedral sheets. The layer thickness is usually 0.95 – 1 nm and the lateral dimensions of the layer may vary from 30 nm to several microns and even larger [Yariv et al. 2002]. These layer stacks are held together by van der Waals forces and electrostatic attraction. Isomorphous substitution of the metal ions in the sheets, for example, Al^{3+} replaced by Mg^{2+} or Fe^{2+}, or Mg^{2+} replaced by Li^{+}, results in a charge deficiency. The negative charges impart basicity to the oxygen plane and are usually balanced by alkali or alkaline cations situated in the gap between the layers, though, there may still be a small portion of negative charges which are not fully balanced leading to a weakly basic oxygen plane or the broken bond plane. The counterbalanced cations are naturally hydrated and weakly bound to the surface of the layer. These inorganic cations can be subsequently exchanged with organic cations such as alkyl ammonium ions and this replacement renders the clay organophilicity, which is a must for the applications of clays as adsorbents of organic compounds or fillers in polymer composites.

Organic modification of a clay mineral alters the hydrophilic nature, improves its compatibility with organic molecules, and at the same time expands the clay, converting it from a microporous (< 2 nm) structure to a mesoporous (> 2 nm) material suitable for guest intercalation into its galleries. According to Lagaly [1976, 1982, 1986], conformation of the intercalated long-chain alkylammonium cations is dependent on length of the alkyl chains of the organic cations, degree of the cationic exchange and the charge density distribution on the clay sheets, resulting in adoption of a lateral monlayer, bilayer, pseudotrimolecular layer, paraffin-type monolayer or paraffin bilayer arrangement, as shown in Figure 2.2.1. n-Alkylammonium ions with chain lengths less than 8 carbons arrange as a lateral monolayer with a constant spacing of ~13.6 Å, while those with longer chains are found in lateral bilayers with basal spacing of 17.7 Å. Higher cationic exchangeable capacity (CEC) particularly in combination with the use of dialkyl or trialkyl substituted ammonium ions leads to a further increase in the basal spacing which is designated as a pseudotrimolecular layer structure with basal spacing of 21.7 Å or the paraffin-type arrangements (monolayer and bilayer) with basal spacings larger than 22 Å. Charge heterogeneity on the silicate sheets is responsible for the non-integral change in basal spacing of organoclays. Studies by Bonczek et al. [2002] showed that there were two dominant configurations based on the proportion of the CEC. Below 70% of CEC the organic cations existed predominantly in heterogeneous monolayers attaining basal spacings of between 14.1 and 14.4 Å, whereas for higher organic loading (up to 100% of CEC) the alkylammonium cations was assumed a predominantly bilayer configuration. The work by Xi et al [2004] confirmed the arrangement of n-alkyl surfactant molecules existing in the galleries of montmorillonite. They found that the variation in the *d*-spacing was a step function of the surfactant concentration and proposed a model that a lateral monolayer of surfactant molecules formed when the surfactant loading was up to 0.4 CEC, a lateral-bilayer arrangement for the loading up to 0.8 CEC, and a pseudotrimolecular layer with excess surfactant adsorbed on the clay surface for the loading above 1.5 CEC.

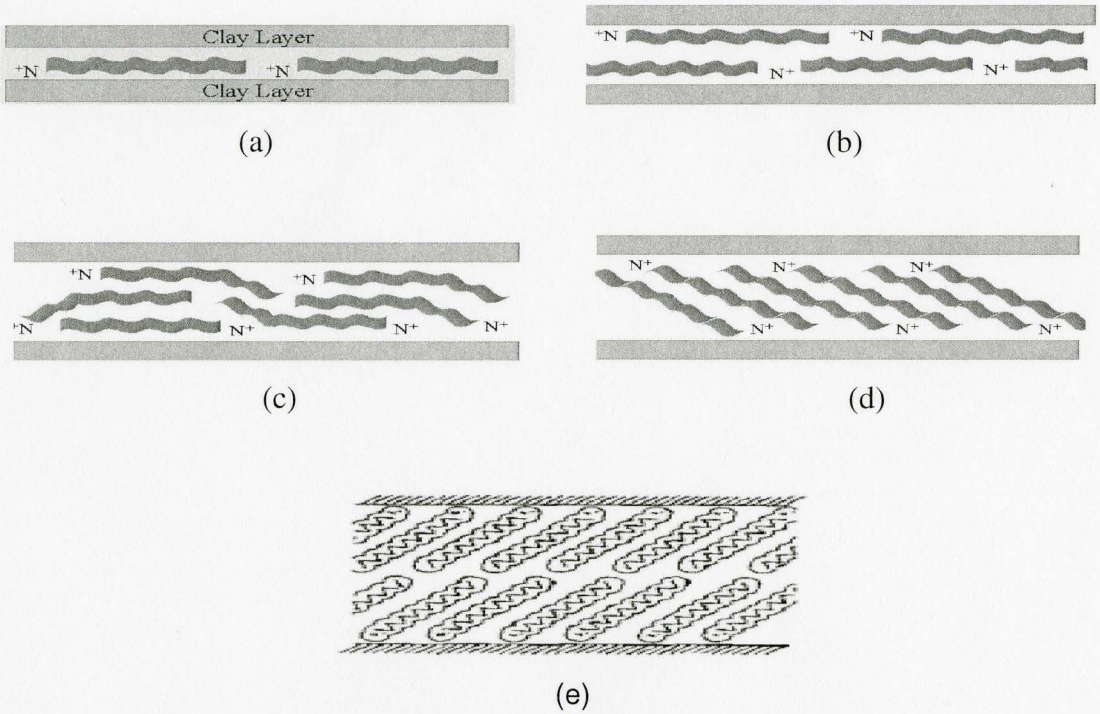

Figure 2.2.1 Alkyl chain conformations in layered silicates: (a) lateral monolayer (13.7 Å), (b) lateral bilayer (17.7 Å), (c) pseudotrimolecular layer (21.7 Å), (d) paraffin-type monolayer (>2.2 Å) [Bonczek et al. 2002], and (e) paraffin-type bilayer [image taken from Vaia et al. 1994]

The proposed structures of organoclays in Figure 2.2.1 are supported by numerous studies. The real distribution of the long-chain alkylammonium cations in an organoclay, however, has proven to not exactly follow these models. One particular problem with these models is the assumption that all surfactant becomes ionically bound within the galleries of montmorillonite as an organoclay is prepared. Studies by He et al. [2006] showed that there were three molecular environments for the surfactant within the clay: i) intercalated within the clay interlayer via cation exchange and electrostatic bonding, ii) located within the galleries of the clay by hydrophobic bonding with the aliphatic tails of the surfactant, and iii) physical adsorption to the external surface. Stability of the

surfactant, in terms of ease of removal (via chemical, thermal or physical means), has been found to follow the order given above, with the intercalated species being most difficult to remove and the exterior adsorbed material being the most easily taken away. Deng et al. [2003] suggested that the surfactant molecules are probably concentrated in the margin area of the interlayer galleries forming an annular ring structure between two neighboring silicate sheets, held back from intercalating more deeply into the galleries due to van der Waals associations.

Inside the structure of clays, there are two kinds of water molecules. One is the hydrated water molecules around the balanced metal cations which accounts for most of the total water molecules; the other is the free water molecules which are held to the oxygen plane by attractive and dispersive forces [Yariv et al. 1992]. The former state of water is more stable and its removals require temperatures as high as 135°C, but for the latter state, a small portion of moisture content is readily removed at temperatures above ambient [Xi et al. 2004]. The hydrated cations, as shown in reaction (2.2), have the ability

$$[M(OH_2)_x]^{m+} \rightarrow [m(OH)(OH_2)_{x-1}]^{(m-1)+} + H^+ \qquad (2.2)$$

to donate protons and thus provide the clay with acidity, while the oxygen-plane surface of clay platelets is able to accept a proton and therefore is alkaline. The dissociation reaction is more energetically favored (10^7 times more within the interlayer than in the bulk) due to the enhanced dielectric constant of the interstitial matter caused by confinement [Touillaux et al. 1968]. The acid strength of the sodium cation is relatively weak, yet increases in strength as the water content decreases within the inner layers. Replacement of the exchangeable cation by an organophilic surfactant would reduce the water-adsorbing capacity of the clay [Jordan 1949].

2.2.2 Thermoplastic Polyolefins and Maleated Polypropylenes

Thermoplastic polyolefins refer to a class of polymer material modified by inorganic fillers and elastomeric particles consisting of block copolymers or rubber. TPOs are non-polar which presents extreme difficulties in intercalation as well as forming a homogeneous and thermodynamically stable nanocomposite because of their incompatibility with the polar inorganic filler.

During the intercalation process, the entropy decreases due to the severe confinement being imposed on the polymer chains. The compensation by the increase in conformational freedom of the tethered alkyl surfactant chains as the interlayer spacing increases is not enough and the total entropy remains negative [Vaia and Giannelis 1997]. In order to overcome the entropic penalty, favorable mixing enthalpic interactions between polymer and clay must be present. According to Vaia and Giannelis, the mixing enthalpy may comprise apolar interactions arising from associations between polymer and surfactant aliphatic chains as well as polar interactions originating from the Lewis acid/base interactions between the layered silicates and the polymer chains. Unfortunately, the two types of favorable enthalpic interactions seem not to exist for the apolar polymer. For example, no organic surfactant attached to montmonrillonite has yet yielded enough organophilicity to provide compatibility with a PP matrix, and the PP chains do not provide sufficient Lewis acid/base interactions with silicate surface. The positive total free energy of the mixing will not allow the intercalation of PP into an organoclay to proceed. To overcome the unfavorable approach of non-polar polymer chains into the interlayer of an organic modified montmorillonite, a polymeric compatibilizer is introduced to the TPO/MMT system in a small quantity sufficient to improve the interaction with the silicate surface yet remain miscible with the polymer matrix. Typically, the most favored polymeric compatibilizers are maleated polyolefins, most often maleic anhydride grafted polypropylenes (MA-PP) due to the presence of tertiary carbons in their backbones and hence the relative ease of free radical grafting.

The mechanism of a compatibilizer assisting in diffusion of polymer chains into clay galleries or dispersion of clay platelets into polymer matrix might be two steps [Vaia et al. 1995 and 1996; Dennis et al. 2001]. Chains of compatibilizer first enter the clay galleries due to strong interaction, probably by hydrogen bonding, between the polar groups on compatibilizer chains and the oxygen groups of the silicate layers, and then chains of non-polar polymer matrix diffused into the expanded interlayer region because of the compatibility of the polymer and the compatibilizer. Therefore, features of a compatibilizer such as molecular weight, polar group concentration, acidity/alkalinity, etc. are important for its compatible effectiveness with the organoclay and the TPO matrix, as well as the final mechanical properties of the nanocomposite. For maleated polypropylenes, higher degrees of grafted maleic anhydride (MA) improve the intercalation capacity of MA-PP [Kato et al. 1997], but lead to immiscibility with the polymer matrix [Kawasumi et al. 1997]. Research by Kawasumi et al.[1997] showed that the dispersibility of orgaoclay in a non-polar polymer matrix was dependent not only on the intercalation capacity of an MA-PP in the clay galleries but also on the miscibility of the MA-PP with PP. The work by Wang et al. [2004] showed that an oligomer with low molecular weight ($M_w = 9100$) led to improved clay dispersion whereas a compatibilizer with high molecular weight ($M_w = 330{,}000$) gave rise to improvement in mechanical properties. Another research study confirmed this result in that MA-PP with lower molecular weight and higher MA content led to better clay dispersion in the polypropylene/clay nanocomposites but also caused deterioration in both mechanical and thermal properties [Yang et al. 2006]. It seems that an MA-PP with both enough polar groups and good miscibility with PP would achieve an exfoliated and homogeneous dispersion of clay platelets in the nanocomposites, but at a cost.

The immiscibility of a compatibilizer within a polymer matrix is attributed to not only its polar groups but also its lower molecular weight. Higher molecular weight for a compatibilizer will definitely increase its miscibility with non-polar polymer matrices, and therefore an MA-PP with higher maleic anhydride content without reduction of its

molecular weight during preparation would be desirable. The unfortunate fact so far is that chain length seems always to be coupled to the grafting degree of the polar functional group due to the reaction used in generating a maleic anhydride modified polypropylene compatibilizer. With higher maleic anhydride grafted onto the polymer backbone, the molecular weight of the polypropylene will be substantially reduced by chain scission which occurs simultaneously with bulk grafting [Shi et al. 2001]. The effect of the degree of grafted maleic anhydride groups on the dispersibility of clay in the polymer nanocomposite is usually studied by not decoupling the molecular weight of MA-PP. Hong et al. [2005] attempted to look at the effect of molecular weight on exfoliation but they were unable to decouple the influence of maleic anhydride content from their results. They used a compatibilizer with MA content of 2.6 wt % and molecular weight of 49,600 g/mol to create a fully exfoliated TPO nanocomposite, while the other two compatibilizers, 1 wt % MA content/157,100 g/mol molecular weight and 0.8 wt % MA content/240,700 g/mol molecular weight, did not lead to fully exfoliated structure. As expected, impact and flexural properties were greater for nanocomposites using the latter two compatibilizers. Another paper trying to study the effect of the compatilizer's molecular weight [Wang et al. 2006] stated that the effect of molecular weight of MA-PP on the exfoliation behavior should be coupled with processing conditions because both are factors influencing the shear viscosity during the melt compounding of PP/clay nanocomposites. They claimed that all studied PP-MAs, i.e. Polybond 3150 with 330,000 g/mol/0.5 wt %, Polybond 3200 with 84,000 g/mol/1.0 wt % and Polybond 3000 with 61,000 g/mol/1.2 wt %, gave rise to similar degrees of dispersion when blended with Nanomer I.30P, an octadecylamine modified MMT clay, at a ratio of 10:1 (w/w) at the optimal temperature. They seemed to conclude from their research that processing temperature or the shear viscosity during the melt compounding were the key factors to clay dispersion or exfoliation. Clearly, their work still did not decouple the influence of the grafting degree of maleic anhydride from molecular weight.

The amount of MA-PP used should be limited because of its negative effects on the thermal stability and even the mechanical properties of the final products [Thompson and Yeung 2006; Wang et al. 2004]. A study by Lertwimolnun and Vergnes [2005] showed that at a constant clay concentration (5 wt %) an improvement in the degree of clay dispersion within PP could be obtained by adding MA-PP at concentrations higher than 10 wt %, but no further improvement on the dispersibility of clay was observed above 25 wt %. The ratio of compatibilizer-to-organoclay is another issue needed to be considered due to the concentration limitation of compatibilizer in the non-polar polymer/clay nanocomposites. A reasonably low ratio of compatibilizer-to-organoclay should be applied when considering shear delamination and mechanical properties, though a higher ratio facilitates clay dispersibility. The work by Kato et al. [1997] indicated that a weight ratio of 3:1 led to the average basal spacing of an organoclay increased up to 72.2 Å. Wang et al. [2004] showed that when the proportion of Polybond 3150 and an organoclay in weight reached 4:1, the organoclay platelets completely dispersed in the MA-PP melt and that when the proportion was 3:1, the characteristic peak in the XRD pattern was very small and the peak location was undistinguishable due to the peak's broadness, which validated the result by Kato et al [1997].

2.2.3 Structures of PLS Nanocomposites

Generally, there are two types of structures for PLS nanocomposites, the intercalated morphology and the exfoliated morphology, shown in Figures 2.2.2(b) and 2.2.2(c), respectively. For the intercalated structure, a single or more than one extended polymer chains intercalate in between each silicate layer resulting in an increased interlayer spacing though the ordered stacking structure remains intact. This morphology is sometimes referred to as an ordered exfoliated structure if the van der Waals forces between adjacent platelets are negligible. For the exfoliated structure, the silicate layers are completely separated and uniformly dispersed in a continuous polymer matrix. Some times in literature this morphology is referred to as a disordered or dispersed exfoliated

structure. When polymer chains are unable to intercalate between clay platelets, only a conventional composite (Figure 2.2.2a) is obtained. The exfoliated structure is most desired because it is felt by researchers that this structure will allow maximum specific mechanical properties. Unfortunately, until this structure can be realized in a stable morphology it is difficult to compare against phase separated and intercalated systems.

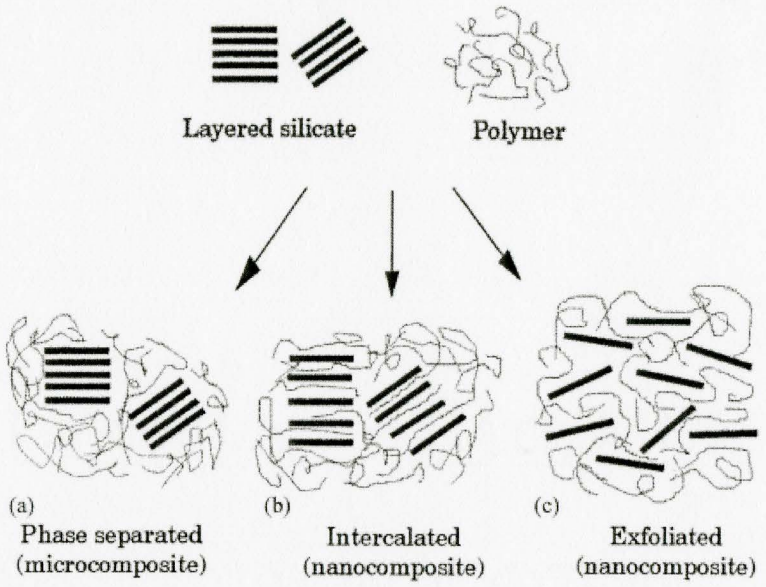

Figure 2.2.2 Structures of PLS nanocomposites [Alexandre and Dubois, 2000]

The structure of PLS nanocomposites depends on the nature of their components and the method of processing because the two factors determine the dispersion degree of clay platelets. In most cases only a nanocomposite with a mixed intercalated and exfoliated structure is obtained, especially for the case of non-polar polymer matrix and melt compounding processing in which fully exfoliated structure is rare.

2.3 Processing and Processing Issues of PLS Nanocomposites

There are basically four strategies for creating PLS nanocomposites: i) exfoliation-**adsorption** by which the layered silicate is exfoliated into single layers using a solvent in which the polymer is soluble, ii) in-situ intercalative **polymerization**, a technique that the layered silicate is swollen within the liquid monomer or a monomer solution so that polymer formation can occur in between the intercalated sheets, iii) **melt intercalation** where the layered silicate is directly mixed with the polymer matrix in the molten state and exfoliation occurs by shear delamination of individual platelets from the silicate stacks after associative forces between adjacent silicate layers have been weakened by intercalation, and iv) **template synthesis** where the silicate layers are formed in-situ in an aqueous solution containing the polymer [Oriakhi, 1998]. Clearly strategy iv) is not available for most polymers and method i) is usually used to produce water-soluble polymer nanocomposites. Therefore, in-situ polymerization and melt intercalation (which is often referred to in this thesis simply as melt compounding) have become the two dominant routes for preparing PLS nanocomposites. For polyolefinic based PLS nanocomposite materials, melt intercalation seems more promising over in-situ polymerization because i) no solvent is involved, ii) the synthesis can proceed on the industrially available extruder, and iii) the monomer is not suited to the intercalation and exfoliation of MMT on a nanometer level by subsequent polymerization from a solution [Pinavaia and Beall 2000]. In addition, the apolar nature of the polymer does not allow it to form a thermodynamically stable morphology with the clay when produced by in-situ polymerization.

For melt compounding, intercalation of polymer chains into the interlayer region of clay is considered a key step in preparing a nanocomposite because the processes of exfoliation and delamination of an organoclay are recognized to happen following this step [Vaia et al. 1995 and 1996, Dennis et al. 2001]. According to these researchers, polymer chains first diffuse into the clay galleries and expand the interspace size between clay platelets. During this stage, the pathway does not require high shear and the major driving force is either physical or chemical affinity of the polymer to the organoclay

surface, overcoming the strong attractive van der Waals forces between the silicate sheets making up the clay crystal by induced basal expansion of its galleries. Following this stage, clay platelets delaminate from the expanded stacks during which shear is the major driving force, and therefore high shear intensity would help the exfoliation. It is the first stage that controls the whole processing because it has been shown to take considerable time [Schmidt et al. 2002]. Since polymer processing operations are typically measure in the order of seconds, the full exfoliation must occur within a faction of the total residence time. It is the rate-limiting step of exfoliation for the clay mineral that becomes a key challenge to advancing the commercialization of these novel polymers.

While complete exfoliation of the clay species is difficult within most polymers, the challenge is seen to be greatest for olefinic resins due to i) the poor interactions between the macromolecule and organoclay, and ii) the high demand for these polymers in commercial applications. Different strategies have been developed recently for improving the extent of exfoliation. The most popular has been the use of compatibilizers which are partially effective. More disruptive technologies such as high energy ultrasound [Lim et al. 2003] and electrical fields [Lu et al. 2006] have also been reported to advance the rate and extent of exfoliation. Treece and Oberhauser [2007] showed how direct injection of supercritical gas into a single screw process could yield exfoliation levels similar to twin screw compounding operations despite the lower shear history. Horsch et al. [2006] proposed using supercritical fluid to pretreat the organoclays before their addition. Among the three methods stated, the use of supercritical fluid can be seen as the most applicable to current industrial processing practices and the least damaging to equipment and the polymer structure.

2.4 Supercritical CO_2 and Its Applications

2.4.1 Properties of Supercritical CO_2

A supercritical fluid is defined as a substance for which both pressure and temperature are above their critical values and the density of which can be tuned from liquid-like to gas-like simply by changing temperature and/or pressure. The vapor-liquid-coexistence state of a fluid above its critical point makes it an excellent solvent with gas-like viscosity and liquid-like density. Supercritical carbon dioxide ($scCO_2$) has a critical temperature (T_c) of 304.05K and critical pressure (P_c) of 7.40MPa [Kemmere and Meyer 2005]. Compared to other supercritical fluids, carbon dioxide has received much more attention due to its easy accessibility to supercritical state (particularly for industrial uses), easy removal simply by depressurization, relative benignity to the environment, chemical inertness, low toxicity, low cost, and non-flammability [Tomasko et al. 2003]. Its ability to solvate under supercritical state is similar to organic solvents and tunable by simply changing temperature and pressure conditions. For most high molecular weight polymers, supercritical CO_2 is not a good solvent, but its solubility in many such polymers is substantial. In such cases, $scCO_2$ acts as plasticizer, suitable for polymer processing and polymer synthesis.

2.4.2 Polymer Processing

Applications of $scCO_2$ in polymer processing have included polymer modification, blending, foaming, etc. In polymer modification, polymers exposed to $scCO_2$ first swell to varying extents leading to increased free volume and chain mobility, which then facilitates the impregnation of modifiers such as monomers, catalysts and other active chemical species. Supercritical CO_2 may also act as a carrier of those modifiers, delivering the solutes into the polymer phase. The swelling of polymers and the enhanced impregnation of active chemical species allows the chemical modification to be carried out at a lower temperature, which is very meaningful for the melt modification in order to avoid degradation. Successful applications of $scCO_2$ in polymer modification are reported to include chemically grafted methyl acrylate [Dong et al. 2004], 2-hydroxyethyl methacrylate [Li et al. 2001], methyl methacrylate [Liu et al. 2002] and maleic anhydride

[Liu et al. 2005] onto polypropylene by radical mechanism with the general aim of increasing hydrophilicity of PP.

Blending is an important technique for scientists and engineers creating new materials using immiscible homopolymers. Property improvements in these created materials strongly dependent on their morphology, i.e. the droplet size of the dispersed phase. Viscosity ratio of the dispersed phase and the continued phase is crucial in determining the size of the droplets. Supercritical CO_2 can help control the viscosity ratio of the two phases because of differences in the solubility of $scCO_2$ in different polymers, and therefore the size of the droplets may be tuned. In supercritical CO_2 controlled blending of poly(methyl methacrylate) (PMMA) and polystyrene (PS) by twin screw extrusion, it was observed that the droplet size of the minor phase (PMMA) decreased sharply when the viscosity ratio of PMMA and PS reached 7.3 at a shear rate of 100 s^{-1} and that the viscosity of PMMA reduced up to 80% and viscosity reduction of PS up to 70% [Elkovitch et al. 2000]. It was believed that the greater reduction in viscosity of the dispersed component lead to better momentum transfer from the more viscous major component and caused the minor component to break up into smaller droplets.

Foaming is another common polymer processing technique that provides products with substantial reduction in weight and high impact strength. Microcellular foaming of polymers using CO_2 as a blowing agent has even been touted as a revolutionary invention in the polymer industry [Simone and Paisner 2003, Liu et al. 2003]. The microcellular foaming technique is especially meaningful for those biodegradable and biocompatible polymers in the applications of tissue engineering, tissue regeneration and protein encapsulation because the microcellular foam combines substantial weight deduction and high impact strength with high toughness and good fatigue life, plus allows production in a clean and safe environment [Barry et al. 2004, Fujiwara et al. 2005]. Physical blowing agents like CO_2 are better than chemical blowing agents when the melting point of the polymer is high and its chemical structure is not thermally stable at high processing

temperature. Furthermore, good control over porosity is possible with CO_2 simply by manipulating temperature and pressure due to the high degree of supersaturation possible at high pressure and low temperature.

The uses of $scCO_2$ for polymer particle formation, fractionation, purification, and dyeing are all quite well established. In polymer particle formation, particle size, particle size distribution and morphology can be better controlled using $scCO_2$ as a solvent or anti-solvent by tuning process parameters such as the amount of dissolved CO_2, temperature, pressure, nozzle diameter and depressurization rate than using other traditional solvents, and this method leaves polymer particles solvent-free. The polymers reported for producing particles by this technique include fluoropolymer [Franklin et al. 2001], poly(ethylene glycol) [Hao et al. 2005], etc. For the polymer fractionation, by sequentially reducing or increasing the pressure of a SCF/polymer solution, narrow molecular weight fractions of the polymer sample are precipitated or extracted from the SCF/polymer solution [McHugh and Krukonis 1994, Kim et al. 1998]. Polymer purification using $scCO_2$ is based on the supercritical fluid extraction of monomers, oligomers, or other residual contaminants from polymer to improve the physical properties of the polymer in some way [Taylor 1996]. The most advantageous use of this technique is the reduction of organic solvent used. Organic dyes can also be transported uniformly into polymer hosts by $scCO_2$ [West et al. 1998, Kazarian et al. 1999 and Kawahara et al. 2001].

2.4.3 Clay Minerals and Organoclays

Supercritical CO_2 is mainly used as a regenerative solvent and an intercalant aid for clay minerals and organoclays. As an extractive or regenerative solvent, $scCO_2$ was reportedly used to clean natural clay soils contaminated with hydrocarbons, especially hydrocarbon polymers, [Reutergardh et al. 1998, Elektorowicz et al. 2007] and regenerate clay minerals [Braida et al. 2007] and organoclays [Mendes and Coelho 2005] containing

adsorbed organic compounds. Supercritical CO_2 has also been used as an aid to exfoliate layered silicate particles [Manke et al 2002], as a processing medium for intercalating natural clay with sugar acetate and β-D-galactose [Gulay et al. 2006] and organically modified clay with 4-phenylazoaniline [Ishii et al. 2002]. These studies were primarily focused on the extent of desorption achieved for various adsorbed organic species and the morphology of intercalated silicate layer structures. They were not concerned with the interaction of the $scCO_2$ with the organic adsorbents, the clay pillars or the clay surface on a molecular level. The study by Horsch et al. [2006] is the only article known to the author exploring the interactions between $scCO_2$ and surfactant modifier of MMT. In that study the researchers attributed the $scCO_2$ effect on clay dispersion to rapid depressurization and proposed that CO_2-philicity to the surfactant of the organoclay might result from the presence of acidic hydrogen atoms on the surfactant.

2.4.4 PLS nanocomposites

For recent years, patents [Mielewski et al. 2004] and papers [Horsch et al. 2006, Yang and Ozisik 2006, Nguyen and Baird 2007, Litchfield et al. 2007, Zhao and Huang 2008] on $scCO_2$ aiding the synthesis of PLS nanocomposites by melt compounding have been present. These researchers generally focused on the processing routes used and the improved dispersion of clay in the polymer matrix due to the addition of $scCO_2$. Two typical processing routes are proposed for the melt compounding synthesis. One is directly injecting $scCO_2$ into a melt mixture of silicate particles and polymer in an extruder, by which the silicates particles are expected to exfoliate in the extruded mixture [Horsch et al. 2006, Yang and Ozisik 2006, Zhao and Huang 2008]. The other route includes two steps: first exfoliating silicate particles using $scCO_2$ and then delivering the exfoliated silicate particles together with $scCO_2$ into a stream of polymer melt in an extruder [Nguyen and Baird 2007, Litchfield et al. 2007]. Batch compounding was also used to prepare polypropylene/sepiolite nanocomposites using $scCO_2$ as assistant solvent [Ma et al. 2007]. All these reports except Yang and Ozisik [2006] claimed that the clay

dispersion was improved and, subsequently the mechanical properties such as modulus and yield stress were likewise increased. Yang and Ozisik [2006] studied the effects of organic modifier of clays and processing parameters on clay dispersion in Nylon-6 matrices and found that high pressure and the addition of $scCO_2$ were not factors contributing towards improving clay dispersion. The authors also had a conclusion that it was necessary to select a proper organic modifier but it was not a sufficient condition to obtain an exfoliated clay morphology. Researches by Zhao and Huang [2008] showed that there was an optimal CO_2 concentration at which the PP/clay nanocomposites tended to be more viscous and that higher CO_2 concentration above the optimal value lead to decrease in the complex viscosity and dynamic moduli. However, these articles seldom probe the molecular level mechanism of interaction between $scCO_2$ and the nanocomposite components. As mention above, only the study by Horsch et al. [2006] discussed the interaction between $scCO_2$ and surfactant modifier of MMT.

Specific knowledge on anticipated interactions of $scCO_2$ with maleated compatibilizers is unavailable; however, it is evident from the available literature that the anhydride group will interact with the gas in some small manner. The most direct evidence of CO_2 interaction with maleic anhydride (MA) can be found in those studies looking at Diels-Alder reactions conducted under supercritical conditions to enhance kinetic rates. Glebov et al. [2001] found that the rate of reaction between maleic anhydride and isoprene under supercritical conditions was substantially increased when the MA concentration was below its solubility limit in CO_2 and only a single phase existed. At higher concentrations of MA, multiple phases existed in their reaction system and the rate of reaction was closer to those without CO_2. Unfortunately, the literature in this area never seems to hypothesize how the gain in reaction rate occurred. Extraction of MA from prepared MA-PP under $scCO_2$ was found by Clark and Lee [2004], but they provided little analysis on how. In the work of Liu et al. [2005], the authors attempted to prepare MA-PP by solid-state free radical reaction aided by $scCO_2$ and found a maximum

in the grafted maleic anhydride content in relation to CO_2 pressure which was attributed to partitioning of MA between different phases present within the mixture.

CHAPTER 3 EXPERIMENTAL

3.1 Materials

3.1.1 Clay minerals and organoclays

Five organoclays, Cloisite 20A, SCPX 1137, SCPX 2934, SCPX 2972 and SCPX 2971 were chosen for the studies. They are all MMT modified with organic quaternary ammonium salt surfactants. Their structural nature and suppliers are summarized in Table 3.1.1. First consideration of clay selections was the commercial availability. The unmodified clay and the organically modified clays were all supplied by Southern Clay Products (SCP). The modified clays had a reported organic loading of 95-100 meq/100g determined based on a titration method using amine salt. The second consideration was the chemical nature of surfactants used to modify the natural clay. Number of long alkyl chains, length of the long alkyl chain and non-aliphatic surfactant were the considered factors in order to examine potential variance in CO_2-philicity. Carbon numbers in the surfactant molecule of SCPX 1137, Cloisite 20A and SCPX 2934 are identical (~18 carbon atoms) but the number of aliphatic tails in a surfactant molecule of them is 1, 2 and 3, respectively. Cloisite 20A and SCPX 2972 have an identical number of long alkyl chains but the length of the alkyl chains is different, namely 18 carbons for Cloisite 20A and 12 carbons for SCPX 2972. Sodium montmorillonite (NaMMT) was the initial clay mineral from which the modified montmorillonites were prepared.

Table 3.1.1 Clays and their properties and suppliers used in the project

Clay	Surfactant type*	Chemical nature	Surfactant MW†	Basal Spacing‡ (Å)	Clay Supplier
SCPX 1137	1 – C_{18}	Trimethylhydrogenated tallow ammonium chloride	340	18.3	SCP
Cloisite 20A	2 – C_{18}	Dimethyldihydrogenated tallow ammonium chloride	574	25.8	SCP
SCPX 2934	3 – C_{16}	Methyltrihexadecyl ammonium chloride, 100 MER	739	33.4	SCP
SCPX 2972	2 – C_{12}	Dimethyldicoco ammonium chloride, 95 MER	417	20.6	SCP
SCPX 2971	Aromatic	Trimethylbenzyl ammonium chloride, 95 MER	186	15.1	SCP
NaMMT	—	—	—	12.2	SCP

* Example, 1 – C_{18} indicates one alkyl chain attached with a length of 18 carbon groups

† Molecular weights of surfactants in the table were provided by the suppliers.

‡ Values of basal spacing of the clays in the table were based on XRD measurement in our labs.

3.1.2 Other materials

Carbon dioxide gas (> 99.5 mole % purity) and nitrogen gas (100 mole % purity) were supplied by Air Liquide Canada Inc. 1-Bromonaphthalene (97 % assay) from Sigma-Aldrich and glycerol (Class IIIB) from Fisher Chemicals were used for surface tension measurement without any further treatment. Their dispersive (γ^d), polar (γ^p) components and the total surface energy (γ) were shown in Table 3.1.2 for 1 atm and 25°C.

Table 3.1.2 Surface property of two liquids [Gokel 2004]

Liquid	**Total, γ**	**Dispersive, γ^d**	**Polar, γ^p**
	mN/m	**mN/m**	**mN/m**
1-Bromonaphalene	42.80	42.52	0.28
Glycerol	60.90	35.54	25.36

3.2 Apparatus

A specially-built high pressure vessel (HPV) was used to process the clays with $scCO_2$. Temperature and pressure in the vessel were controlled by a temperature controller and a high pressure syringe pump (ISCO Model 260D). The setup of the processing apparatus is shown in Figure 3.2.1.

Another in-house built apparatus was the high pressure cell (HPC) for in-situ XRD measurement, shown in Appendix A. The tubes of the XRD-HPC were made from sapphire and polyetheretherketone (PEEK). Single-crystal sapphire is transparent and exhibits no detectable basal reflections by XRD in the range of interest. Unfortunately, the wall thickness of the tube (3 mm) necessary to withstand high enough pressures for

this work was too thick to allow X-rays generated from the Cu sealed X-ray tube or Mo sealed X-ray tube to pass. Instead of the sapphire tube, a PEEK tube of similar dimensions was selected and proved efficient for this application.

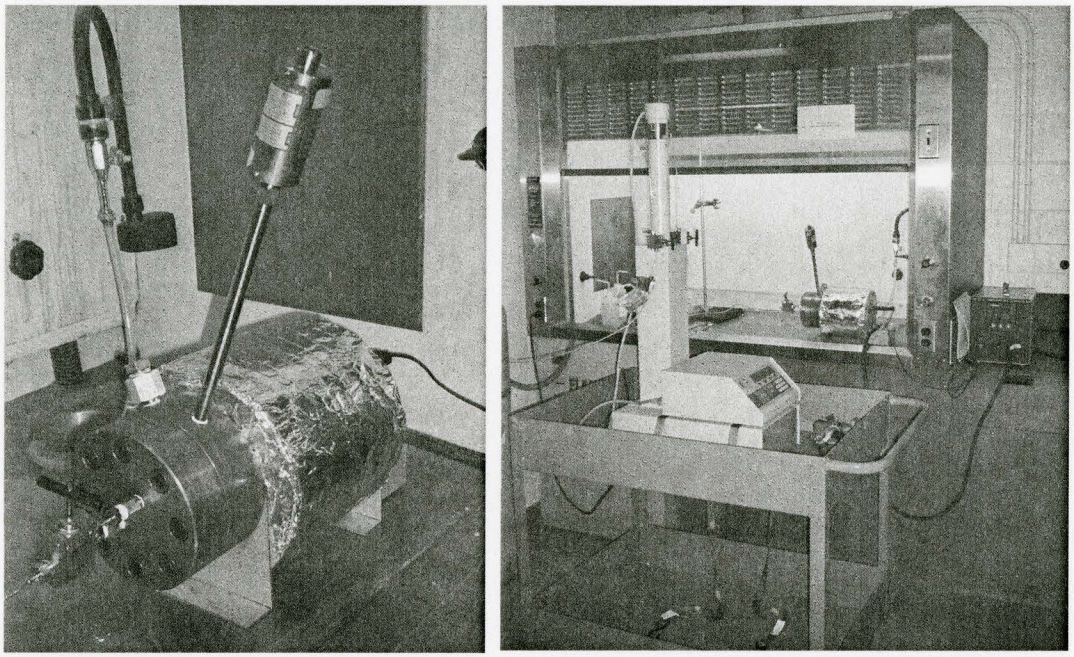

Figure 3.2.1 High pressure vessel (left) together with Syringe pump and temperature controller (right)

3.3 Experimental Design

3.3.1 Organoclays treated with single solvent — $scCO_2$

In order to investigate the general behavior of organoclays under $scCO_2$ atmosphere at different conditions (i.e. temperature, pressure, pressure release rate), a two-level full factorial design of experiment (DOE) was used. Variables and specific level values of the DOE are shown in Table 3.3.1. Low levels of temperature (50°C) and

pressure (7.6 MPa) were chosen to ensure that CO_2 was in its supercritical state (CO_2 critical point: P_c = 7.4 MPa and T_c = 31 °C) while the high levels of each factor (200°C and 9.7 MPa) were selected based on the practically applied processing temperature of TPO or PP in industry and a pressure possibly achieved inside the barrel of a twin screw extruder. Considering that the expansion of clay particles may be the result of explosive depressurization, we also chose pressure release rate as a parameter. The high level value (4.8 MPa/s) was the largest release rate that the needle valve on the HPV could reach while the low level (0.2 MPa/s) was the value selected for slowly releasing the gas from the vessel. The pressure release rate was controlled manually. The duration of the experiment was determined by the temperature used and was not considered a variable here but rather a requirement to ensure full adsorption of the CO_2 prior to depressurization. Appendix B lists detail of the full factorial design of experiment. The experimental procedure for the trials is discussed in Section 3.4.

Table 3.3.1 Parameters and levels in the DOE

Variables	**Levels**
Organoclay	Cloisite 20A, SCPX 1137, SCPX 2934 SCPX 2972, SCPX 2971
Temperature, °C	50 and 200
Pressure, MPa	7.6 and 9.7
Pressure release rate, MPa/s	0.2 and 4.8

Characterizations of the $scCO_2$ processed clay samples included organic weight fraction, the hydration properties, pH of the clay in water suspensions, thermal properties, interlayer distance, surface tension, etc. The interlayer distances of the clays examined above would be those after gas depressurization. In-situ observations of organoclay behavior under high CO_2 pressure were made to examine if there was any difference in surfactant morphologies while the $scCO_2$ was present.

3.3.2 Organoclays treated with $scCO_2$ and water co-solvent

Considering the potential strong interaction of the uncoated surface of an organoclay with water and the reports on PLS nanocomposites successfully synthesized in water slurry [Hasegawa et al 2003, Xu et al. 2006], water may be a suitable co-solvent to assist the clay expansion. In order to ascertain the effectiveness of water as a co-solvent to CO_2 in the expansion of the clay galleries, a small set of experiments was designed.

3.4 Experimental Procedure

3.4.1 Clay treatment with $scCO_2$

Supercritical CO_2 processing of the clays alone followed this procedure: i) drying about 2g of a selected clay in a vacuum oven at 40°C overnight (16 hours), ii) pre-heating the HPV for 1 hour to allow the temperature in the HPV to be uniform, iii) placing the dried clay into the HPV chamber, iv) purging the air in the chamber with CO_2, v) pressurizing the chamber up to the designated pressure, vi) maintaining the pressure and temperature during the whole processing, vii) depressurizing the chamber rapidly or slowly, and viii) collecting the treated samples for subsequent analysis. The processing pressure was controlled by a syringe pump. Gas in the vessel was released manually.

3.4.2 Organoclay treatment with $scCO_2/H_2O$ co-solvent

For the small set of experiments looking at the effect of water co-solvent on expansion of the clay galleries, two organoclays were chosen, namely Cloisite 20A and SCPX 2934. The clays were first dried in an oven at 40°C overnight (16 hours) and then hydrated for 10 days to an equilibrium weight. The hydration was performed by placing several grams of each organoclay in a small confined chamber where a dish filled with

distilled water sat to obtain a higher moisture environment. The relative humidity in the chamber was found to be 77%. Then a hydrated sample was treated with $scCO_2$ in the batch vessel under one of two conditions: 9.7 MPa, 200°C and 0.2 MPa/s; and 9.7 MPa, 50°C and 0.2 MPa/s.

3.4.3 Organoclay washing

As mentioned in Chapter II, there is a portion of surfactant physically adsorbed on the external surface of clay particles and the margin areas of the interlayer galleries. In order to resolve the effect that $scCO_2$ had on the interlayer region compared to the exterior of clay, the physically adsorbed surfactant needs to be removed. It has been shown by other researchers that a mixture of water/ethanol (4:1 in volume) is an appropriate solvent which primarily removes the physically adsorbed surfactant onto the external clay surfaces and not the surfactant present in the interlayer region [He et al. 2006]. The specific procedure and conditions of this extraction method used in our research were as follows: i) wrap the organoclay within filter paper, ii) put the wrapping into a liquid mixture of water/ethanol (4:1 in volume), iii) reflux the liquid for 6 hours, iv) wash the refluxed clay with distilled water and filter the washed clay using a Buchner funnel, and v) dry the clays in a vacuum oven at 80°C overnight.

3.5 Characterization

3.5.1 Organic content, pH and hydration

The organic content of organoclays was obtained by burning the organic material from the samples. The burning process ('ashing') was performed in a muffle furnace at 600 ℃ and air environment for 1 hour. The organic content was calculated from difference in the mass based on the sample immediately collected from the batch vessel

after treatment and compared to the weight of the ashed product. This measurement gave a maximum standard deviation up to 1.0 wt % in the percentage organic content.

pH values were measured using a Mettler Toledo pH meter. The measurements were accomplished by: i) preparing aqueous suspension of a clay by adding 0.2 wt % of the modified mineral into distilled water under magnetic agitating; ii) sonicating the suspension for 30 seconds before pH measurement; iii) immersing the pH probe in the suspension while stirred magnetically; and iv) reading the stabilized pH value. Three to five measurements were taken and standard deviation of each sample will be displayed in the results.

Hydration of the $scCO_2$ processed clays proceeded by placing the known weight of a clay sample in an enclosed humidification chamber and measuring the weight of the hydrated sample every day until equilibrium was reached, about 7-10 days. The chamber featured an enclosed space containing a beaker of water at room temperature and its relative humidity was 77%.

3.5.2 Surface energy and interfacial tension

Surface energy is determined by two interfacial forces, van der Waals dispersive interactions (γ^d) and electron donor/acceptor polar interactions (γ^p), attributed to Lewis acid-base theory. The two types of interactions are considered independent and additive:

$$\gamma = \gamma^d + \gamma^p \tag{3.1}$$

Surface energy of a material can be obtained by measuring the contact angle (θ) that a liquid droplet of known properties forms on the flat surface of the material. The interaction terms were estimated from the contact angle measurement by using the Young-Dupre equation:

$$(1+\cos\theta)\gamma_l = 2\left(\sqrt{\gamma_s^d \gamma_l^d} + \sqrt{\gamma_s^p \gamma_l^p}\right) \tag{3.2}$$

where θ is the measured contact angle. To solve the two unknowns, γ_s^d and γ_s^p, in Equation (3.2), two liquids with known dispersive and polar components must be used in the contact angle measurement. Here 1-bromonaphalene and glycerol were chosen. Surface energy was calculated using the Owens and Wendt method [Owens and Wendt, 1969]. Surface tension is temperature dependent and for the majority of compounds the value of surface tension decreases at a rate of 0.1 dyn·cm^{-1}/°C with temperature [Gokel 2004].

For powder samples, surface energy can be determined using direct contact angle measurement or thin layer wicking. For clays, a suitable flat surfaces for measurement is generally questionable on account of macroscopic surface roughness [van Oss and Giese 2003], leading to larger than expected contact angles. However, with swelling clays a wicking approach can not be used since the capillary rise velocity is significantly retarded for polar liquids due to swelling. It is for this reason that direct contact angle measurements were used in this work. The flat surface required for this approach was prepared by filling a highly polished tablet-press die with an organoclay sample and subsequently compressing the powder under a pressure as high as 340 MPa. The diameter of the clay disk was 10 mm and the thickness was about 1.5 mm. An example of the final tablet produced by each of the five organoclays was analyzed by a KLA-Tencor surface profilometer. The profilometer has a vertical resolution of 5 Å on the kilo angstrom range and 5 nm on the micron range, and a horizontal resolution of 400 Å. The surface topography (an example texture profile given in Figure 3.5.1) was measured to confirm that the surfactants did not produce significantly different surface properties for their pressed disks; capillary effect resulting from large asperities can negatively influence the measured contact angle by the sessile drop technique and therefore, comparison of results between the different organoclays required similar surfaces. As we can see from the

summarized data in Table 3.5.1, tablets with low surface roughness resulted from the preparation method though minor differences were noted between SCPX 1137 and SCPX 2971, and the other organoclays. While for the author of this thesis there is no known study showing the relationship between the dimensions of roughness and the magnitude of capillary forces which affect the contact angle of a liquid droplet, as it will be shown later that the determined surface energy values were consistent with published data for similar organoclays tested by different measurement technique.

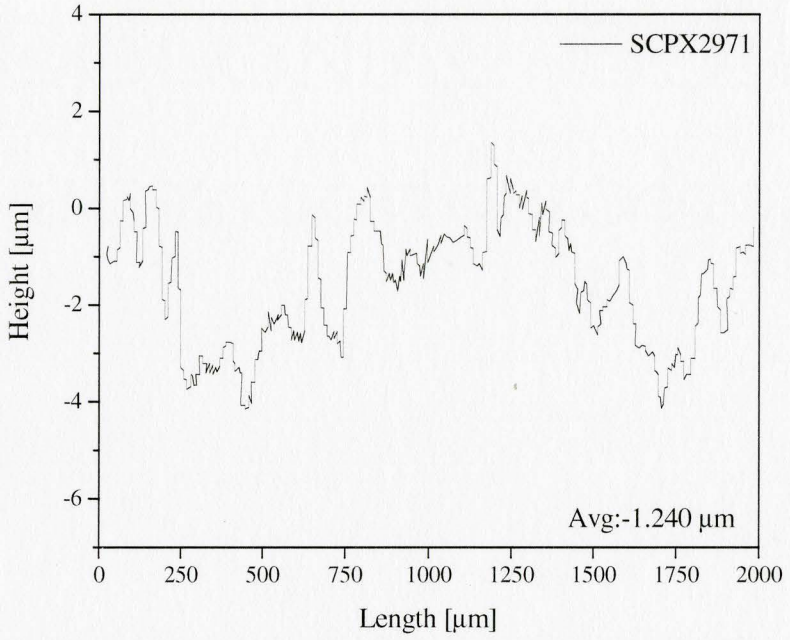

Figure 3.5.1 Surface roughness of SCPX 2971

Table 3.5.1 Surface roughness of organoclay tablets prepared by the hydraulic press

Type	SCPX1137	C20A	SCPX2934	SCPX2972	SCPX2971
Roughness (µm)	1.7 ± 0.4	0.5 ± 0.3	0.5 ± 0.1	0.5 ± 0.2	1.8 ± 0.4

Surface energy measurement was performed on a custom-built sessile-drop apparatus consisting of a temperature-controlled cubic chamber with two quartz windows on opposite sides for illumination and observation. The chamber was also connected to a gas cylinder allowing continuously purging of the atmosphere in it. A low magnification microscope coupled with a CCD camera took the images of the liquid drop or the molten polymer drop on a clay tablet and the image analysis software, FTÅ (First Ten Angstroms Inc.) measured the shapes of the acquired images to give the contact angle. The size of liquid droplet was controlled by a 10 – 100 μl VWR-brand pipet. The measurement followed this procedure: i) elevated the sample chamber temperature to 50°C, ii) placed a clay disk into the chamber, iii) opened gas N_2 valve and waited for 5 minutes for the air purging and sample heating, iv) put a liquid droplet of 0.2 μl on the surface of the disk, and v) output contact angle values by the software.

3.5.3 X-Ray Diffraction

Observations of the gallery spacing of the samples were performed on three diffractometers, Bruker D8 and Bede Scientific D1 using Cu Kα (λ = 1.54 Å) as radiation source and Bruker Smart APEX II using Mo as X-ray tube (λ = 0.71 Å); availability dictated where the measurement was made. Powder samples were mostly analyzed using Bede Scientific D1 diffractometer at an accelerating voltage of 40kV and a current of 40mA. Analysis on Bruker D8 X-ray diffractometer was carried out at an accelerating voltage of 40kV and a current of 20mA. Both of the instruments were calibrated using silver behenate crystal powder.

The in-situ observations under pressure could not be accomplished using the CuKα diffractometers due to the thickness of the wall of the PEEK tube. Radiation energy of a CuKα tube was insufficient to penetrate the tube wall, and therefore, Bruker Smart APEX II with higher energy Mo X-rays was used. The Mo X-ray tube can produce higher radiation energy and proved to work for observing interlayer distance of clays confined in

the PEEK tube. The in-situ XRD measurement was performed as follows: i) fully and tightly fill the PEEK tube with an organoclay, ii) pressurize to 9.7 MPa with CO_2, iii) keep the tube pressurized for 2 hours, and iv) take an XRD scan for 5 minutes. The whole processing could only be run at room temperature, and therefore the CO_2 environment in these observations was not supercritical but rather in a subcritical state.

3.5.4 Transmission Electron Microscopy

The exterior of the clay particles and their lamellar microstructure were studied using TEM. The powder of a clay was placed on a carbon grid and observed directly using the CM 12 PHILIPS TEM at an accelerating voltage of 120 kV. The magnification used was mostly 200K times.

3.5.5 Scanning Electron Microscopy

Particle size and detail structure of clays were visually analyzed by using scanning electron microscopy (SEM). The clay powder was spread on the sticky surface of a plate, gold-sputtered and observed on a PHILIPS SEM 515 with an accelerating voltage of 20 kV at magnifications of 300, 1100 and 5000 times.

3.5.6 Thermogravimetric Analysis

The change in surfactant mobility and distribution within an organoclay and similarly for their mixtures with compatibilizers and/or TPO was evaluated using TGA. The analysis was performed by a STA 409 (Netzsch Instruments) over a temperature range of 20 – 600 °C, a ramp rate of 10°C/min and under an atmosphere of CO_2. The isothermal TGA was done with the same instrument by heating the sample from ambient

temperature to 200 ℃ at 30 ℃/min ramp rate and CO_2 atmosphere and holding the sample under the conditions for 2 hours.

3.5.7 Differential Scanning Calorimetry

DSC is another way to evaluate thermal properties of our materials. The changes in melting temperature or melting range and heat capacity were expected to reflect re-crystallization or extraction happened during $scCO_2$ processing. Regular DSC analysis was performed on a DSC 2910 (TA Instruments) by a temperature span of 0 – 200°C, ramp rate 10°C/min and N_2 atmosphere. Conventional modulated DSC measurements of clays were done using Tzero technology on a DSC Q200 (TA Instruments) at a temperature range of –10°C ~ 130°C, a modulated period of 60 seconds, a modulated amplitude of ± 1°C, a heating rate of 1°C/min and N_2 atmosphere.

3.5.8 Fourier Transform Infrared Spectrometry

FT-IR spectrometry was used to assess the interactions of $scCO_2$ with the organoclays. Transmittance FT-IR spectra were collected at a frequent range of 400 – 4000 cm^{-1} using a Bio-Rad FTS-40 spectrometer at a resolution of 2 cm^{-1} and N_2 atmosphere. The scanning times for each collection were 64. Powder samples were mixed with KBr and compressed into tablets. During the measurement, care was taken to ensure that the atmosphere in the sample chamber was completely replaced by N_2 to avoid interfering with the observation of CO_2 that might exist in our treated samples.

3.5.9 Atomic absorption spectrometry

The sodium content of the pristine and organic modified clays was identified by a Perkin-Elmer 5100 ZL atomic absorption spectrometer. The analysis was conducted at the McMaster Environmental Lab.

CHAPTER 4 ORGANOCLAYS PROCESSED WITH SUPERCRITICAL CARBON DIOXIDE

4.1 Thermal Stability of Surfactants

To ensure equilibrium conditions were achieved in the high pressure batch vessel with regards to adsorption of carbon dioxide into the interlayer spacing of the different clay species, the experiments were carried out for 3 hours at 200°C and 6 hours at 50°C. With such prolonged exposure to an elevated temperature up to 200°C, there were concerns that degradation of the surfactant would result [Shal and Paul 2006], thereby complicating our analysis in regards to the influence of $scCO_2$ on the structure of the organoclay. In order to respond this concern, both isothermal and non-isothermal TGA were conducted under a blanket of CO_2 (~300 kPa). Note that the results in this section specifically pertain only to the as-supplied organoclays and not any clay treated by $scCO_2$.

Non-isothermal TGA results of the five organoclays and NaMMT were plotted in Figure 4.1.1. It can be seen that thermally-initiated degradation for the five organoclays did not begin before 212°C, which corresponded with the degradation study by Shah and Paul [2006]. All the five surfactants were, therefore considered to be thermally stable in the CO_2 environment at 200°C. The graph shows that the onset temperature for degradation of the five organoclays was the order of SCPX 1137 < SCPX 2972 < SCPX

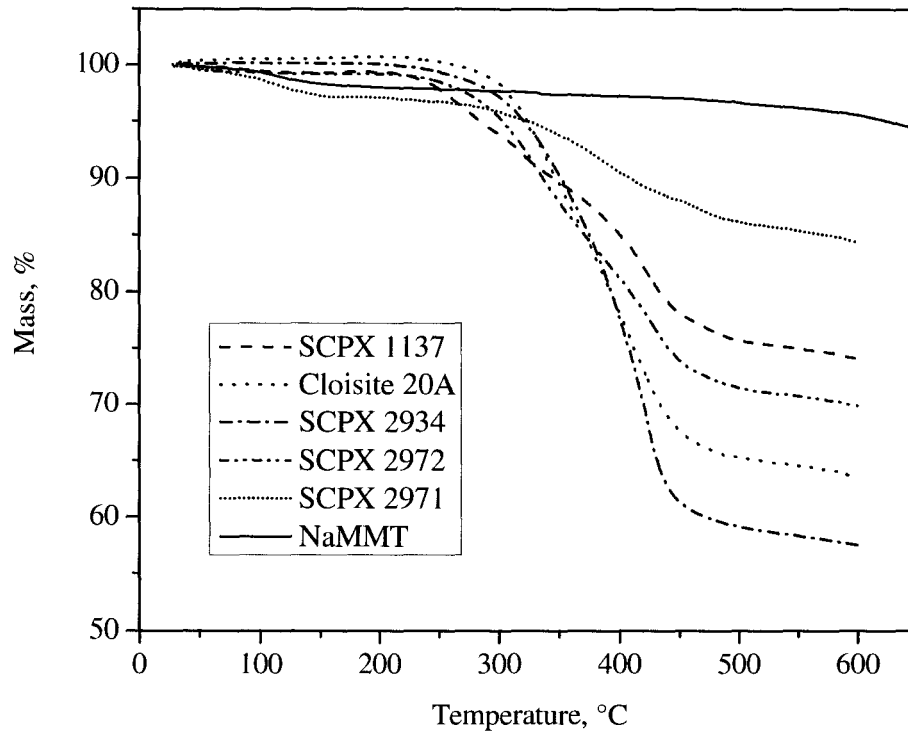

Figure 4.1.1 TGA plots of five organoclays and NaMMT under CO_2

2934 < Cloisite 20A < SCPX 2971. Above 100°C, SCPX 2971 exhibited obvious mass loss which should be attributed to moisture evaporation from this clay. As shown in Table 4.1.1, the moisture content of SCPX 2971 was close to NaMMT. Part of moisture contained in the two clays was not able to be removed during the drying at 40°C; a higher drying temperature was not used in order that all surfactants remained as solids and no morphological details were lost. The moisture stayed in the clays and continuously evaporated when elevating the heating temperature. Therefore, we can see in Figure 4.1.1 that SCPX 2971 and NaMMT had similar curves below about 200°C. It was noted from the TGA curve for NaMMT that de-hydroxylation from the clay mineral itself started to occur at 450°C, which should be one of the reasons that mass of the organoclays still decreased slightly after the majority of organic modifiers burned. Another reason for the

slight decrease in mass above 450°C may be the continuous removal of the residue of the organic materials [Soares et al 2004].

Table 4.1.1 Moisture content of organoclays and NaMMT dried at 40°C for 6 hrs, wt%

SCPX 1137	Cloisite 20A	SCPX 2934	SCPX 2972	SCPX 2971	NaMMT
2.83	1.90	1.04	2.16	5.11	5.77

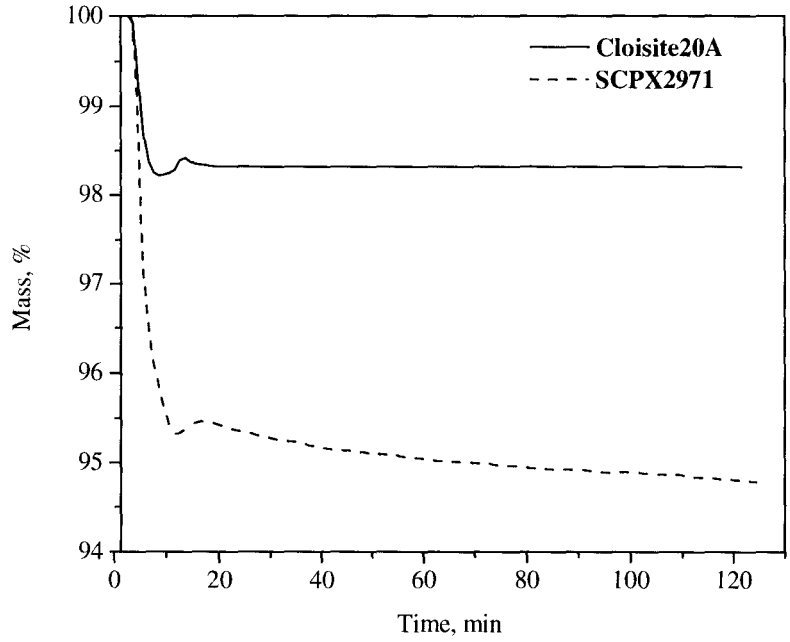

Figure 4.1.2 Isothermal TGA analysis under carbon dioxide environment

Isothermal TGA was conducted on a selection of the surfactants, namely C20A, the representative of aliphatic chain surfactants, and SCPX 2971, the aromatic surfactant.

The weight loss in Figure 4.1.2 was quite rapid (within the first 10 minutes) and in comparison to Table 4.1.1 the losses for both materials are more likely attributed to water rather than any organic degradation.

The comparatively high moisture content of SCPX 2971 has two feasible reasons: i) incomplete coverage of the silicate surface by the surfactant and ii) H_2O binding with the aromatic group. The incomplete coverage may result from the steric effect of benzyl ring which would be described later in this chapter based on XRD analysis. Slight solubility of benzene in water has been proved through weak hydrogen bond between water and the benzene π-electron cloud [Backs and Goldman 1981, Ravishanker et al. 1984]

4.2 Organic Content, Hydration and Acid-Base Character

Changes in organic content, water absorption and pH value of the five organoclays before and after $scCO_2$ treatment under the designed conditions were summarized in Table 4.2.1 – Table 4.2.5. Discussion of the data will be given in the respective Sections 4.2.1-4.2.2. For the organic content measurements, in comparison to the TGA data shown in Figure 4.1.1, we see that the organic content by ashing was in reasonable agreement with the TGA results. For example, Cloisite 20A was found to be 38.4 wt% by ashing and 34.7 wt% by TGA. The smaller sample size used for the TGA may present sampling errors while the oven used for ashing operates for a longer sustained time at 600°C. This temperature is close to the decomposition temperature for the hydroxyl groups from the broken bond plane of the clay [Xie et al 2001]. Actually, the TGA curve of NaMMT in Figure 4.1.1 shows that the hydroxyl group decomposition might start to occur when temperature went above 500°C. Unfortunately, a lower furnace temperature was found to leave a considerable amount of carbon along with the clay and therefore was not useful. In addition, the temperature control of muffle furnace used can

not be programmed accurately, which may also introduce an error among tested samples. However, the ashing method was proved to be repeatable with a standard deviation of less than 1.0 wt % for the five untreated organoclays, and the ash-determined organic contents were consistent with the published data by Paul [Shah and Paul 2006] for untreated Cloisite 20A, SCPX 1137, and SCPX 2934, indicating that the ashing method is reproducible.

The equilibrium moisture content was selected as the value measured after 10 days of hydration because the onset of a plateau was noted as early as 5 days of hydration, though for some clay samples this onset was delayed to as late as the eighth day. Fig 4.2.1 shows the weight gain arising from water adsorption over the first 9 days.

Table 4.2.1 Surfactant content, water absorption and pH — Cloisite 20A

Processing condition	**Surfactant content, %**	**Water absorption, %**	**pH (std)**
Un-processed	38.45	6.28	7.07 (0.01)
9.7 MPa / 200°C/ 4.8 MPa/s	38.44	5.32	6.87 (0.01)
9.7 MPa / 200°C/ 0.2 MPa/s	39.34	3.76	7.21 (0.08)
7.6 MPa /200°C/ 4.8 MPa/s	39.05	5.70	7.03 (0.04)
7.6 MPa / 200°C/ 0.2 MPa/s	38.74	4.23	6.95 (0.03)
9.7 MPa / 50°C/ 4.8 MPa/s	41.58	3.15	7.33 (0.03)
9.7 MPa / 50°C / 0.2 MPa/s	38.96	4.91	7.23 (0.00)
7.6 MPa / 50°C / 4.8 MPa/s	39.09	3.86	7.37 (0.03)
7.6 MPa / 50°C / 0.2 MPa/s	37.67	4.07	7.12 (0.02)

Table 4.2.2 Surfactant content, water absorption and pH value — SCPX 1137

Processing condition	Surfactant content, %	Water absorption, %	pH (std)
Un-processed	26.77	6.30	7.15 (0.02)
9.7 MPa / 200°C/ 4.8 MPa/s	25.90	6.20	6.94 (0.04)
9.7 MPa / 200°C/ 0.2 MPa/s	27.49	4.93	7.29 (0.10)
7.6 MPa /200°C/ 4.8 MPa/s	25.45	4.13	6.50 (0.03)
7.6 MPa / 200°C/ 0.2 MPa/s	27.63	5.41	6.80 (0.01)
9.7 MPa / 50°C/ 4.8 MPa/s	29.37	4.27	7.29 (0.00)
9.7 MPa / 50 °C/ 0.2 MPa/s	27.70	5.79	7.23 (0.00)
7.6 MPa / 50°C/ 4.8 MPa/s	27.58	5.05	7.21 (0.01)
7.6 MPa / 50°C/ 0.2 MPa/s	28.04	5.06	7.03 (0.01)

Table 4.2.3 Surfactant content, water absorption and pH value — SCPX 2934

Processing condition	Surfactant content, %	Water absorption, %	pH (std)
Un-processed	44.04	6.59	6.34 (0.05)
9.7 MPa / 200 °C / 4.8 MPa/s	44.28	6.41	6.46 (0.00)
9.7 MPa / 200°C / 0.2 MPa/s	44.09	3.02	6.79 (0.02)
7.6 MPa /200°C / 4.8 MPa/s	43.18	3.76	6.34 (0.12)
7.6 MPa / 200°C / 0.2 MPa/s	45.45	3.46	6.10 (0.00)
9.7 MPa / 50°C / 4.8 MPa/s	45.66	2.32	6.81 (0.12)
9.7 MPa / 50°C / 0.2 MPa/s	44.61	3.83	6.61 (0.03)
7.6 MPa / 50°C / 4.8 MPa/s	44.68	3.19	6.94 (0.03)
7.6 MPa / 50°C / 0.2 MPa/s	44.74	3.21	6.20 (0.01)

Table 4.2.4 Surfactant content, water absorption and pH value — SCPX 2971

Processing condition	Surfactant content, %	Water absorption, %	pH (std)
Un-processed	16.82	17.51	7.81 (0.13)
9.7 MPa / 200°C / 4.8 MPa/s	16.49	17.42	7.66 (0.04)
9.7 MPa / 200°C / 0.2 MPa/s	17.26	11.78	7.74 (0.02)
7.6 MPa /200°C / 4.8 MPa/s	14.72	11.17	8.66 (0.02)
7.6 MPa / 200°C / 0.2 MPa/s	16.08	12.35	7.84 (0.04)
9.7 MPa / 50°C / 4.8 MPa/s	18.05	10.40	7.82 (0.06)
9.7 MPa / 50°C / 0.2 MPa/s	16.31	10.46	7.88 (0.00)
7.6 MPa / 50°C / 4.8 MPa/s	18.60	10.32	7.91 (0.03)
7.6 MPa / 50°C / 0.2 MPa/s	18.03	10.21	7.54 (0.02)

Table 4.2.5 Surfactant content, water absorption and pH value — SCPX 2972

Processing condition	Surfactant content, %	Water absorption, %	pH (std)
Un-processed	30.56	11.01	7.56 (0.023)
9.7 MPa / 200°C / 4.8 MPa/s	30.19	9.75	7.34 (0.01)
9.7 MPa / 200°C / 0.2 MPa/s	33.69	5.06	7.62 (0.00)
7.6 MPa /200°C / 4.8 MPa/s	31.28	7.15	7.51 (0.15)
7.6 MPa / 200°C / 0.2 MPa/s	30.77	5.62	6.52 (0.02)
9.7 MPa / 50°C / 4.8 MPa/s	31.98	5.40	7.53 (0.01)
9.7 MPa / 50°C / 0.2 MPa/s	30.04	5.68	7.69 (0.06)
7.6 MPa / 50°C / 4.8 MPa/s	32.71	5.66	7.87 (0.01)
7.6 MPa / 50°C / 0.2 MPa/s	31.89	6.13	7.03 (0.01)

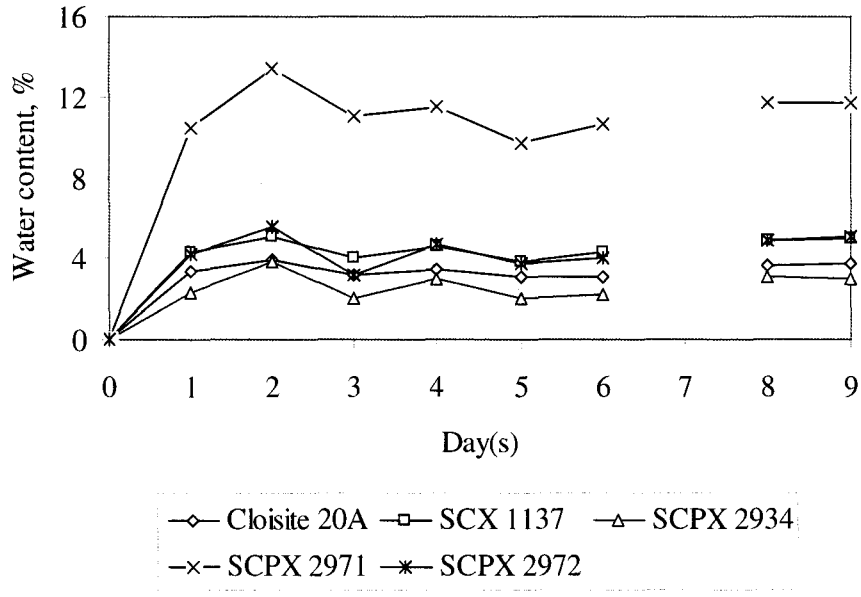

Figure 4.2.1 Moisture adsorption into selected $scCO_2$ treated organoclays over a nine day period within the humidification chamber

4.2.1 Five pristine (as-supplied) organoclays

All measurements for the pristine organoclays from Tables 4.2.1-4.2.5 plus sodium content and surface tension are included in Table 4.2.6 to summarize and allow easy comparison between properties. Sodium montmorillonite was also listed in the table for comparison. The summarization shows that the order of untreated organoclays in terms of organic content was SCPX 2934 > Cloisite 20A > SCPX 2972 > SCPX 1137 > SCPX 2971. The order of surface tension of the five organoclays was exactly in the reverse of the organic content order, and acidity of the five organoclays largely follows this trend except SCPX 2972. However, changes in moisture uptake for the five organoclays are quite different from these two former properties. Cloisite 20A and SCPX 1137 exhibited the same moisture content in spite of their significant difference in

intercalant organic content and their hydration values were not higher than that of SCPX 2934 which had the highest organic content. Though the organic content of SCPX 2972 was third highest in the series, its hydration content was much higher than everything but SCPX 2971. SCPX 2971 had the lowest organic content and its hydration content was the highest among the five organoclays. Water content and the pH value for NaMMT, which contains no organic modifier, was much higher than all other organoclays.

Table 4.2.6 Organic content, hydration and acidity of pristine organoclays and NaMMT

Organoclay species	**Organic cotent wt %**	**Hydration content wt %**	**Acidity (pH)**	**Surface tension mJ/m^2**	**Sodium content wt %**
SCPX 2934	44.0	6.6	6.3	33.4	0.23
Cloisite 20A	38.5	6.3	7.1	34.7	0.25
SCPX 2972	30.6	11.0	7.6	39.5	0.46
SCPX 1137	26.8	6.3	7.2	45.2	0.27
SCPX 2971	16.8	17.5	7.8	55.4	0.39
NaMMT	—	30.7	9.4	—	2.84

As mentioned in Chapter II, the main sites for water molecules to exist in clay are the metal cations present to counterbalance the negative charges of the clay's oxygen plane and the hydroxyl groups of the broken bond plane. With the replacing of the metal cations by the organic cations, the silicate surface is covered with an organic surfactant. Generally speaking, the more organic loading to the organoclay, the more organic coverage on the silicate surface, especially the surface of the clay particles, and therefore decreased hydration ability and basicity. NaMMT exhibited alkalinity with a pH value of 9.4 while the organoclays are basically neutral. However, the surfactant distribution on the silicate surface changes with the increase in organic loading, and even in the interlayer region, the arrangement mode of surfactant molecules changes with increasing surfactant content [Xi et al 2004, Fornes et al, 2002]. Excess amounts of surfactant over

the cation exchange capacity are adsorbed on the silicate surface and added to the galleries of the silicate layers. The similarity in the moisture uptake for SCPX 1137, Cloisite 20A and SCPX 2934 might be interpreted that the degree of metal cations exchanged and the coverage of the silicate surface are the similar and that Cloisite 20A and SCPX 2934, especially the latter, are excessively loaded with their surfactants. The similar sodium contents for three organoclays shown in Table 4.2.6 confirm the assumption. The relatively high hydration for SCPX 2972 is probably due to the incomplete coverage of the silicate surface by the surfactant because we see that its sodium content is higher than the three organoclays mentioned. The surfactant for SCPX 2972, dimethyl dicoco ammonium chloride mainly with 12-carbon chains, is different from the other three whose alkyl chains were considerably longer, 16 ~18 carbons.

The acidity or basicity of the organoclays reflects their Brønsted sites on the surface of a smectite clay located at the hydrated cations coordinated with the oxygen plane and the hydroxyl groups of the broken bond plane. As mentioned above, more sodium cations are exchanged with increased organic ammonium loading until excessive surfactants are loaded onto the silicate surface and into silicate galleries. The exchange substantially reduces the number of the Brønsted base sites on the clay surface. The pH trends among the tested clays were SCPX 2934 < Cloisite 20A ≤ SCPX 1137 < SCPX 2972 ≤ SCPX 2971 < NaMMT, basically follows the organic loading. However, considering a maximum standard deviation of ± 0.2, the pH values of Cloisite 20A and SCPX 1137 can be considered the same though their organic contents were significantly different yet their hydration contents were similar. Again, the relatively high sodium content and the incomplete surfactant coverage of SCPX 2972 may lead to it high pH value though it was not as significant as its hydration value. The atomic absorption analysis gave a relative standard deviation of 18%, therefore it was no surprisingly found that pH values of SCPX 2972 and SCPX 2971 were close even if there were minor differences in their sodium contents. The slightly higher pH values for SCPX 2972 and

SCPX 2971 than Cloisite 20A and SCPX 1137 indicates that pH value was not as sensitive as the hydration content.

4.2.2 Supercritical CO_2 treated organoclays

Tables 4.2.1-4.2.5 showed that for each organoclay species the organic content of the $scCO_2$ treated sample under all tested conditions were either similar or above the determined content for the untreated organoclay. The batch vessel and sample holder were examined after each test to ensure that no possible loss of surfactant occurred between runs. Considering the standard deviation of this method (see Chapter III), the fluctuation of the organic content compared to the pristine value were within the range of error. Therefore, it is reasonable to conclude that no significant change in organic surfactant was observed due to the $scCO_2$ treatment or that no surfactant extraction happened during the $scCO_2$ treatment and gas release. Another intention of the organic content measurement was to establish the feasibility of evaluating the adsorption-desorption characteristics of CO_2 onto the clay as a result of the selected surfactant. The available data proved that this measurement failed for this purpose either because of no CO_2 retained onto the clays after gas releasing or because of the amount of CO_2 adsorbed too small to be detected. The following FT-IR analysis will show that no CO_2 was retained in the treated clays. No change in organic content does not rule out an altered surfactant morphology. Actually, we will see from the water content in these tables and following XRD, TEM and TGA results that the surfactant morphology changes significantly for some organoclays and minimal for others.

As indicated in the Tables 4.2.1 – 4.2.5, treatment of these organoclays with $scCO_2$ had no significant influence on the Brønsted character of the clays. The negligible change in pH would be reasonably expected if the Brønsted sites were primarily the sodium, as CO_2 would have little affinity for the cation or any resulting salt from cation

exchange, and therefore, would not be likely removed by the treatment. Atomic absorption measurements confirmed that the sodium content was unaffected by the supercritical solvent, with both C20A and SCPX 1137 found to contain 0.26 wt% Na^+ after $scCO_2$ treatment at 9.7 MPa and 200°C followed by a gas release rate of 0.2 MPa/s. Furthermore, the hydroxyl groups of the broken bond plane would have remained unchanged regardless of any change in the morphology of the surfactant. Therefore, the pH measurement provided no evidence to support the possibility of acidification of the clay by $scCO_2$ (i.e. reaction of the $scCO_2$ with residual interstitial water).

However, the hydration of these $scCO_2$ treated organoclays was found to reduce significantly. Since no reductions in sodium content, in Brønsted sites and in organic intercalants were found, the possible reason left for reduction in moisture uptake resulted from the $scCO_2$ treatment would be the increase in the coverage of oxygen plane with the organic surfactant. It may be reasonable to assume that: i) $scCO_2$ increased the mobility of surfactant molecules, ii) the movable melt surfactant molecules physically adsorbed on the outside of clay particles then enters the galleries of clay platelets, iii) the entered surfactant together with those intercalated species bound by van der Waals forces exchanged further with the metal cation on the platelet surface leading to increased ion-dipole (end-tethered) surfactant, and iv) the exchanged sodium cation still stays in clay galleries. According to Yariv and Michaelian [2002], the hydration of the interlayer would account for associations of water by Lewis acid/base interactions with the oxygen plane of the clay's siloxane groups, and hydrophilic hydration of the exchangeable cation. The further cation exchange reduces the Lewis acid/base interactions with the oxygen plane, and therefore, reduces the moisture uptake.

In terms of the influence of the processing conditions on the hydration, the experiment data were re-written in Appendix C according to the standard DOE arrangement. If x_1, x_2 and x_3 are assigned for temperature, pressure and pressure release

rate, respectively, and y for the moisture content, linear models for the five organoclays are fitted as follows.

C20A:

$$y = 4.4 + 0.35x_1 - 0.10x_2 + 0.15x_3 - 0.13x_1x_2 + 0.63x_1x_3 - 0.17x_2x_3 + 0.20x_1x_2x_3 \quad (4.1)$$

SCPX 2934:

$$y = 3.7 + 0.52x_1 + 0.22x_2 + 0.27x_3 + 0.30x_1x_2 + 0.65x_1x_3 + 0.20x_2x_3 + 0.57x_1x_2x_3 \quad (4.2)$$

SCPX 1137

$$y = 5.1 + 0.03x_1 + 0.18x_2 - 0.18x_3 + 0.21x_1x_2 + 0.18x_1x_3 + 0.13x_2x_3 + 0.51x_1x_2x_3 \quad (4.3)$$

SCPX 2972

$$y = 6.3 + 0.57x_1 + 0.17x_2 + 0.67x_3 + 0.35x_1x_2 + 0.85x_1x_3 + 0.40x_2x_3 + 0.37x_1x_2x_3 \quad (4.4)$$

SCPX 2971

$$y = 11.8 + 1.4x_1 + 0.76x_2 + 0.56x_3 + 0.66x_1x_2 + 0.56x_1x_3 + 0.81x_2x_3 + 0.86x_1x_2x_3 \quad (4.5)$$

From the fitted linear models, we see that for C20A, SCPX 2934, SCPX 2972 and SCPX 2971 temperature had a relatively significant effect on the moisture uptake, while pressure and pressure release rate affected this parameter very little. The C20A model (4.1) and SCPX 2934 model (4.2) reveal that pressure release rate itself did not show significant influence on the hydration for C20A and SCPX 2934 but its coupled interaction with temperature exhibited the most effect on the moisture uptake of the two organoclays. The SCPX 1137 model (4.3) shows that temperature had a limited effect on the hydration whereas pressure and the coupled interaction of temperature on pressure had the strongest effects on this surfactant. Pressure release rate itself seems only to have

an influence on SCPX 2972 and again its coupled interaction with temperature showed the strongest effect shown in model (4.4).

4.3 Basal Spacing

Basal spacing of clay crystals has been taken as one of the most important variables evaluating their structure and intercalated ability by polymer intercalants. In general, higher interlayer distance of an organoclay is thought to facilitate the intercalation. Due to their well ordered crystal structure, the interlayer distance of the organoclays is readily characterized by using XRD methods. Table 3.1.1 gives the d_{001} spacing values of the five organoclays and NaMMT determined by the XRD method showing their differences in this property. Swelling with organic surfactants at concentrations close to 1.0 CEC for the clay mineral increased the basal spacing of montmorillonite, where longer chains and greater numbers of chains bound to the ammonium functionality induced larger basal expansion by their incorporation as a result of steric effects. The interlayer spacing values for the as-supplied organoclays corresponded well with reported X-ray data in the literature [Xi et al. 2007, Xie et al. 2001, Osman et al. 2003, Lee and Kim 2002] and indicated that different arrangements were being assumed by the different alkylammonium surfactants within the smectite clay. The terminology being adopted here for surfactant conformation corresponds to the work of Lagaly [1976, 1994] and summarization by Bonczek et al. [2002]. In this section, basal spacing was used to examine the interaction between a surfactant and $scCO_2$ by observing changes in this property.

4.3.1 Effect of $scCO_2$

NaMMT

Un-modified MMT was examined to demonstrate if $scCO_2$ interacts with the unmodified silicate surface and hence to compare the organoclays with un-modified MMT, which would simplify our evaluation on the interaction of $scCO_2$ with surfactants. Figure 4.3.1 shows that for the pristine MMT there were two diffraction peaks at 2θ = 7.24° and 8.78° at d_{001} corresponding d-spacing of 12.2Å and 10.1Å, respectively. The larger gap spacing corresponded to hydrated MMT with a monolayer of water in the interlayer region [Bongiovanni et al. 2006], while the d-spacing value, 10.1Å, is very close to the thickness of the MMT silicate sheet, 0.95 ~ 1.0 nm, (see section 2.2.1) indicating that water distribution was not uniform in the MMT galleries. Considering that this d-spacing value of the second peak is a little higher than that of the anhydrous MMT, it is also possible that there might be small amount of mineral impurity, for instance, mica [Simon 2006]. The two diffraction peaks are broad and of low intensity, reflecting the poor ordering of MMT (often referred to as a mixed layered structure). After 3-hour $scCO_2$ treatment at 9.6 MPa and 200°C followed a pressure release rate of 0.2 MPa/s, the

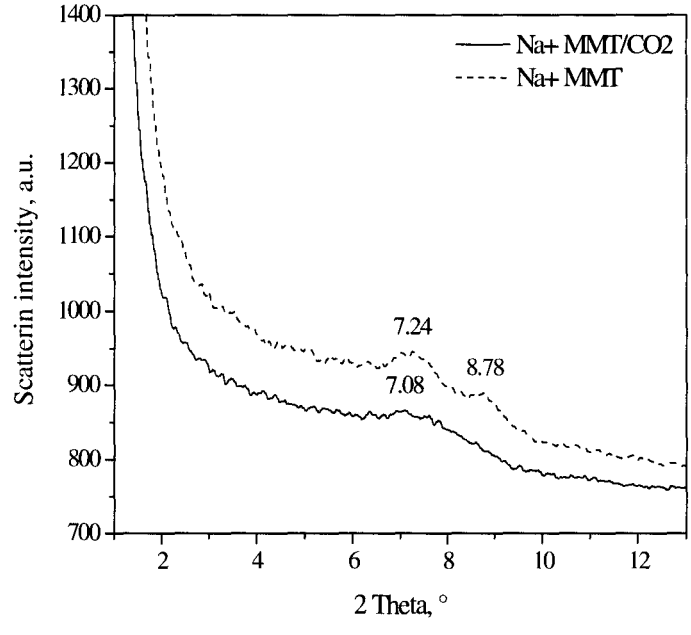

Figure 4.3.1 XRD Patterns of MMT before and after $scCO_2$ treatment at 200°C and 9.6 MPa following by pressure release rate of 0.2 MPa/s

two diffraction peaks for the untreated MMT combined together forming one broader peak with a highest scattering intensity value at $2\theta = 7.08°$. The disappearance of the second peak for the pristine MMT may suggest that it was the anhydrous MMT other than impurity that existed in the clay. The heterogeneous distribution of water molecules in pristine MMT galleries may be attributed to the heterogeneity of charge density on the clay sheets [Lagaly et al. 1976]. The galleries with fewer negative charges on silicate sheets attract fewer alkali cations and consequently contain fewer water molecules. Annealing of NaMMT at high temperature, high pressure and CO_2 environment probably improved the uniform charge distribution and, therefore, resulted in better water distribution. In addition, water has some solubility in the $scCO_2$ and therefore became better spread out throughout the clay mineral after the CO_2 treatment.

SCPX 1137

For the monoalkyl surfactant, SCPX 1137, the XRD patterns are shown in Figure 4.3.2. If the silicate sheet is considered to be 9.7Å in thickness [He et al. 2006, Yariv and Michaelian 2002, Xi et al. 2007], the XRD detected gallery spacing for the pristine SCPX 1137 would be 8.6 Å (i.e. 18.3 Å – 9.7 Å). The approximate molecular size of the surfactant was 4.3 Å in diameter and 23.8 Å in length when fully extended according to the calculations by He et al. [2006]. It is reasonable to assume that the arrangement of the surfactant was bilayer, with the alkyl chain laying flat against the two opposing silicate surfaces. The exposure of the organoclay to $scCO_2$ in the batch vessel under 9.7 MPa and 200°C followed by a pressure release rate of 0.2 MPa/s changed the conformation of the surfactant. The crystal structure of the clay became more heterogeneous as seen in Figure 4.4.2 with its diffraction peak becoming much wider than the untreated species. Position of the main peak shifted to a higher 2 theta angle ($2\theta = 5.1°$) indicating that collapse occurred during the treatment. On the other hand, a few weak peaks at lower 2 theta angles may suggest that there were parts of the clay that expanded due to the $scCO_2$ processing.

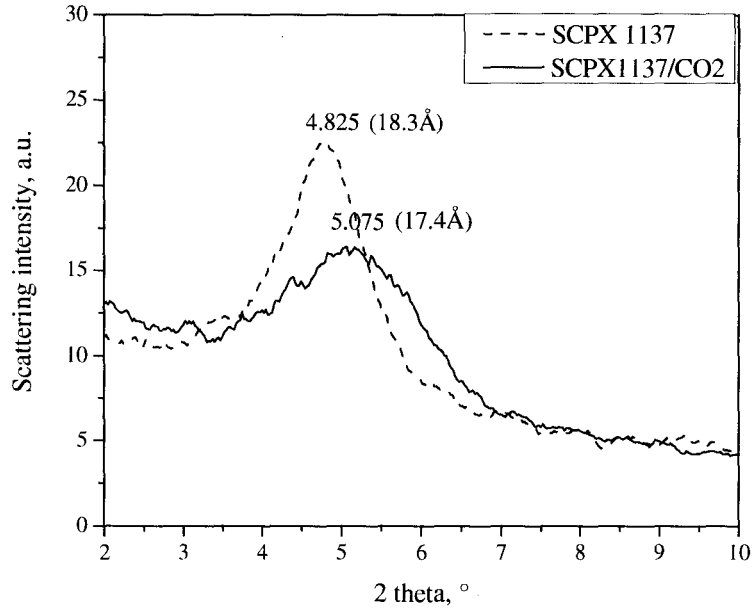

Figure 4.3.2 XRD Patterns of SCPX 1137 before and after $scCO_2$ treatment at 200°C and 9.6 MPa following by pressure release rate of 0.2 MPa/s

Cloisite 20A

The surfactant of Cloisite 20A is dialkyl and the basal spacing of it, 26.8 Å, was larger than that of the clay with monoalkyl surfactant above. The XRD patterns of C20A are shown in Figure 4.3.3. The pristine C20A exhibited an intense diffraction peak of the d_{001} crystal plane at 2θ value of 3.4° showing a well organized crystal structure. The gallery spacing of 16.1 Å (i.e. 25.8 Å – 9.7 Å) suggested that the intercalated surfactant assumed a paraffin-type monomolecular arrangement with the end-tethered molecules partially tilted away from the silicate surface. After the C20A was treated with $scCO_2$ at 200°C and 9.7 MPa then released at 0.2 MPa/s, the diffraction peak shifted to a lower 2θ angle of 3.2° with significantly decreased intensity of the peak. The left shift of the diffraction peak indicates that basal spacing of C20A increased slightly (Δ 2.0 Å) as result of $scCO_2$ treatment. The expansion of the clay galleries probably resulted from the increase in the tilt angle of the intercalated molecules. The lowered intensity of the

diffraction peak may suggest that crystal structure of C20A became relatively more heterogeneous compared to the untreated C20A. The increase in basal spacing suggests that removal and rearrangement of surfactant molecules occurred during the CO_2 treatment.

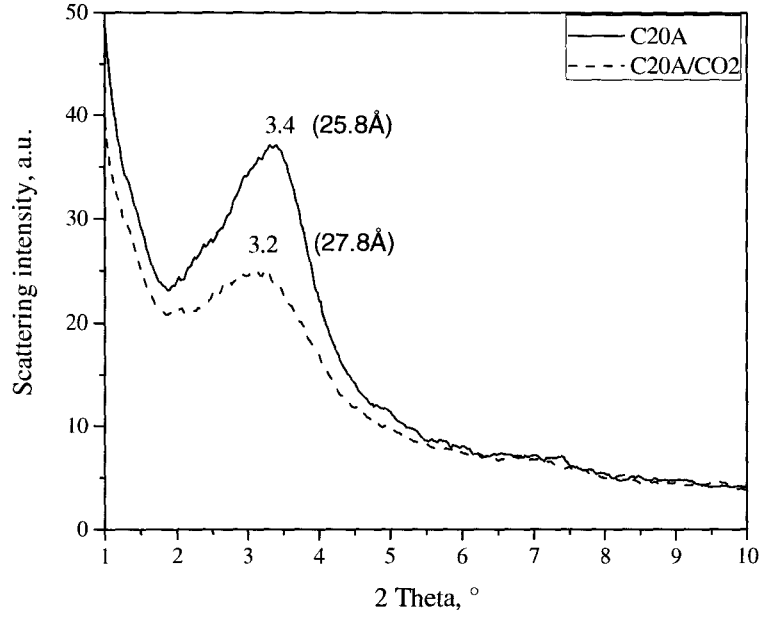

Figure 4.3.3 XRD Patterns of Cloisite 20A before and after $scCO_2$ treatment at 200°C and 9.6 MPa following by pressure release rate of 0.2 MPa/s

SCPX 2934

The trialkyl-surfactant organoclay exhibited the largest basal spacing value among the three organoclays intercalated with $C_{16 \sim 18}$ chain length surfactants. Its interlayer spacing, 23.7 Å (i.e. 33.4 Å – 9.7 Å), suggested a paraffin monolayer structure with the end-tethered molecules, just like C20A, but with greater tilted angle. Considering the fully extended length of C_{18} chains, 23.8 Å, [He et al. 2006], the surfactant molecules, actually, could be assumed to stand up completely with a tilted angle of 90°. As shown in Figure 4.3.4, the diffraction peak (001) moved to a higher 2 theta angle after $scCO_2$

treatment under 200°C, 9.7 MPa and 4.8 MPa/s, indicating a decrease in basal spacing (Δ = 2.1 Å). The sharpness and similar pattern of both peaks for before and after $scCO_2$ treatment exhibited that the crystal structure of organoclay was well ordered and that $scCO_2$ treatment did not significantly alter its crystal structure.

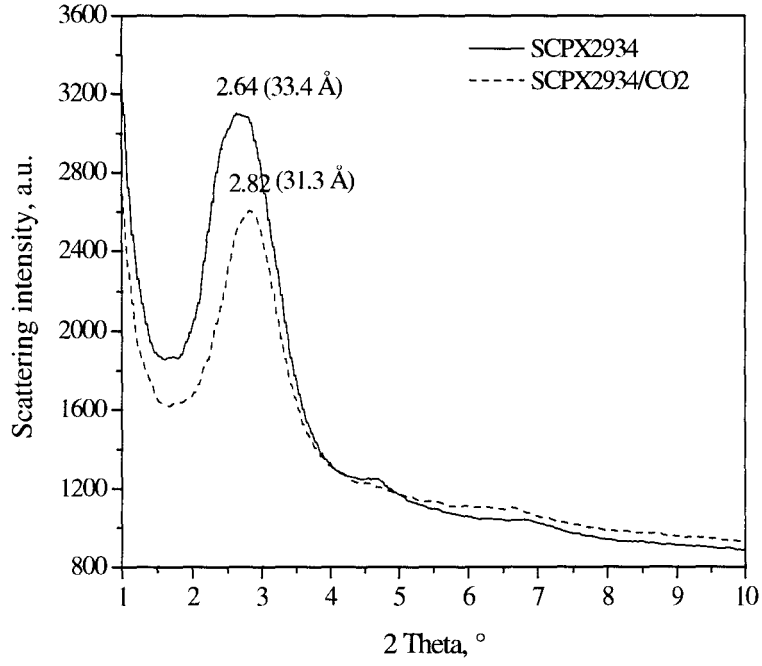

Figure 4.3.4 XRD Patterns of SCPX 2934 before and after $scCO_2$ treatment at 200°C and 9.6 MPa following by pressure release rate of 4.8 MPa/s

SCPX 2972

Figure 4.3.5 shows the XRD patterns of SCPX 2972 before and after $scCO_2$ treatment. Like SCPX 2934, the treatment was carried out at 200°C and 9.7 MPa/s followed by a pressure release rate of 4.8 MPa/s. The surfactant of this clay, dicocodimetyl ammonium chloride, is dialkyl like C20A but with a shorter chain length of 12 carbons. If length of a fully extended C_{18} alkyl chain is 23.8 Å [He et al. [2006], estimated length of a fully extended C_{12} chain should be about 15.8 Å. Considering the gallery spacing of 10.9 Å (i.e. 20.6 Å – 9.7 Å) for SCPX 2972, the surfactant arrangement

may be assumed as paraffin type monolayer with a tilt angle less than 90°, just like C20A. Clearly, the shorter chain surfactant induced a smaller gallery spacing for a similar number of sites occupied on the clay surface if the assumption was true. At 1.0 CEC, the basal spacing of the as-received SCPX 2972 (20.6 Å) was 5.2 Å smaller than that of C20A. However, surfactant arrangement for SCPX 2972 may be assumed in another way: considering 4.3 Å in diameter size for a single chain and repulsing force between two alkyl chains, diameter size of one dicocodimethyl molecule should be more than simple addition of diameters of two alkyl chains i.e. 8.6 Å and may be close to 10.9 Å, and thus an assumption of a lateral monolayer structure for this clay may also be reasonable. Also like SCPX 2934 and 1137, the CO_2 treatment caused collapse of the crystal layers but the collapse was not significant, indicating that surfactant molecules were mobile under $scCO_2$.

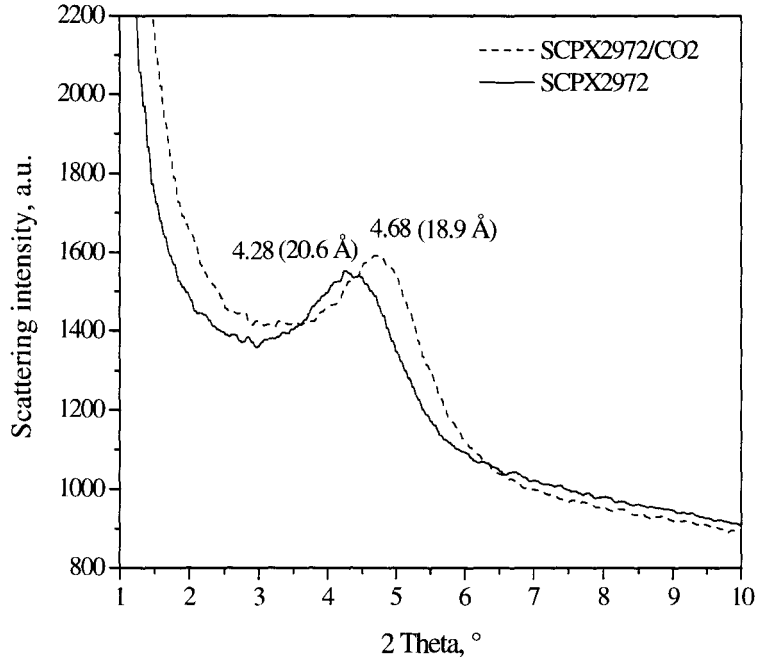

Figure 4.3.5 XRD Patterns of SCPX 2972 before and after $scCO_2$ treatment at 200°C and 9.6 MPa following by pressure release rate of 4.8 MPa/s

SCPX 2971

This organoclay was found least affected by the tests in this thesis compared to the other ones examined. The X-ray diffraction peak (001) for SCPX 2971 in Figure 4.3.6 is the narrowest and sharpest among the five organoclays, exhibiting the best crystallized structure. The basal spacing detected, 15.1 Å corresponding to the peak position (2θ = 5.8°) is consistent with the literature [Koh and Dixon 2001, Polubesova et al. 1997]. The gallery spacing was only about 5.4 Å (i.e. 15.1 Å – 9.7 Å), and therefore the arrangement of the surfactant in between the silicate sheets should be a monolayer structure. Considering the rigid molecular structure attributed to the phenyl ring in the benzyltrimethyl surfactant, it was expected that the monolayer structure would not change significantly after the $scCO_2$ treatment in spite of the plasticization of the organic surfactant by $scCO_2$. As shown in Figure 4.3.6, no change was found for the diffraction peak of (001) plane. The lack of change by the $scCO_2$ treatment may also be attributed to

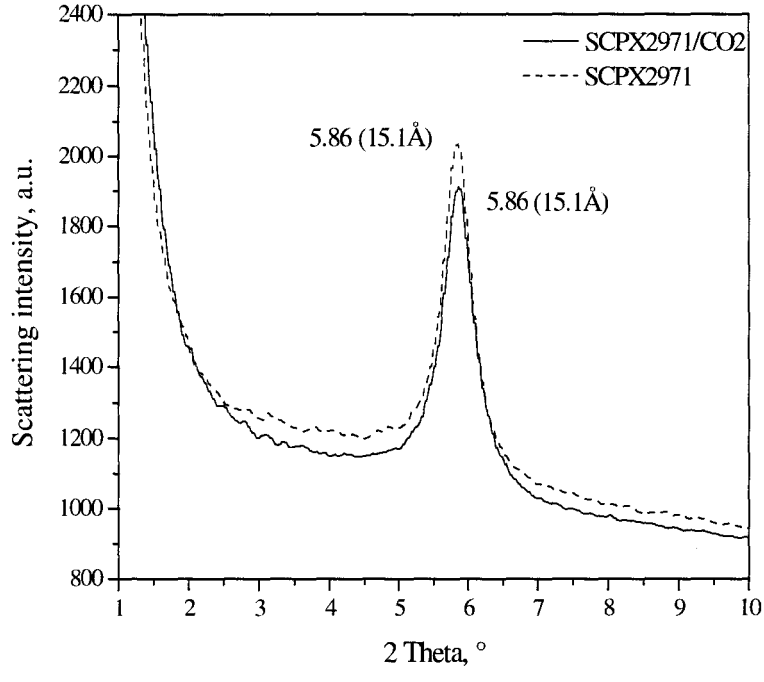

Figure 4.3.6 XRD Patterns of SCPX 2971 before and after $scCO_2$ treatment at 200°C and 9.6 MPa following by pressure release rate of 4.8 MPa/s

the strength of the interactions between the aromatic ring and adjacent silicate sheets. Benzyltrimethyl ammonium exhibited a larger dipole moment due to the aromatic ring than the long alkyl chain surfactant [Backx and Goldman 1981] and, therefore, its interactions with silicate sheet would be stronger than those with long alkyl surfactants. The strong interaction may restrict the intercalant molecules because studies by Kol and Dixon [2001] showed that regardless of the benzyltrimethyl surfactant concentration, the basal spacing remained relatively constant, i.e. the modified clay was not willing to adsorb a second interlayer.

4.3.2 Effect of processing conditions

Effects of treatment conditions on the basal spacing of the organoclays were focused on the alkyl surfactants with C_{16} – C_{18} chains, i.e. SCPX 1137, Cloisite 20A and SCPX 2934. Basal spacing values of all $scCO_2$ treated organoclays were summarized in Table 4.3.1. For the monoalkyl surfactant, SCPX 1137, Figure 4.3.2 shows that CO_2 treatment at 200°C and 9.7MPa caused the silicate sheet to collapse to a small degree. However, at the same pressure release rate, 0.2 MPa/s, treatments at lower temperature and/or lower pressure, as shown in Table 4.3.1, did not show any influence on the gallery distance. The reason responsible for the minor change in basal spacing when applying high temperature and high pressure and no change when processed at lower temperature and/or lower pressure may be the melting point of the confined surfactant which was high up to 116°C, see the first-run DSC result in the following section. Even under high pressure, low processing temperature of 50°C may not induce the surfactant molecules to move. Even if the temperature was elevated to 200°C, the processing pressure of 7.6 MPa might not high enough to drive the molecules to move. Surfactant mobility increased with temperature and the solvation strength of $scCO_2$ (i.e. density of the fluid). At 200°C, density of $scCO_2$ under pressure of 7.6 MPa is 0.090 g/mL, much lower than that under 9.7 MPa, 0.117 g/mL. When the temperature and pressure were both at their highest

levels, surfactant molecule were driven to move; however, this mobility was mainly towards the transition to a lateral monolayer with only a small fraction of chain transitioned towards the paraffin type monolayer, as indicated in Figure 4.3.2. It probably was the fact that both transitions occurred that increased heterogeneity in the interlayer spacing. Based on the discussion, it may be concluded that CO_2 influenced surfactant morphology of SCPX 1137 only when both of temperature and pressure were high enough. Pressure release rate was not examined here since we will see that this parameter did not significantly affect basal spacing of SCPX 2934. Results of the TGA and FT-IR, to be discussed in later sections, will assist in identifying the changes in morphology for this surfactant.

Table 4.3.1 Basal spacing of $scCO_2$ treated organoclays

Processing conditions	**SCPX 1137**	**Cloisite 20A**	**SCPX 2934**
Original	18.3	25.8	33.4
50°C, 7.6 MPa, 0.2 MP/s	18.5	26.2	33.3
200°C, 7.6 MPa, 0.2 MP/s	18.1	26.8	—
50°C, 9.7 MPa, 0.2 MP/s	18.2	26.2	31.5
200°C, 9.7 MPa, 0.2 MP/s	17.5	27.8	31.2
50°C, 7.6 MPa, 4.8 MP/s	—	28.2	—
200°C, 7.6 MPa, 4.8 MP/s	—	27.6	31.5
50°C, 9.7 MPa, 4.8 MP/s	—	26.6	31.2
200°C, 9.7 MPa, 4.8 MP/s	—	27.7	31.2

For SCPX 2934, we see in Table 4.3.1 that when the three parameters were all at their lowest level, i.e. 50°C, 7.6 MPa and 0.2 MPa/s, d-spacing of this clay retained its original value indicating that CO_2 at this condition was not able to affect the surfactant

morphology. However, basal spacing values at other processing conditions all resulted in a reduced gallery spacing of about 2.1 Å. This variation indicated: i) rearrangement of the trialkyl surfactant occurred only through elevating either temperature or pressure or both of them, ii) the reduction in interlayer distance by the rearrangement was limited to a fixed value (limited packing reorganization was possible due to steric hindrance), iii) temperature and pressure appeared to have a negligible influence on reduction in basal spacing, and iv) pressure release rate had no significant effect on the basal spacing of SCPX 2934. The reduction in basal spacing probably resulted from the decrease in the tilted angle of surfactant molecules confined in the interlayer region from 90° to some lower degree. The following DSC, TGA and FT-IR analyses will assist in determining how the morphology changed.

Cloisite 20A was the only clay for which gallery spacing exhibited an increase after $scCO_2$ processing. Therefore, more attention was paid to this clay throughout this chapter. Keeping x_1, x_2 and x_3 assigned to the factors of temperature, pressure and pressure release rate, respectively, and setting y for the basal spacing, a linear model was determined to aid analysis:

$$y = 27.1 + 0.34x_1 - 0.16x_2 + 0.39x_3 + 0.21x_1x_2 - 0.21x_1x_3 - 0.49x_2x_3 + 0.09x_1x_2x_3 \quad (4.6)$$

From the Equation (4.6), we can see that among the main factors temperature and pressure release rate had a stronger affect on basal spacing whereas pressure had a relatively minor effect except when coupled with pressure release rate. Therefore, higher temperatures and higher pressure release rates are drivers towards increasing the basal spacing of C20A.

From the results of basal spacing of C20A above and the results of moisture uptake in Section 4.2, we knew that pressure release rate seemed to be in the second place after temperature influencing the surfactant morphology, especially for the case of C20A.

Horsch et al. [2006] claimed that an organoclay having good CO_2-philicity (Cloisite 93A) achieved substantial reduction in the number of tactoids present after $scCO_2$ treatment at 8.6 MPa and 90°C for 20 hours followed by rapid depressurization. Thus, we made two more trials on the pressure release rate at conditions of 9.7 MPa and 200°C except for the two tests in the DOE. All the other processing conditions (temperature, pressure and duration) for the new experiments were same as those two in the DOE, i.e. 200°C, 9.7 MPa and 3 hours. For one trial the pressure release rate was manually controlled as low as possible. The whole depressurization lasted 30 minutes, the pressure release rate was about 0.005 MPa/s, and therefore the pressure release rate for this trial was named 0. Since the higher level of pressure release rate in the DOE was the highest value that the needle valve used could achieve, it was impossible for another trial at higher pressure release rate if the needle valve was still used. Instead of the needle valve, a new ball valve was installed which allowed the depressurization to be instant (less than 1 second). Therefore the pressure release rate was more than 9.7 MPa/s, which was named here for comparisons. XRD patterns of the $scCO_2$ processed C20A at 0, 0.2 and 9.7 MPa/s were shown in Figure 4.3.7. XRD pattern for C20A at 4.8 MPa/s obtained by another instrument using different sample holder was not included in the figure due to more than one magnitude difference in their scattering intensity, but the d_{001} peak position was at 2θ angle of 3.2° corresponding to basal spacing value of 27.7 Å listed in Table 4.3.1.

It can be seen from Figure 4.3.7 and Table 4.3.1 that there was almost no difference in diffraction peak position among pressure release rates of 0, 0.2 and 4.8 MPa. However, we do see that there was a trend that intensity of the diffraction peaks decreased with increase of pressure release rate (XRD scans of the samples of 0, 0.2 and 9.7 MPa/s were performed for the same mass of sample loaded in the same sample holder) indicating that number of C20A tactoids reduced or part of the tactoids dispersed due to the faster depressurization, which was consistent with results by Horsch et al. [2006]. For the case of 9.7 MPa/s, except for the reduction in scattering intensity, the d_{001} diffraction pattern became broader and peaked at lower 2θ angle (2.9°), indicating that except for the

dispersion of partial tactoids there were some tactoids which swelled due to the explosive depressurization. It seems to conclude that elevated pressure release rate improved the expansion or dispersion of C20A particles.

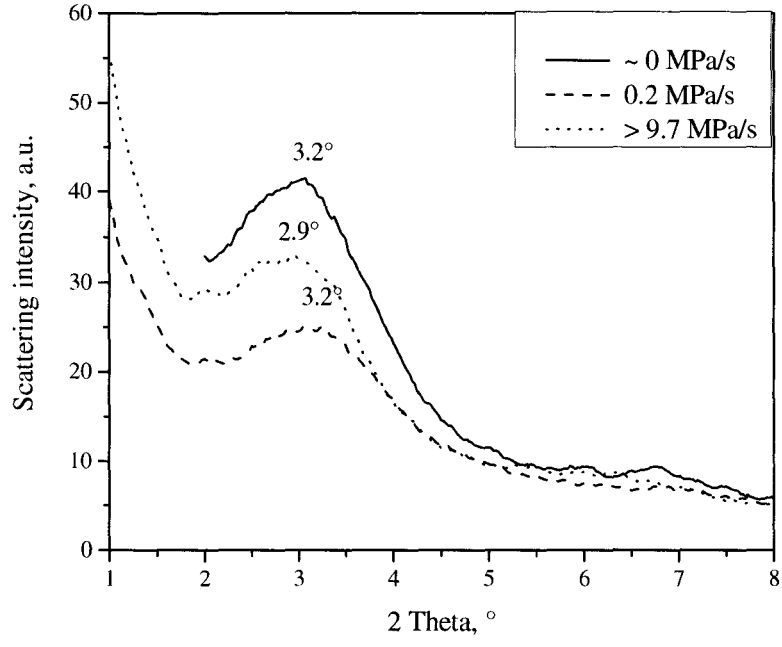

Figure 4.3.7 XRD patterns of C20A processed with CO_2 at 200°C, 9.7 MPa and different depressurization at a gas release rate of 0 MPa/s, 0.2 MPa/s and 9.7 MPa/s

4.3.3 In-situ observation

The XRD observations on $scCO_2$ processed clays mentioned above are all based on analysis after depressurization. In order to improve our understanding of how the microstructure of an organoclay at the presence of the supercritical fluid (i.e. without the pressure release rate factor coupled to the measurement), the clays were also examined *in-situ* using XRD. Due to the experiment limitation of the built apparatus and X-ray detector system, the high pressure device could not be heated. The measurement was

performed at room temperature and an elevated pressure (9.7 MPa) and, therefore, CO_2 during this measurement was not in supercritical state but rather in its subcritical state. In spite of this restriction in solvation power, we could still learn a substantial amount on the microstructure of an organoclay while being conditioned. Figure 4.3.8 shows the results of NaMMT and the five organoclays using Mo as the X-ray source (Mo wavelength, λ = 0.7107 Å). Results for pristine (i.e. no CO_2 present) SCPX 1137, SCPX 2972 and SCPX 2971 obtained by Mo X-ray radiation were consistent with those by Cu X-ray radiation but d-spacing values of pristine NaMMT, C20A and SCPX 2934 by using Mo X-ray were, smaller than by using Cu X-ray. The reason for the difference between the two methods was not explored since our interest was in the variation in d-spacing before and after CO_2 treatment.

For the NaMMT, Figure 4.3.8(a) shows that the diffraction peak shifted to a lower 2 theta angle and became much more intense indicating it exhibited expanded interlayers which were more homogeneous in spacing under high pressure than the pristine species. This change was not found for the treated species after depressurization, as shown in Figure 4.3.1. The most interesting variation was found for C20A shown in Figure 4.3.8(c), where the gallery spacing increased 3.9 Å while the largest increase in gallery spacing for those depressurized species was only 2.4 Å according to Table 4.3.1. This variation trend is thought to be very meaningful for our following melt compounding in creating a TPO nanocomposite. Interlayer spacing and microstructure of SCPX 1137 and SCPX 2971 (Figure 4.3.8b and f) showed almost no change when the clay was under the subcritical state of CO_2, which were consistent with those depressurized samples, indicating that the lateral mono- or bi- layer arrangements of these surfactants were not readily altered by $scCO_2$. Interlayer spacing of SCPX 2934 remained same when under subcritical CO_2, but the intensity of the diffraction peak at (001) plane became much stronger, as shown in Figure 4.3.8(d), suggesting that the amount of crystal increased when the clay was under subcritical CO_2, which was not found for the $scCO_2$ treated species after depressurization.

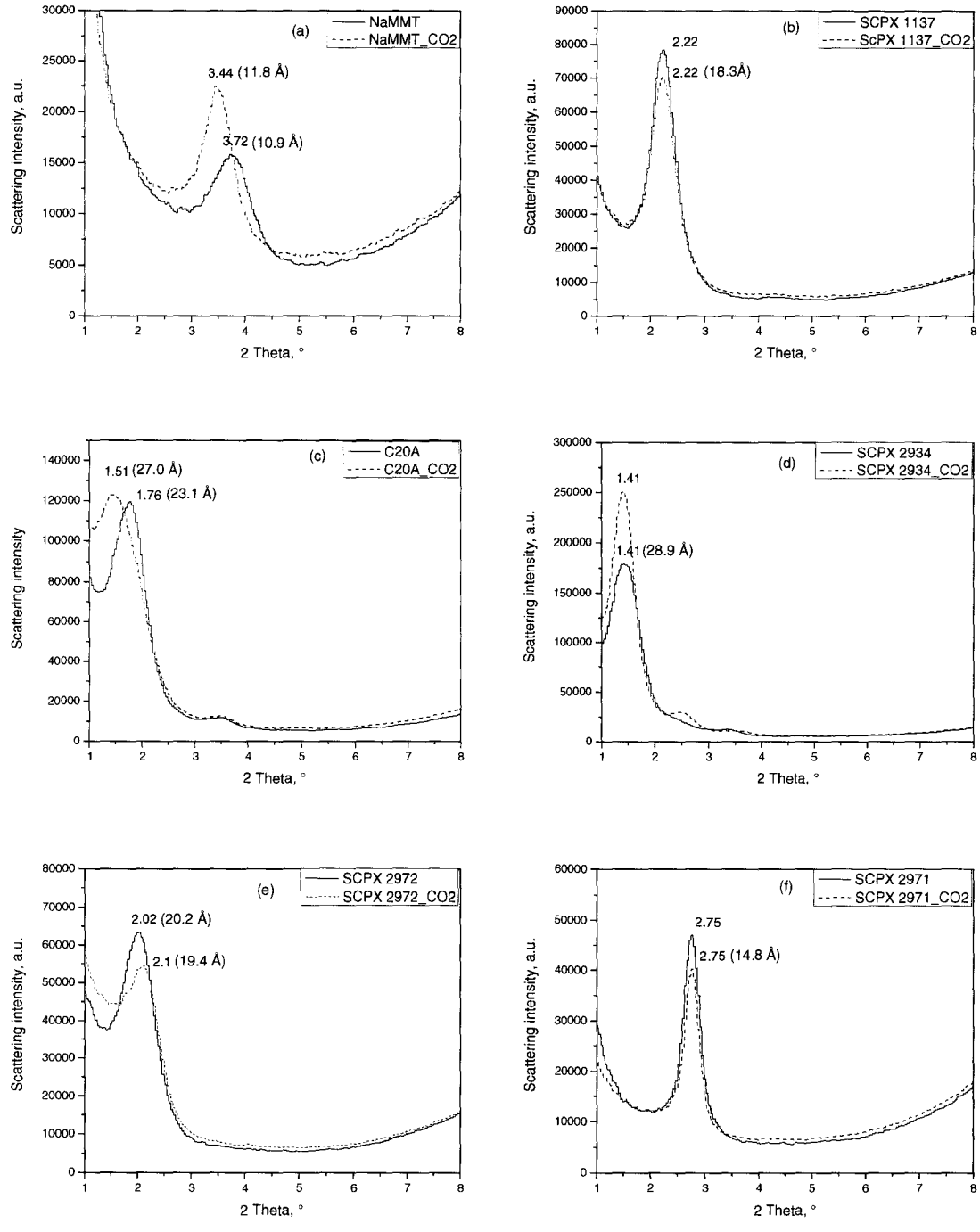

Figure 4.3.7 XRD patterns of in-situ observations of clays at the environment of CO_2 in sub-critical state

SCPX 2972 exhibited a decrease both in basal spacing and in diffraction peak intensity when under the subcritical state of CO_2, just like the $scCO_2$ treated and depressurized sample, showing that the layer structure collapsed readily and that the pillar intercalant were vulnerable under CO_2.

The data above show that the basal spacing was not substantial different in-situ from the samples retrieved after the gas was removed, and that the interpretation made were not strongly affected by the depressurization procedure. For a deeper understanding of how the microstructure of an organoclay is influenced by the supercritical fluid, temperature should also be elevated. Other researchers in this project have performed those studies where they explored how the organclays with mono-, bi- and tri- alkyl surfactants with similar chain length were affected by CO_2 at different temperature from 50°C to 200°C and different pressure from atmospheric to supercritical [Thompson et al. 2008]. Their work gives detailed *in-situ* X-ray powder diffraction studies on organoclays in a CO_2 environment but again the basal spacing was not much different from the depressurized samples. The detailed study revealed thermodynamic pressure effects on the melting point of the surfactants, i.e. how the mobility of the chains was strongly coupled to both pressure and temperature.

4.4 Thermal Properties

4.4.1 Melting range of surfactants

DSC curves in Figure 4.4.1 show that there were mainly three phase transitions for each organoclay, indicating that each surfactant existed with three typical kinds of crystalline arrangement. For SCPX 1137 (Figure 4.4.1(a)), the first phase transition occurred at 90°C and the last one at 125.5°C, showing that a disordered liquid behavior could not be achieved below 90°C and that the surfactant confined in clay galleries will melt completely when heated above 125.5°C. At room temperature or 50°C (the low level

of temperature used in the experiments), the surfactant molecules would be confined in their crystalline lattices, which may be the reason that the basal spacing did not show any change when processed with $scCO_2$ at 50°C and with subcritical CO_2 at room temperature (i.e. *in-situ* XRD data).

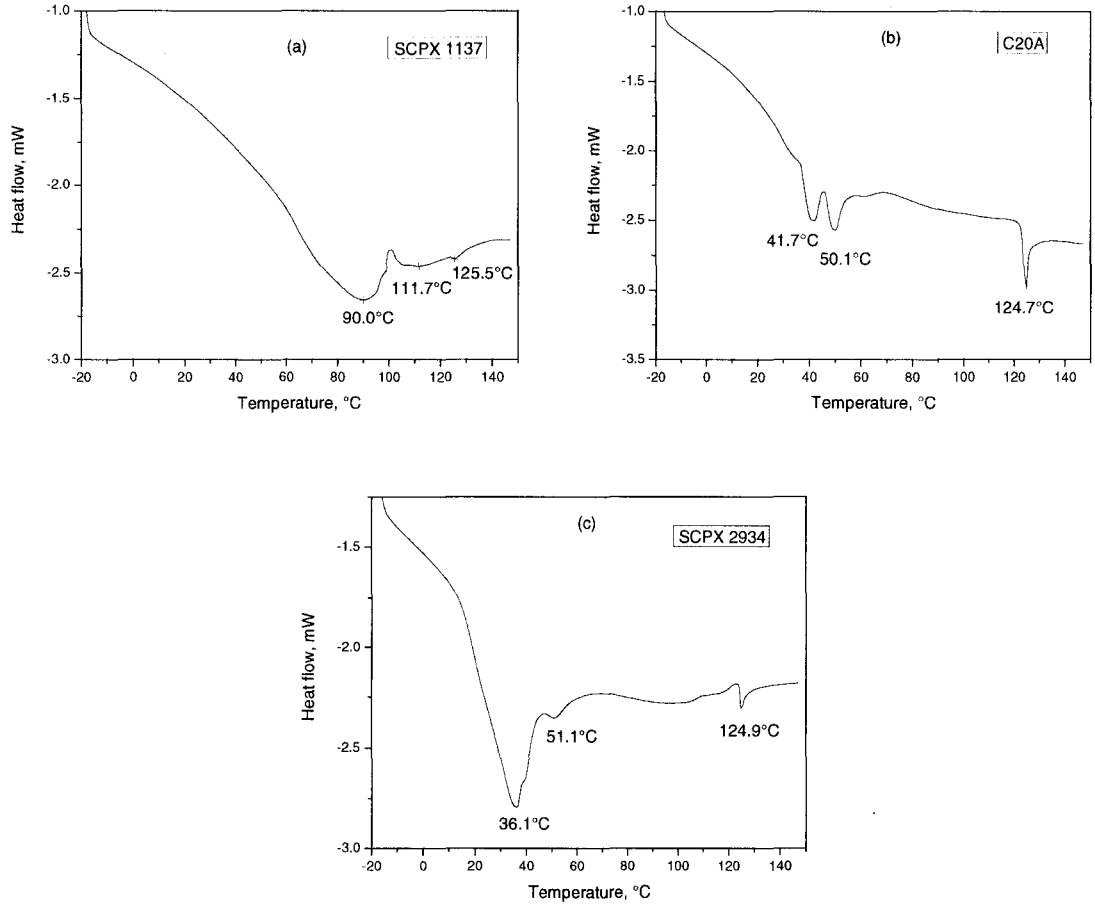

Figure 4.4.1 DSC graphs of pristine SCPX 1137 (a), Cloisite 20A (b), and SCPX 2934 (c)

For C20A, two phase transitions appeared at, 41.7°C and 50.1°C, with a third transition noted at 124.7°C (Figure 4.4.1(b)) similar to that of SCPX 1137. Partial melting of the surfactant at 50°C is probably one of the reasons for the d-spacing changes observed when the clay was processed with $scCO_2$ at this temperature. However, the

surfactant morphology changed significantly even when exposed to CO_2 at room temperature, see Figure 4.3.8(c), a possible explanation for which may be that CO_2 density at room temperature and 9.7 MPa (0.884 g/mL) is much higher than that at 50°C (0.347 g/mL) and at 200°C (0.117 g/mL) under the same pressure and it, therefore, is of larger solubility. Solubility of CO_2 at this condition (room temperature and 9.7 MPa) might be high enough to plasticize the surfactant molecules corresponding to the first two melting points leading to a decrease in their melting point. CO_2 may help these mobile surfactant molecules to transition from one crystalline phase (a lower tilt angle) to another crystalline phase (a higher tilt angle) and therefore increase the basal spacing of the clay [Osman et al. 2000].

The melting range of SCPX 2934, i.e. 36 ~ 125°C, was similar to that of C20A, but the majority of crystals melted before 36.1°C (Fig 4.4.1(c)). Though the majority of surfactant molecules of SCPX 2934 was movable at 50°C and probably mobile at room temperature when exposed to subcritical CO_2, the morphology of this surfactant did not exhibit an alteration as significantly as C20A. In spite of the greater mobility of the surfactant molecules, it may be difficult for a paraffin-type monolayer structure to transition into the paraffin-type bilayer structure under the present conditions applied. The increased amount of crystals under subcritical CO_2 shown in Figure 4.3.8(d) may be attributed to the removal and rearrangement to some extent, i.e. CO_2 may help more surfactant molecules into the crystal phase.

4.4.2 Thermogravimetric analysis

Three molecular environments exist for a surfactant within these organically pillared clays, which can be readily distinguished by TGA as demonstrated by the work of several authors [Osman et al 2003 and 2000, Soares et al 2004, Xi et al 2004]. The differential mass loss peaks between 200-450°C tend to correspond to intercalated organic surfactant while peaks at lower temperatures are related to adsorbed and cation-

bound water, and peaks above 600°C are attributed to mass loss by the clay mineral itself. Though dependent on the chemical structure of the surfactant, it has been generally found by the work of those earlier authors that surface-adsorbed species exhibit decomposition temperatures similar to the pure surfactant which lie in the range of 180-250°C, while intercalated molecules show greater thermal stability afforded by the confined environment within montmorillonite. The intercalated surfactant bound predominantly by van der Waals forces (i.e. tail-to-tail bound) or ion-dipole interactions (end-tethered) typically decomposed at temperatures between 250-350°C or 350-450°C, respectively. Therefore, this technique can provide morphological details on surfactant rearrangement which are not necessarily observed by XRD. Figure 4.4.2-7 show the differential mass loss plots determined by TGA for the washed or $scCO_2$ treated organoclays, and include the original organically modified clays for comparison.

SCPX 1137

Plot for the original monoalkyl modified clay, SCPX 1137, in Figure 4.4.2 shows the significant presence of surfactant adsorbed onto the exterior surface, as noted by the peak at 240°C, compared to the other organoclays (shown later) which only showed shoulder peaks; the externally adsorbed surfactant was in near equivalent concentration to the untethered intercalated molecules for SCPX 1137. The TGA results for two selected $scCO_2$ treated samples of this organoclay were also included in Fig 4.4.2. Unlike the corresponding washed sample, the $scCO_2$ treated SCPX 1137 showed minor differences in both surface-adsorbed and van der Waals intercalated surfactant. However, it was seen that the concentration of both surface-adsorbed and van der Waals intercalated surfactant significantly decreased compared to the original species and yet the increase in the concentration for the ion-dipole associated species was not significant. In terms of the effect of pressure release rate, the difference in the three surfactant environments for the two processing conditions was very limited. As indicated in the discussion regarding XRD data, these changes with $scCO_2$ had little affect on the basal spacing of the modified clay due to the surfactant's lateral bilayer arrangement. In addition, significant mass loss

was found by TGA at temperatures above 450°C, as indicated by the shoulder in the plot between 450-530°C. The peak has not been previously reported by other researchers, though it is suspected that the finding corresponded to the broad variance in particle size (and hence surface area) for this clay.

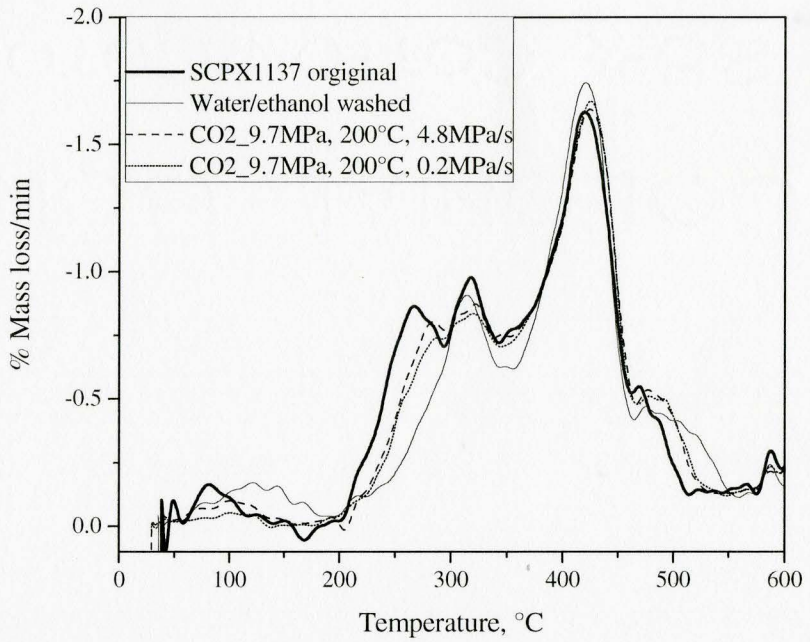

Figure 4.4.2 Differential mass loss plot determined by TGA for SCPX 1137

Cloisite 20A

The mass loss curve in Figure 4.4.3 for pristine Cloisite 20A indicated that the majority of the surfactant was intercalated into the galleries of the clay and that end-tethered molecules were more than those present as tail-to-tail bound. Washing the organoclay resulted in removal of the minor exterior adsorbed species as noted by the loss of the shoulder between 200-275°C in the plot. An increase in the intensity of the peak at 420°C and a decrease in the peak at 330°C were observed, indicating that washing allowed some of the tail-to-tail bound species to further intercalate into the galleries of the clay and react via cation-exchange with the residual sodium ions. The treatment of C20A

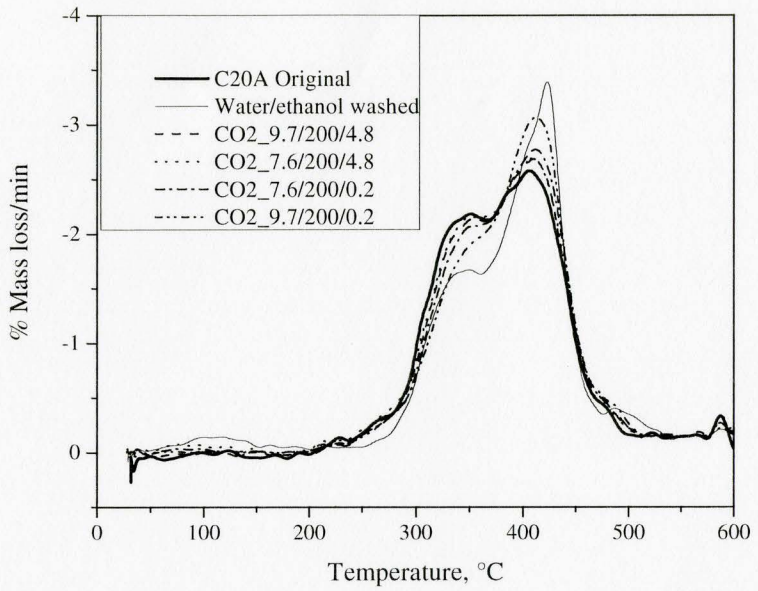

Figure 4.4.3 Differential mass loss plot determined by TGA for Cloisite 20A

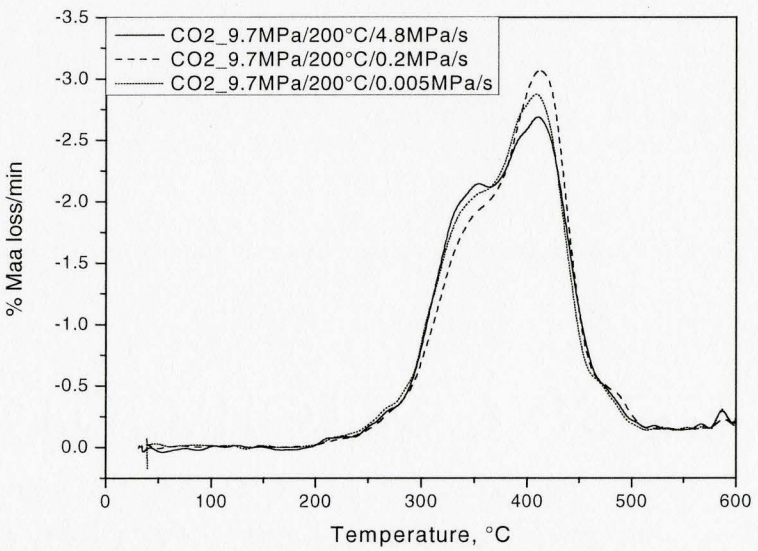

Figure 4.4.4 Differential mass loss plot determined by TGA for Cloisite 20A at three different pressure release rates

by $scCO_2$ showed the greatest change in surfactant morphology compared to the other clays, as it had in the XRD analysis. The TGA data indicated that the surface-adsorbed content, corresponding to mass loss between 200-300°C, was unaffected as a result of the supercritical fluid but the ratio of ion-dipole bound material increased with respect to van der Waals bound molecules. The observed increase in end-tethered species would have increased the tilt angle of the bound surfactant as the adjacent free space was reduced, thus bringing about the basal expansion noted by XRD. The effect of the treatment conditions on the differential mass loss was examined only for pressure and pressure release rate. At 200°C and a followed pressure release rate of 4.8 MPa/s, processing pressure exhibited no influence on the ratio of ion-dipole bound material to van der Waals bound molecules, but at the same temperature and a lower pressure release rate of 0.2 MPa/s, higher processing pressure resulted in much higher this ratio, indicating that high treatment pressure might facilitate the transition of surfactant molecules from tail-to-tail bound to end-tethered bound when the gas was released slowly. In terms of the influence of pressure release rate, it was observed that lower pressure release rate seemed to readily improve this ratio value. Therefore, an extra experiment was run with a very low pressure release rate at 200°C and 9.7 MPa. For this run, the pressure release rate was controlled manually as low as possible and was estimated at 0.005 MPa/s. The comparison among the three pressure release rates was expressed in Figure 4.4.4 where it can be seen that the ratio of the end-tethered material to the tail-to-tail molecules for the lowest pressure release rate was between those of the two other situations. It seemed that there was an optimum pressure release rate when the treatment was processed at 200°C and 9.7 MPa. Unfortunately, in actual compounding processes for a nanocomposite, it is unlikely this factor can be controlled.

SCPX 2934

Figure 4.4.5 shows that the original SCPX 2934 gave a mass loss plot indicating that the majority of the surfactant was end-tethered to the clay. Washing brought about a

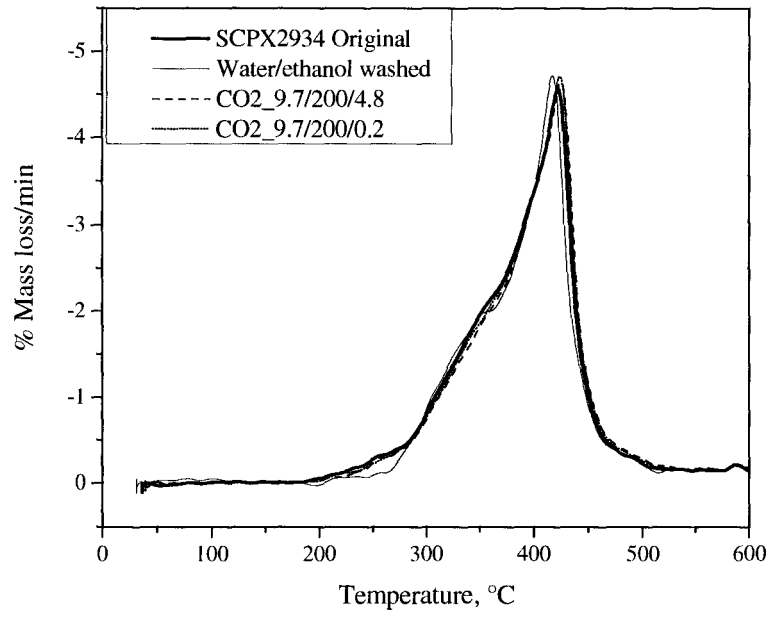

Figure 4.4.5 Differential mass loss plot determined by TGA for SCPX 2934

decrease in the exterior adsorbed surfactant, as indicated by the loss of the shoulder peak in the plot between 200-300°C, and consequently led to an increase in the number of end-tethered molecules. The mass loss plot for the $scCO_2$ treated SCPX 2934 showed a small increase in the intensity of the peak at 410°C with a subsequent slight decrease in the shoulder peak centered at 340°C. This small change in surfactant morphology – furthering of cation exchange by the intercalated species – resulted in minor variations in the basal spacing as shown in the XRD data. Overall, the distribution ratio of species within the galleries varied only slightly as a result of the washing or the $scCO_2$ treatment.

SCPX 2972

As shown in Figure 4.4.6, like the three previous organoclays the majority of the SCPX 2972 surfactant was intercalated into the galleries of the clay but those molecules were equally present as tail-to-tail bound and end-tethered. Washing the organoclay

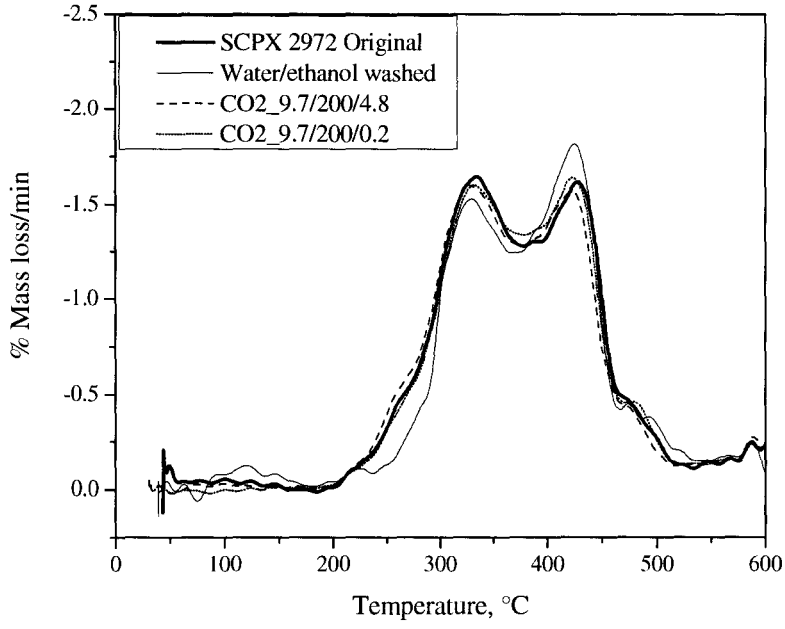

Figure 4.4.6 Differential mass loss plot determined by TGA for SCPX 2972

resulted in removal of the exterior adsorbed material corresponding to the shoulder at 200-300°C and the intercalated species bound by van der Waals force corresponding to the peak at 335°C, which consequently led to the increase in the intensity of the peak at 428°C, i.e. washing allowed part of the untethered species to become end-tethered. The $scCO_2$ treatment at 200°C and 9.7MPa followed by 4.8 MPa/s pressure release rate resulted in a small decrease in the amount of both the tail-to-tail and the end-tethered bound surfactant molecules. The removal of the surfactant from the interlayer resulted in the partial collapse of the galleries noted by XRD. However, the $scCO_2$ treatment at the same temperature and pressure but followed by 0.2 MPa/s pressure release rate exhibited slight difference in that a small decrease in the tail-to-tail bound surfactant concentration and a small increase in the end-tethered molecules could be discerned.

SCPX 2971

For SCPX 2971, as almost no change in the surfactant morphology occurred when processed with $scCO_2$ the TGA analysis was only considered for the pristine and washed species. As Figure 4.4.7 indicated, washing only reduced the exterior adsorbed surfactant molecules corresponding to shoulders at about 200-320°C, and probably only a small part of the removed material entered the galleries because it was noticed that the increase in the van der Waals bound surfactant peaked at 391°C and the ion-dipole bound species peaked at 467°C was very limited. It was also noticed that washing did not significantly alter the concentration of the adsorbed water on to this clay corresponding to the peak at 113°C, indicating that surfactant distribution for SCPX 2971 did not exhibit a significant change due to the washing.

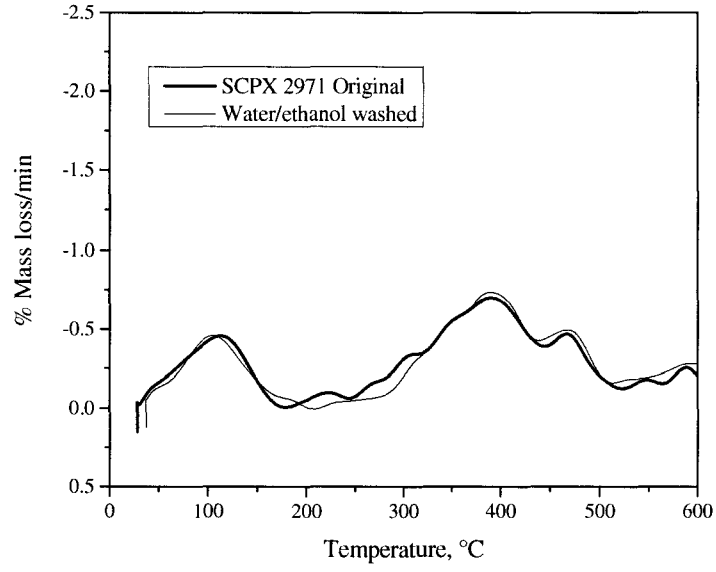

Figure 4.4.7 Differential mass loss plot determined by TGA for SCPX 2971

In general, the results in this section indicate that solvation of the clays by $scCO_2$ increased the mobility of the alkyl organic molecules, though not often resulting in basal expansion. The free volume expansion afforded by the supercritical solvent within the

continuum of the organic medium (i.e. surfactant) allowed the externally adsorbed and intercalated species to migrate further into the galleries of the clay and in some cases, become exchanged with remaining sodium cations.

4.5 FT-IR analyses

Carbon dioxide can behave as a weak Lewis acid within ionic media [Kazarian et al. 2000, Huang et al. 2005], it is feasible that the CO_2 molecule itself can balance the charge on the silicate – at least until H_2O could replace it. If this occurs, organic cations will be removed and CO_2 will retain to the silicate. The frequency and the width of asymmetric stretching mode of methylene, $\nu_{as}(CH_2)$, are reported to be sensitive to the gauche-trans conformation and the packing density of methylene chains [Vaia et al 1994, Wang et al 1993, Frost et al. 2008]. Lower frequencies and width means highly ordered all-trans conformations while higher frequencies represent the increased chain disorder due to a higher number of gauche conformers along the hydrocarbon chain. In order to determine whether residual CO_2 or carbonic acid were present and whether changes in the morphology could be detected by IR technique, transmission FT-IR analysis was performed. The samples were initially dried in a vacuum oven at 40°C over night and either stored for analysis or subsequently processed with CO_2 at 200°C and 9.7 MPa for 3 hours. All samples were stored in a desiccator under vacuum till FT-IR analysis could be performed. Since the duration of samples waiting for analysis was usually several hours or days, during which the possible residual CO_2 might escape from the processed organoclays, one FT-IR analysis of $scCO_2$ treated clay (i.e. C20A) was performed immediately after the treatment. The spectra of the selected clays before and after $scCO_2$ treatment were shown in Figure 4.5.1.

IR spectrum of entrapped CO_2 in the v bending mode should give rise to a strong peak at 660 – 668 cm^{-1}. The stretching peaks for CO_2 at 2330 – 2360 cm^{-1} can be quite

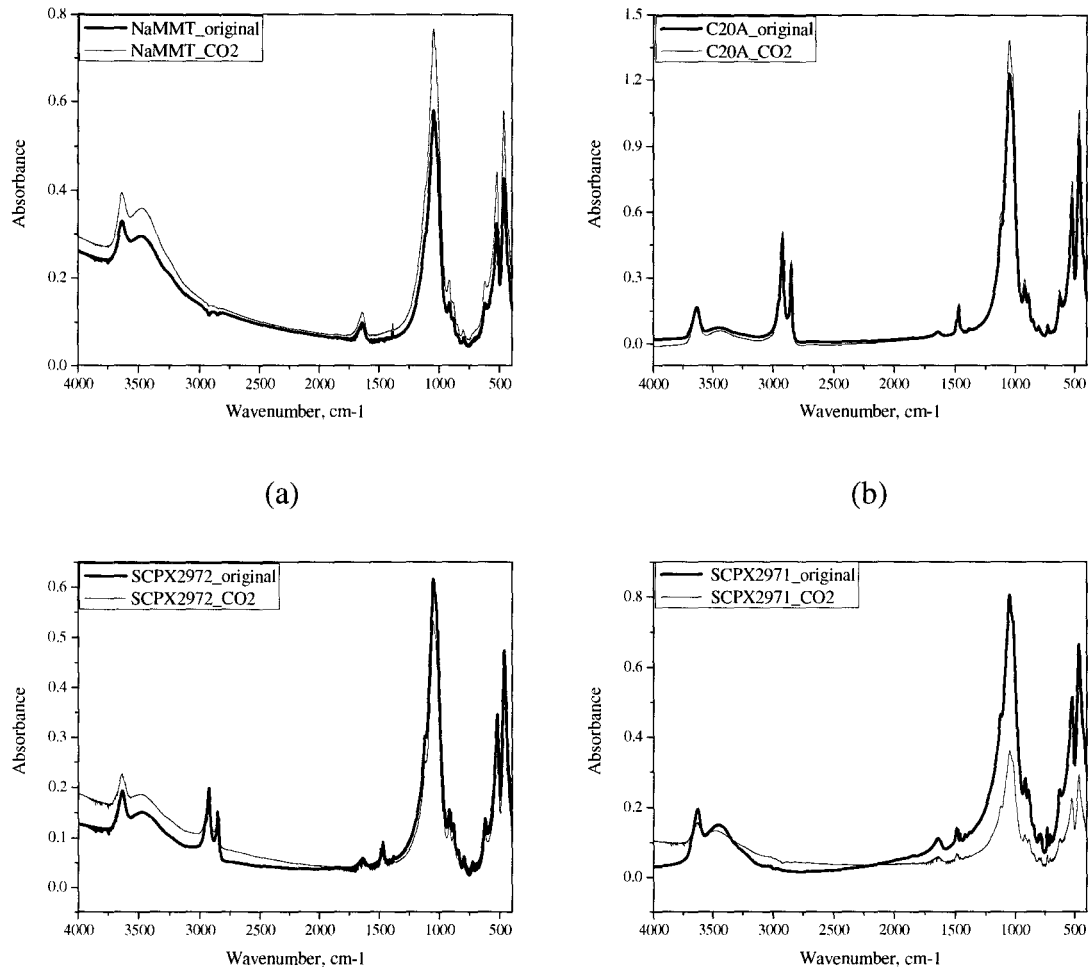

Figure 4.5.1 FT-IR spectra of (a) NaMMT, (b) Cloisite 20A, (c) SCPX 2972 and (d) SCPX 2971 before and after CO_2 treatment at 200°C and 9.7 MPa

informative regarding the bonding state of the molecule within the clay — CO_2 has been found to associate with anions in ionic liquids ascribed to a charge-quadrupole moment interaction. Figure 4.5.1 shows that no CO_2 absorbances at band 660 – 668 cm^{-1} and at 2330 – 2360 cm^{-1} were found in all the $scCO_2$ treated samples, indicating that there were no CO_2 molecules entrapped within galleries after the gas was released. Graphs in the

figure also show that there were no new chemical species such as carbonic acid or free amines present as a result of $scCO_2$ treatment. These results confirm the previous observations that the clays were thermally stable at the processing conditions and that no surfactant extraction occurred during the processing.

Close looks at the FT-IR analyses at band 2800 – 3000 cm^{-1} for the organoclays with alkyl chain surfactants showed that the change in asymmetric stretching frequency of methylene groups corresponded to their basal spacing. Supercritical CO_2 led to C20A and SCPX 2972 a significant increase and decrease, respectively, in their interlayer distance, so correspondingly their frequencies of ν_{as} (CH_2) exhibited difference. Figure 4.5.2 shows the detail of FT-IR results of C20A and SCPX 2972 at this band. The asymmetric stretching frequency of methylene groups for C20A surfactant (Figure 4.5.2a) increased 2 cm^{-1} from the original species of 2923cm^{-1} to the $scCO_2$ species of 2925 cm^{-1}, indicating that $scCO_2$ increased the surfactant chain disorder. Though $scCO_2$ treatment may allow more un-tethered surfactant molecules to transfer to the end-tethered species for this clay, as discussed above, the packing density in the galleries may not increase much. The increased gallery space provided more free volume for surfactant molecules, which may result in the increase in the surfactant chain disorder.

The interlayer of SCPX 2972 collapsed to some extent due to the $scCO_2$ treatment, as shown in the XRD data in Figure 4.3.5 indicating the free volume in its galleries decreased which increased the surfactant packing density and therefore promoted increase in chain order. The decrease of 1 cm^{-1} in asymmetric stretching frequency after $scCO_2$ treatment (Figure 4.5.2b) reflected this change in chain order. The resolution used for this measurement was 2 cm^{-1}, so the frequency change of 1 cm^{-1} for SCPX 2972 may not be enough to illustrate the change in its surfactant conformation. To confirm this, higher resolution, for instance, 0.5 cm^{-1}, is recommended to use for future experiments.

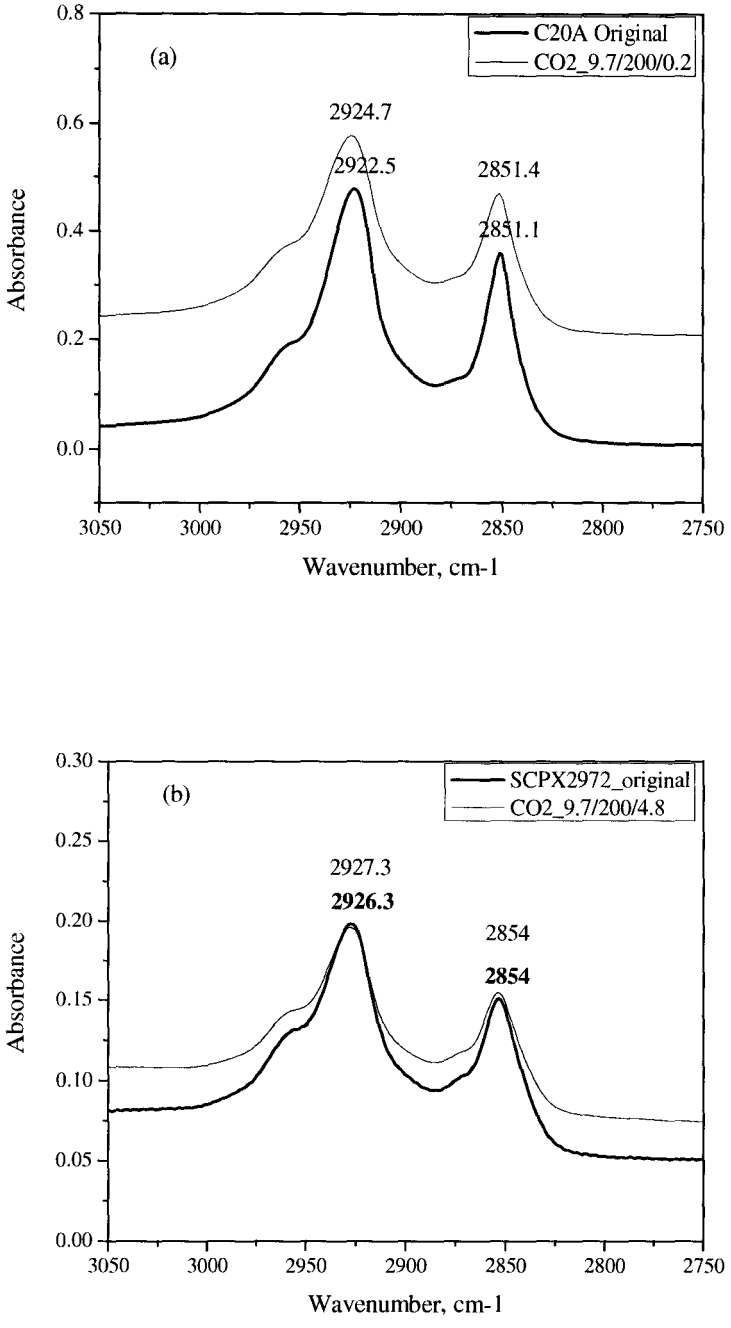

Figure 4.5.2 FT-IR spectra of Cloisite 20A (a) and SCPX 2972 (b) before and after treatment with $scCO_2$ at frequency of 2750 – 3050 cm^{-1}

4.6 TEM analyses

Further observations of the clay structure and surfactant morphology were made by powder TEM. The technique avoided concerns of whether a mounting material like an epoxy resin would further altering the clay structure prior to analysis, though it restricts observations to only the exterior regions of a particle where the electon beam can penetrate. Figure 4.6.1-5 show TEM micrographs of the five organoclays in the original state and $scCO_2$ treated state. Figure 4.6.1 includes the TEM micrograph of the water/ethanol washed C20A as well as the original and $scCO_2$ treated species; all three states were chosen to be displayed for this organoclay as it had shown the most notable changes in its structure based on the other analyses in this chapter. The micrographs show the exterior of the organoclay which consisted of tactoid structures and some platelets encapsulated in the surfactant. The darker body seen in the figure indicates a denser structure which lies below the ~80-130 nm outer layer — the thickness of the particle closer to its interior was too great for the electron beam to fully penetrate. The tactoids typically viewed in the outer region appeared to be made up of 10-20 sheets with some curling at the edges to indicate intercalation of the surfactant. After water/ethanol washing, the exterior surfactant was largely removed and a denser packing of the clay mineral could be seen. Few loose tactoids and no platelets were observed after the washing. As a result of the $scCO_2$ treatment, C20A showed a thickening of the exterior layer with many more separated tactoids observed. These observations by powder TEM indicated meso- and macro-scale changes to the organoclay particles by the $scCO_2$ treatment which could not be properly identified by XRD.

In Figure 4.6.2, it can be seen that the original SCPX 1137 exhibited a denser exterior region, more similar to the washed C20A, with clay aggregates visible and a few tactoids. The $scCO_2$ treated SCPX 1137 showed improved coverage of the surfactant within the clay galleries, but little change in the packing density of the clay sheets. The original and $scCO_2$ treated SCPX 2934 species shown in Figure 4.6.3 revealed an exterior

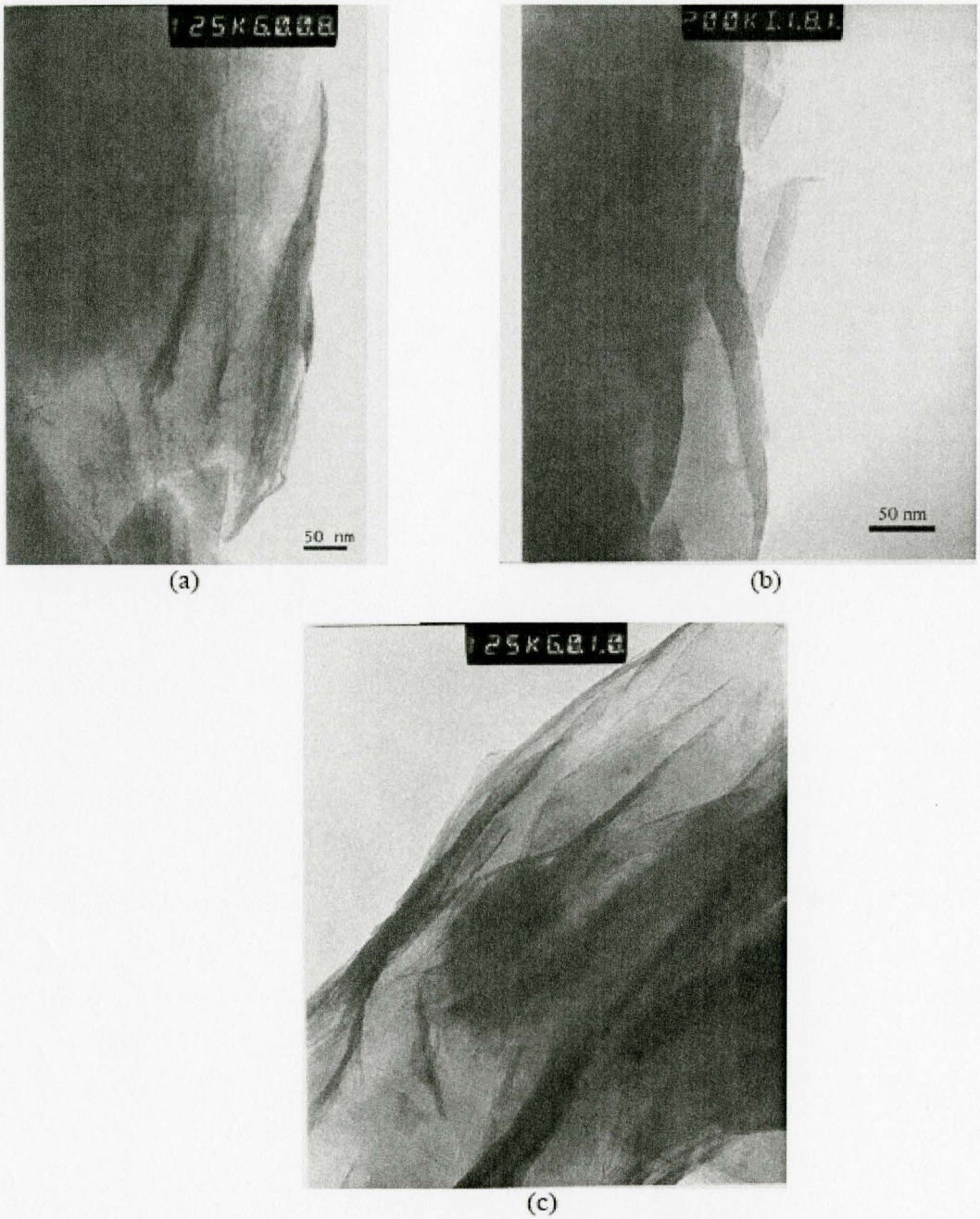

(a) (b)

(c)

Figure 4.6.1 C20A Powder TEM micrographs of Cloisite 20A in its original state (a), water/ethanol washed state (b) and $scCO_2$ treated state at 9.7 MPa and 200°C followed with 0.2 MPa/s gas release rate (c)

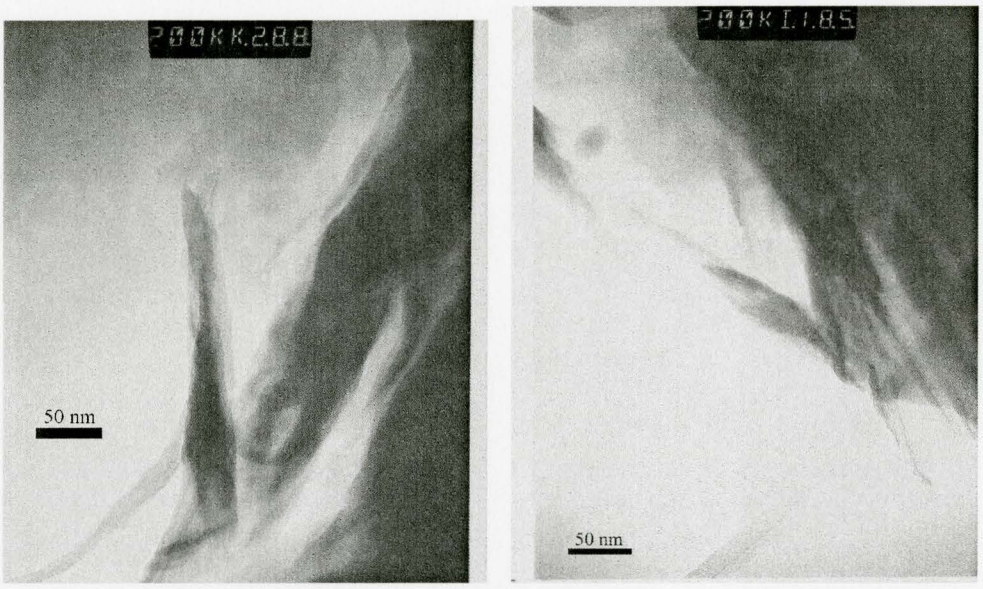

(a) (b)

Figure 4.6.2 Powder TEM micrographs of SCPX 1137: the original (a) versus $scCO_2$ treated (b)

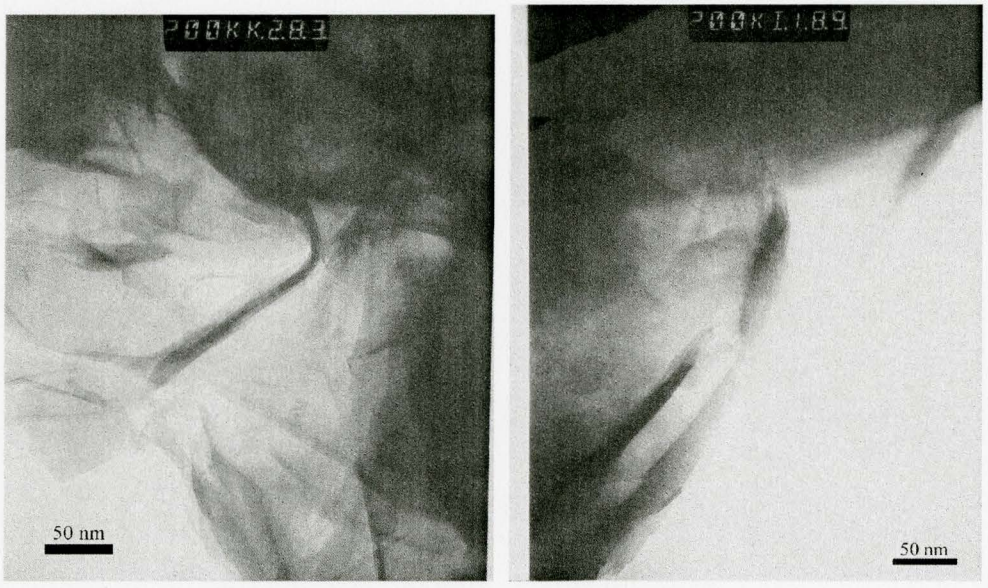

(a) (b)

Figure 4.6.3 Powder TEM micrographs of SCPX 2934: the original (a) versus $scCO_2$ treated (b)

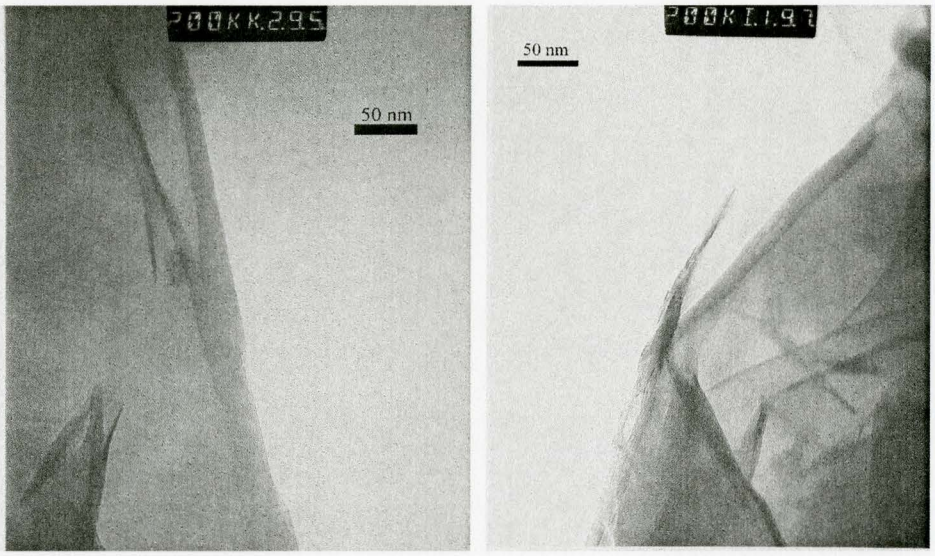

(a) (b)

Figure 4.6.4 Powder TEM micrographs of SCPX 2972: the original (a) versus $scCO_2$ treated (b)

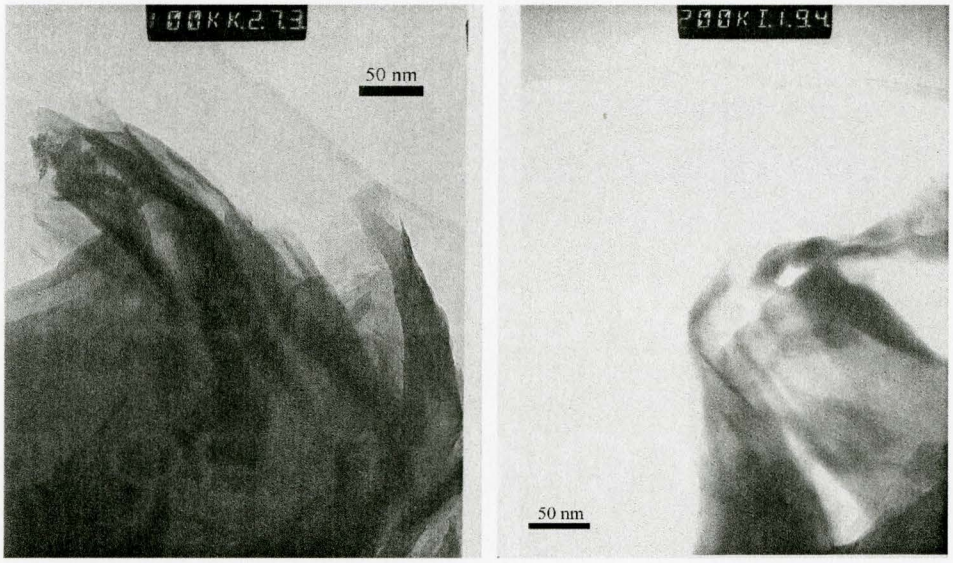

(a) (b)

Figure 4.6.5 Powder TEM micrographs of SCPX 2971: the original (a) versus $scCO_2$ treated (b)

layer similar to the untreated C20A, showing reasonably good dispersion of tactoids in the surfactant. Consistent with the TGA and XRD data, the crystal structure of the clay in the exterior region for SCPX 2934 was not affected by the supercritical solvent. The original SCPX 2972 exhibited good tactoid dispersion in the exterior and the $scCO_2$ had little effect on the tactoid dispersion. For the original SCPX 2971, the tactoids dispersed loosely on the exterior of the particle displayed in Figure 4.6.5, but not as well as other clays. Similarly, the $scCO_2$ treatment did not show any effect on the exterior layer structure.

4.7 SEM analyses

At present it is unclear in the literature as to the mechanism which results in greater exfoliation of a nanocomposite when $scCO_2$ is used as a processing aid during compounding. Certainly the results presented in this thesis to this point indicate that the supercritical fluid acts to improve dispersion of the surfactant throughout the clay particles and may further aid cation exchange with the remaining sodium, but there has been no evidence of major basal expansion to support a theory of substantial weakened van der Waals attractive forces between adjacent silicate sheets. In a study by Horsch et al. [2006], it was postulated that fracturing of clay particles resulted from the rapid depressurization that occurred upon removal of $scCO_2$, and that this particle size reduction beneficially aided in the dispersion/exfoliation of the organoclays in polymers. Certainly, the work by Favre and Lagaly [1991] has shown that the lower charge density of smaller particles leads to preferential binding of longer alkyl surfactants — a beneficial property during compounding of the organoclay within the matrix of a polymer resin. To test their hypothesis, SEM was used to study the organoclay most affected in our trials by the supercritical solvent, namely C20A, and look for evidence of particle fracture. Figure 4.7.1 shows SEM micrographs of C20A, both original and after $scCO_2$ treatment (9.7 MPa, 200°C, 0.2 MPa/s), at similar resolution under the microscope. Image analysis of the original and $scCO_2$ treated species revealed a particle size of 6 ± 3 μm and 9 ± 5 μm,

(a)

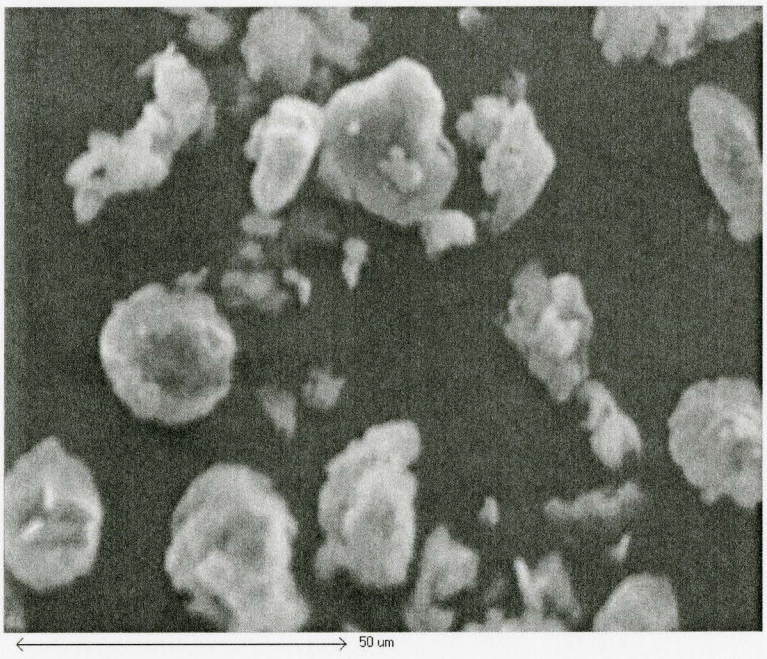

(b)

Figure 4.7.1 SEM micrographs of C20A before (a) and after (b) $scCO_2$ treatment

respectively. Qualitatively, the C20A species showed evidence of a rougher surface after solvation with $scCO_2$. It would seem unlikely based on these observations that a substantial reduction in particle size could arise from rapid expansion of the organoclays under the conditions tested in this work. The minor increase in particle size and particle roughening is more likely attributed to increased porosity of the particles as a result of swelling with the supercritical solvent. Such porosity would be beneficial for subsequent diffusion of polymer chains for intercalation. The observations by powder TEM certainly support this hypothesis as it was noted that the packing efficiency of the silicate layers was reduced after $scCO_2$ treatment. There was not evidence from our study that particle fracture occurred during the rapid depressurization that takes place during the $scCO_2$ treatment.

4.8 Surface energy

Determining the surface energy of the organoclay species meets two objectives, i) providing a basis for evaluating the ideal organoclay for dispersion with the polymer matrix in preparation of a nanocomposites, and ii) allowing critical analysis of the changes in surface chemistry produced by treatment with supercritical carbon dioxide. The former objective relates to the apparently strong reliance of platelet delamination on the extent of transmitted stresses across the interface between the melt and particles during processing. Evaluating the interfacial energy of such a system requires knowledge of the surface energy for the individual components. As a minimum criterion for intercalation and exfoliation to occur, similarity in the surface energy between the organoclay and polymer matrix is required. Originally, sodium montmorillonite exhibits a surface energy of ~200 mN/m. Applying an organic surfactant decreases the surface energy of the mineral to match those typical of many polymers (i.e. 20 – 40 mN/m).

In this analysis, it was important to bear in mind that not all surfactant becomes bound to the silicate surface during initial cation exchange, as seen by TGA. While

questions arise as to the importance of the physically adsorbed surfactants during nanocomposite processing (for instance, does the chemical species locally plasticize the polymer matrix?), we can be certain that its loss will alter the interfacial energy of the system. In the presence of $scCO_2$, we have observed changes in the surface chemistry of organoclays which could be attributed to surfactant removal or interactions with the broken bond plane. In this work, we compare the effect that $scCO_2$ has on the surface energy of our five organoclays in comparison to the same organoclays which had much of their physically adsorbed surfactant removed by water/ethanol washing.

Table 4.8.1 Extraction of physically adsorbed surfactants by a mixture of water/ethanol

Type	SCPX1137	C20A	SCPX2934	SCPX2972	SCPX2971
Mass Loss (wt%)	3.2 ± 0.2	3.3 ± 0.9	7.6 ± 0.4	1.9 ± 1.0	2.3 ± 0.2

Table 4.8.1 presents the observed change in surfactant content for the five different organoclays after washing. The mass loss varied from 1.9 to 7.6 wt% depending on the organoclay. We were somewhat surprised that any loss was observed for SCPX 2971 due to its relatively low organic content (Table 4.2.6) and poor surface coverage on the montmorillonite (noted by pH and hydration results in the previous section) as well as the fact that the benzyl group associates with the oxygen plane of the adjacent silicate sheets to the molecule [Yariv 2002]. It has been shown by other researchers that any removed component by this solvent extraction method was primarily physically adsorbed onto the external clay surfaces, and not intercalated within the interlayer region [He et al. 2006]. The confined surfactant is much more difficult to remove.

In order to confirm that the surfactant removed by washing was the physically adsorbed species and understand the surface chemistry of these washed organoclays, XRD analysis was performed. We expected that there should be no change in basal spacing if the hypothesis of physically adsorbed surfactant removal was true. The XRD

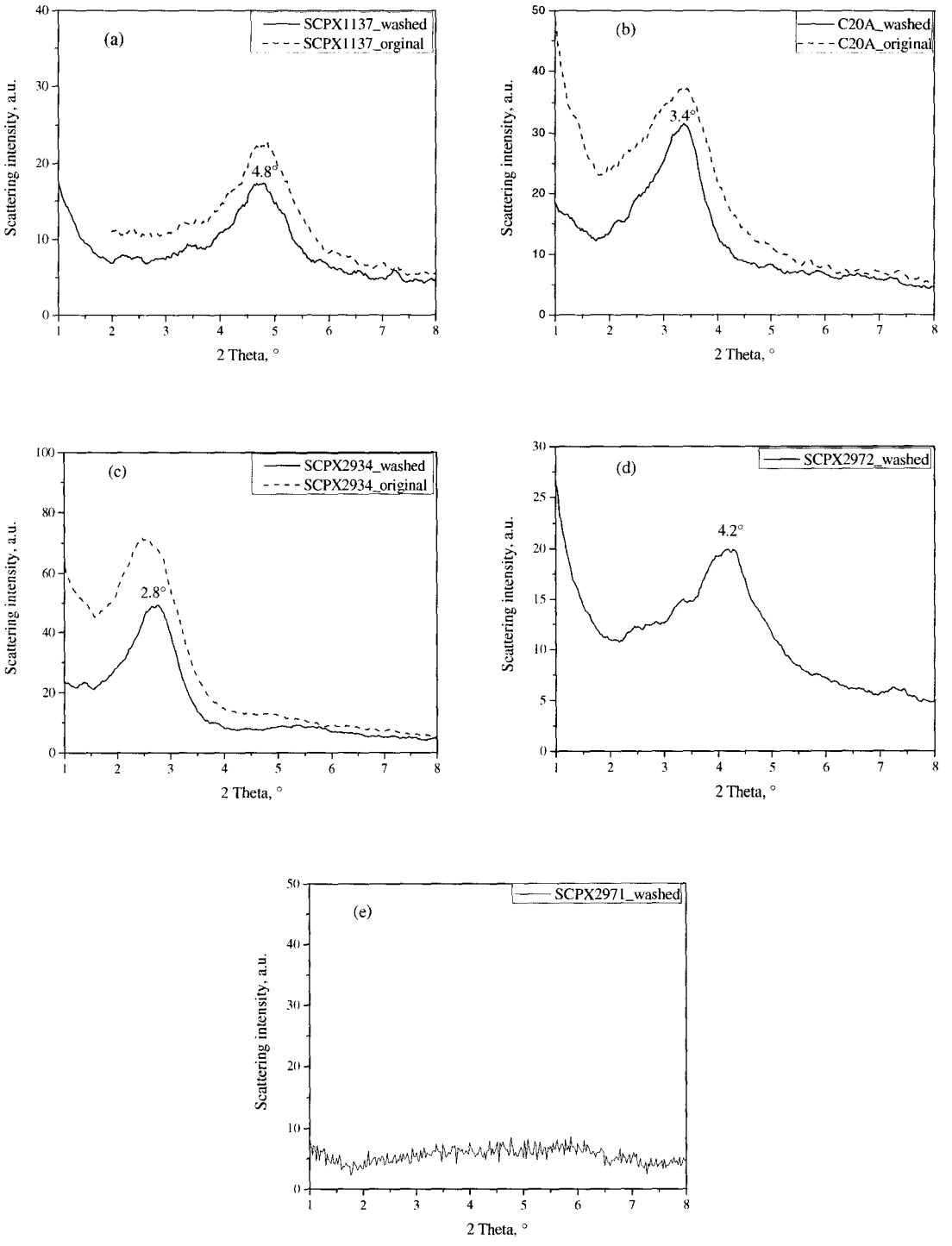

Figure 4.8.1 XRD patterns of washed SCPX 1137 (a), C20A (b), SCPX 2934 (c), SCPX 2972 (d) and SCPX 2971 (e)

results were shown in Figure 4.8.1, in which the as-received data was included for comparison. As-received data for SCPX 2972 and SCPX 2971 could not be included as the two samples were tested on a different XRD instrument and their magnitude scattering intensity failed to overlay with the washed species on a single graph. For SCPX 1137 (Figure 4.8.1a), C20A (Figure 4.8.1b) and 2972 (Figure 4.8.1d and Figure 4.3.5), basal spacing of the washed species did not exhibit any change indicating that the surfactant removed was externally adsorbed as and that washing did not alter the crystalline structure of these clays. For SCPX 2934 (Figure 4.8.1c), 2θ angle of the (001) diffraction peak for washed species increased 0.2°, indicating that the crystal structure of this clay was slightly altered due to the washing. The decrease in basal spacing may attribute to the removal of adsorbed surfactant in the galleries. We noted in Table 4.2.6 that the organic loading of SCPX 2934 was the highest (44 wt %) and in Table 4.8.1 that the surfactant extracted was similarly high up to 7.6 wt %, much higher than others. As mentioned above, we were somewhat surprised by the mass loss for SCPX 2971 due to washing. The possible reason for it may be that this surfactant, trimethyl-benzyl ammonium, had higher solubility in the water/ethanol solvent than other long alkyl chain surfactant. We were also somewhat surprised that the highly ordered crystal structure of SCPX 2971 in its as-received state (Figure 4.3.6) vanished after washing. The sharp X-ray diffraction peak seen at $2\theta = 5.9°$ for the as-supplied material disappeared completely after washing. This phenomenon is interesting to us because the clay may completely exfoliate by the washing (TEM analysis is needed for this state) and the dispersed clay platelets did not reunite to form crystalline structure after drying.

4.8.1 As-supplied organoclays

The determined surface energy of the five organoclays in their as-received state was shown in Figure 4.8.2. As expected for the organophilic surfactants applied to these montmorillonite samples, the dispersive component was higher than the polar counterpart.

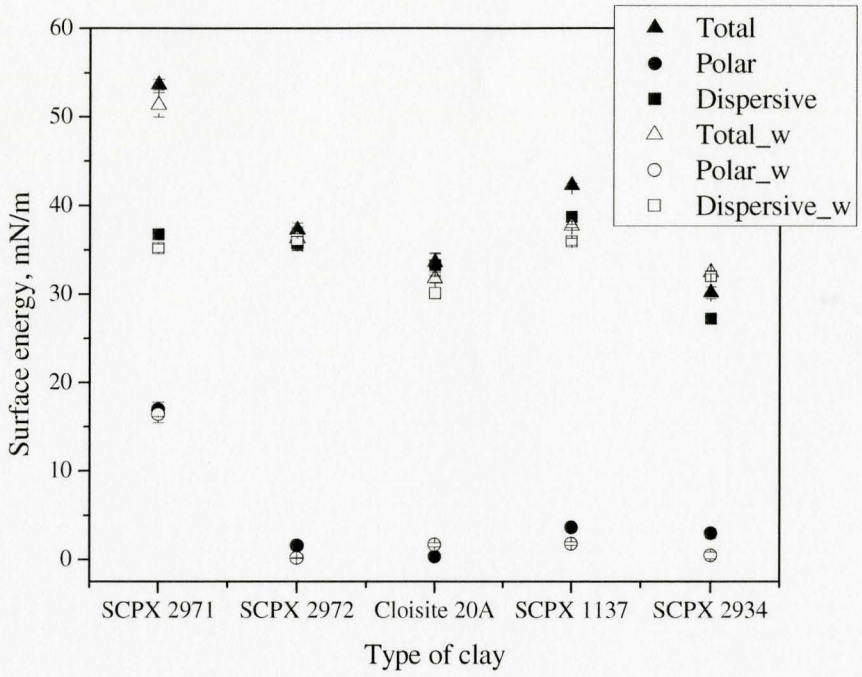

Figure 4.8.2 Determined surface energy for the as-received organoclays (w means washed at water/ethanol mixture)

However, polar component of SCPX 2971 was substantially higher than the other surfactants, which follows along with the other testing methods finding lower organic content and higher moisture content in this clay. This surfactant does not appear to be an ideal candidate for future compounding studies with polyolefins considering its relatively high hydrophilicity, small interlayer spacing, and high surfactant melting point (T_m = 239°C, which is above normally polymer processing temperatures of 200 – 220 °C for polyolefins). C20A, SCPX 2934 and SCPX 2972 showed very similar behavior. Despite the apparent similarity in molecular structure with the other alkyl chain surfactants, the surface energy (both dispersive and polar components) of SCPX 1137 was substantially higher. Higher surface energy of SCPX 1137 may be attributed to the surfactant content. The organic content of SCPX 1137 was only 26.8 wt%, far lower than those of the other organoclays with alkyl chain surfactants, 44.0 wt% for SCPX 2934, 38.5 wt% for C20A,

and 30.6 wt% for SCPX 2972 (Table 4.2.6). Lower surfactant content means less possibility for organic coverage on the surface of silicate sheets especially the surface of clay tactoids and therefore increases the surface energy of the clay. Actually, the order of the surface energy of the five organoclays, SCPX 2971 > SCPX 1137 > SCPX 2972 > C20A > SCPX 2934, inversely followed the surfactant content order of SCPX 2971 < SCPX 1137 < SCPX 2972 < C20A < SCPX 2934.

4.8.2 Washed organoclays

As noted in Figure 4.8.2, polar component for each washed clay except SCPX 2934 changed little while dispersive component decreased slightly or maintained unchanged. These results were consistent with observations by XRD shown in Figure 4.8.1 where we could see that microstructure was not altered by the washing (excluding SCPX 2971). A similar phenomenon was observed by He and coworkers [2006]. SCPX 2934 was the only organoclay to demonstrate a significant increase in dispersive component and decrease in its polar component after washing. The increase in dispersive component was larger than the decrease value in polar component and therefore the total surface energy exhibited small increase. These changes for SCPX 2934 can be attributed to the large amount of surfactant extraction, especially the surfactant reduction on exterior surface of the clay tactoids. The extraction by washing consequently resulted in an increase of dispersive component and reduction in polar component.

4.8.3 Supercritical CO_2 treated Organoclays

Figures 4.8.3 – 7 show the changes in surface energy of the five unwashed organoclays before and after $scCO_2$ treatment at temperatures of 50°C and 200°C, pressures of 7.6 MPa and 9.7 MPa and pressure release rates of 0.2 MPa/s and 4.8 MPa/s. For SCPX 1137 after $scCO_2$ treatment, surface energy of the clay did not show significant change (Figure 4.8.3). This result was reasonably expected because we had known that

an interesting result. TGA analysis in the following section may help us understand the phenomena. Figure 5.2.2 shows the difference in XRD patterns of the hydrated C20A treated with $scCO_2$ at 200°C and 50°C. Though positions of the (001) diffraction peak for the two case were identical, peak intensity for 50°C was significantly higher than that for 200°C, indicating that high temperature led to more heterogeneity in microstructure of the clay.

Observations of the powder particles for the $scCO_2/H_2O$ treated C20A by TEM confirmed the XRD results. Figure 5.2.3 gives the TEM micrographs for C20A treated with $scCO_2/H_2O$ at both conditions of 200°C and 50°C. In comparison with Figure 4.6.1 showing C20A treated with only $scCO_2$ at 9.7 MPa, 200°C and 0.2 MPa/s, we note that the co-solvent treated particles exhibited a looser packing of tactoids within the viewable exterior region of the particle. In fact, for the 50°C condition, some tactoids had been replaced with ordered exfoliated structures while none were evident at 200°C.

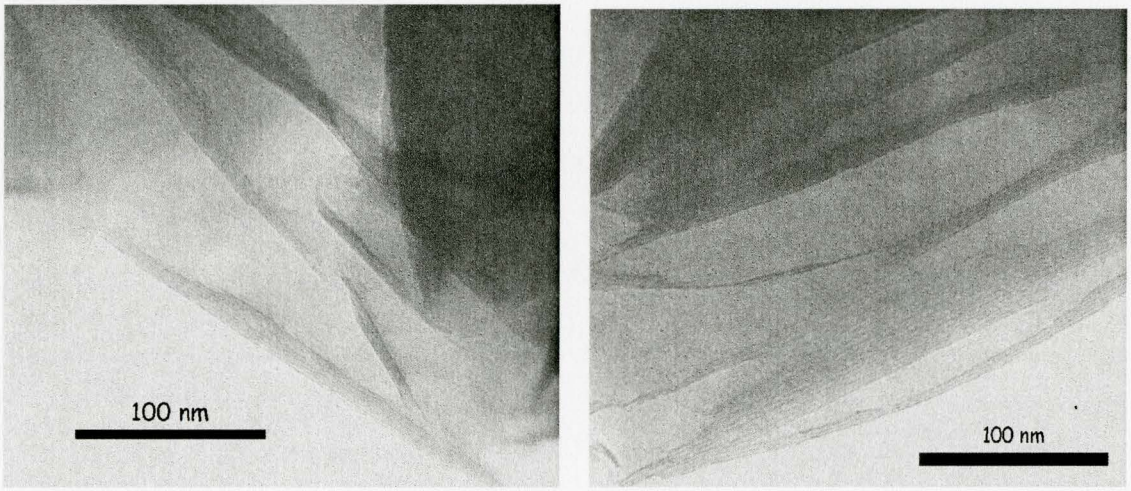

(a) (b)

Figure 5.2.3 TEM images of C20A processed with $scCO_2/H_2O$ at (a) 9.7 MPa, 200°C and 0.2 MPa/s and (b) 9.7 MPa, 50°C and 0.2 MPa/s

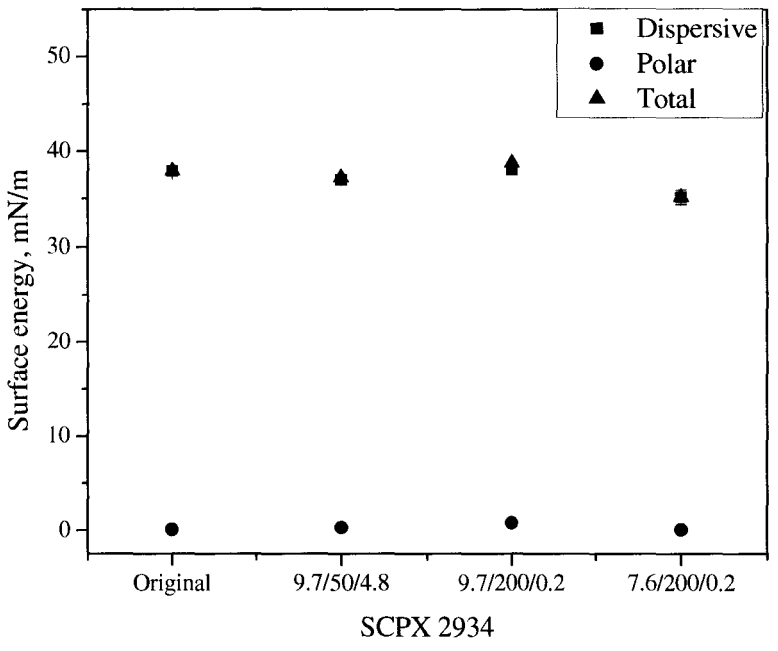

Figure 4.8.4 Surface energy of SCPX 2934 before and after $scCO_2$ treatment. X-axis labels refer to the CO_2 pressure (MPa)/vessel temperature (^oC)/pressure release rate (MPa/s)

4.8 MPa/s and high value for 9.7 MPa, 200°C and 0.2 MPa/s, as shown in Figure 4.8.4. Similarly, Table 4.2.3 shows that the organic content for treated SCPX 2934 at 9.7 MPa, 50°C and 4.8 MPa/s was higher than those of the un-treated species and the treated at 9.7MPa, 200°C and 0.2 MPa/s, and the amount of hydrated water was much lower than with the other two. It seems that temperature and pressure release rate had a synergetic effect on the surface energy of SCPX 2934 and SCPX 1137. Equation (4.2) quantified that the coupled interaction of temperature and pressure release rate on the hydration of treated SCPX 2934 was larger than the main factors, temperature, pressure and pressure release rate. The higher organic content and lower hydration value of the two organoclays treated at 9.7 MPa, 50°C and 4.8 MPa/s may be partially understood as this: drying of an organoclay at 40°C before the $scCO_2$ treatment did not completely remove the moisture in the clay, part of the moisture still stayed in the clay after the $scCO_2$ treatment at 50°C, and

that remaining moisture was accounted into the organic content and at the same time reduced the moisture uptake during the following hydration of the treated clay. The 200°C temperature condition for the $scCO_2$ treatment was high enough to remove the moisture left by the drying. Similar situations will be seen in next chapter for the clays treated with $scCO_2$ and water co-solvent. However, it was still unclear to the author how the dispersive component was related to the coupled conditions of temperature and pressure release rate.

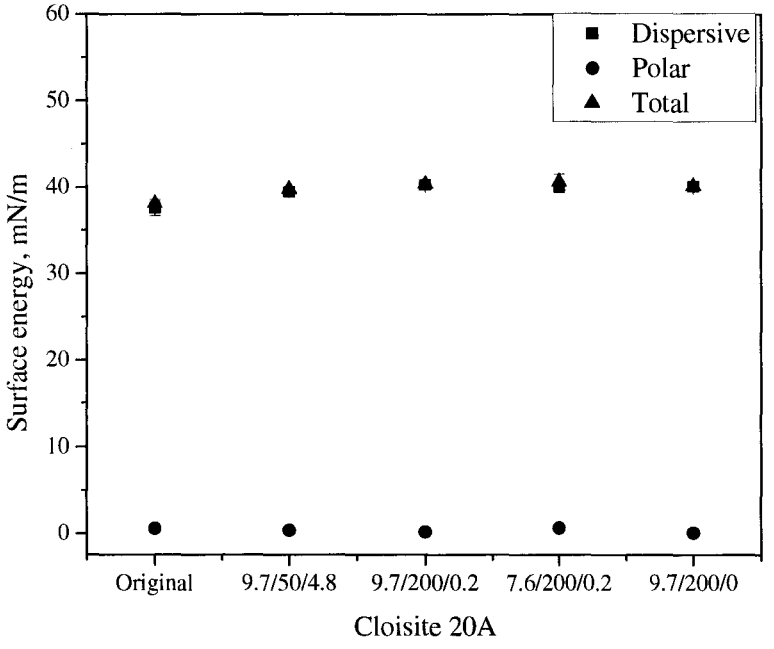

Figure 4.8.5 Surface energy of Cloisite 20A before and after $scCO_2$ treatment. X-axis labels refer to the CO_2 pressure (MPa)/vessel temperature (°C)/pressure release rate (MPa/s)

In Figure 4.8.5, the treatment conditions examined for C20A were same as those for SCPX 1137 and SCPX 2934 in earlier figures, but an extra condition of 200°C, 9.7MPa and 0 MPa/s was now included. The change in surface energy for C20A was quite different from the two mentioned organoclays. The polar component for C20A after

$scCO_2$ treatment changed negligibly whereas the dispersive component obviously increased. Surface energy of treated C20A among varied conditions, however, did not exhibit significant difference. In Section 4.3, we saw that C20A was the only organoclay that its basal spacing increased after the $scCO_2$ treatment. In comparison of surface energy with organoclays with similar surfactant structures (i.e. SCPX 1137 and SCPX 2934), C20A was the one that its surface energy increased significantly due to the $scCO_2$ treatment. It seems that there is some kind of relationship between surface energy and basal spacing, though with such small changes in values for either measurement, it is difficult to make this statement with any certainty. In previous sections, we attributed the increase in basal spacing of C20A to rearrangement of the surfactant molecules and surfactant transition from the external adsorbed state to the galleries by continuing cation exchange with residual Na^+. The swelling of clay particles increased their surface area. In the rubber industry it is understood that the surface energy of carbon black grows with surface area [Erman and Mark 2005]. Noting that contact angle measurements are an exterior property of the clay materials, reduction in physically adsorbed surfactant on exterior surface of clay sheets may also be the reason for the increase in surface energy.

For SCPX 2972 shown in Figure 4.8.6, the polar component exhibited a slight decline due to the $scCO_2$ treatment. In spite of the reduction in polar component, the total surface of this clay still increased due to relatively larger increase in its dispersive component. The increase in the dispersive component for SCPX 2972 can not be explained by surfactant extraction with $scCO_2$ because no decrease in organic content was observed (Table 4.2.5). It can also not be explained by swelling of clay particles since XRD data did not show evidence supporting any swelling of this clay. The most possible reasoning was a reduction in the exterior surfactant. However, TGA analysis in Figure 4.4.6 does not provide adequate resolution of features to confirm this hypothesis. Under $scCO_2$ conditions, it can again be seen that the surface energy of SCPX 2972 treated at 9.7 MPa, 50°C and 4.8 MPa/s was slightly less than the other two conditions. Similar to the results for SCPX 2934, Equation (4.4) showed that effect of coupled interaction of

temperature and pressure release rate on the hydration of treated SCPX 2972 was the biggest (larger than the main factors).

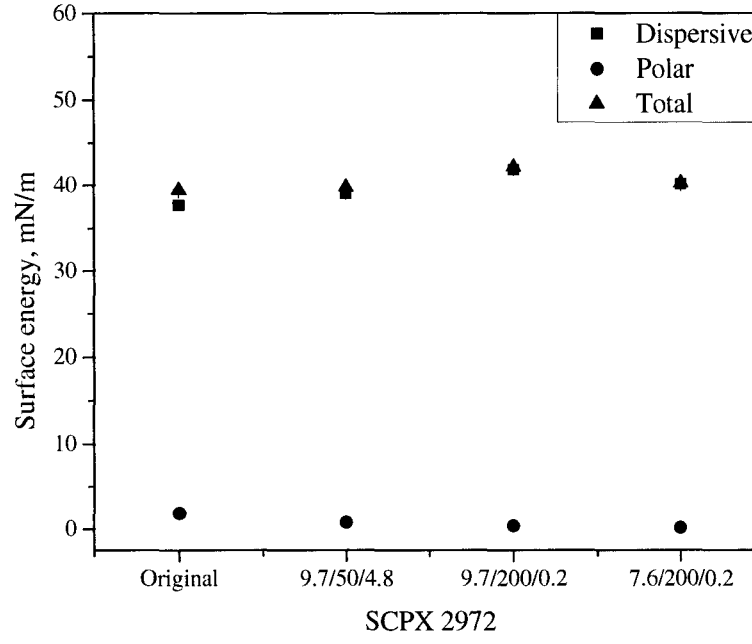

Figure 4.8.6 Surface energy of SCPX 2972 before and after $scCO_2$ treatment. X-axis labels refer to the CO_2 pressure (MPa)/vessel temperature (^{o}C)/pressure release rate (MPa/s)

For SCPX 2971, the surface energy slightly increased after $scCO_2$ treatment. Similar to SCPX 2972, the organic content in Table 4.2.4 and XRD result in Figure 4.3.6 do not support the increase in surface energy for SCPX 2971. Again, the possible reason may be the reduction in the exterior surfactant. Unfortunately, no related test such as TGA was available to confirm this reason.

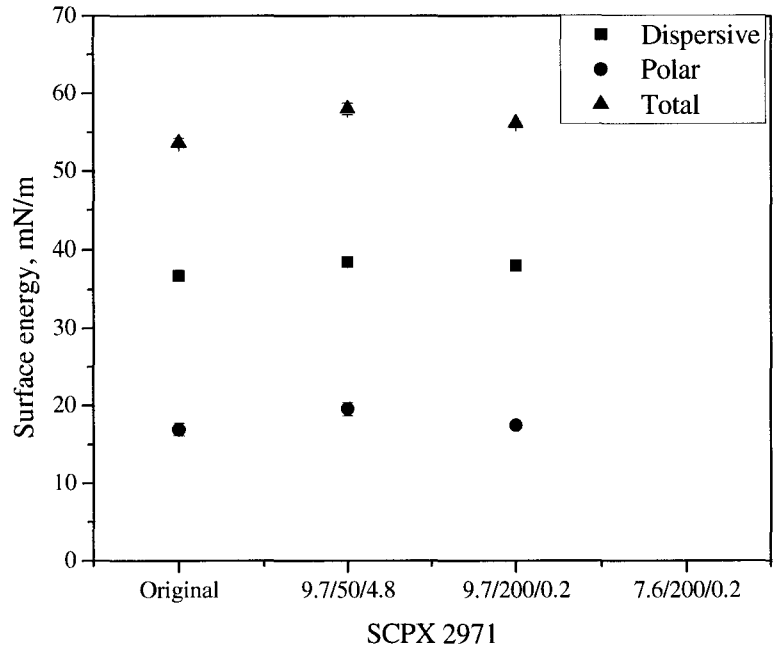

Figure 4.8.7 Surface energy of SCPX 2971 before and after $scCO_2$ treatment. X-axis labels refer to the CO_2 pressure (MPa)/vessel temperature (^oC)/pressure release rate (MPa/s)

4.9 Conclusions

All five surfactants, trimethyl-hydrogenated tallow alky ammonium, dimethyl-di-hydrogenated tallow alkyl ammonium, trihexadecyl methyl ammonium, dimethyl-di-coco alkyl ammonium, and trimethyl-benzyl ammonium, were determined to be thermally and chemically stable at the examined conditions. In spite of solubility of the organic surfactants in $scCO_2$ solvent, no organic extraction occurred during the $scCO_2$ treatment. However, this solubility led to greater mobility for the surfactant molecules. Under the $scCO_2$ environment, surfactant molecules physically adsorbed on clay surface and those intercalated by van der Waals forces were able to become end-tethered species by the

further cation exchange at residual sodium ion sites. The rearrangement of the surfactant molecules improved the organic coverage of the silicate interlayer, which resulted in a reduced availability of hydratable sites for these new materials. The reduced hydratable sites on these clays would be expected to improve their compatability with non-polar polymer resins and suggest a beneficial reason to pre-condition the clays prior to their addition to a nanocomposite compounding process. The surfactant rearrangement also resulted in changes in crystalline structure of the organoclays, i.e. the variation in basal spacing. The variation in basal spacing of an organoclay was determined by the surfactant conformation in between clay platelets. Basal spacing of oranoclays with their surfactants in conformations of lateral monolayer (SCPX 2971), lateral bilayer (SCPX 1137 and SCPX 2972), and completely paraffin-type (90° tilt angle) monolayer (SCPX 2934) were usually not affected significantly by the $scCO_2$ solvent. Only the organoclay with paraffin-type structure with a tilt angle less than 90°, i.e. Cloisite 20A, exhibited any increase in its interlayer distance. The expansion may be assumed as a result of increasing its tilt angle within the clay galleries. Higher temperature and pressure release rate facilitated expansion of the clay galleries and pressure showed little effect on the clay crystalline structure.

Change in surface energy of the organoclays resulted from the $scCO_2$ treatment was dependent upon the individual clays. Surface energy of SCPX 1137 and SCPX 2934 did not show significant variation after conditioning by $scCO_2$ whereas that of Cloisite 20A, SCPX 2972 and SCPX 2971 increased. Processing conditions did not show significant effect on this property.

The data in this chapter does not support any hypothesis of major swelling of the clay or particle fracture as a result of conditioning with supercritical carbon dioxide – either during exposure to the gas or upon its rapid removal. The minor swelling that did occur was not likely caused by an expanded radius of gyration for the alkyl moieties.

Rather the analysis suggested that the supercritical solvent was primarily a plasticizing aid leading to surfactant rearrangement.

CHAPTER 5 ORGANOCLAYS PROCESSED WITH SUPERCRITICAL CARBON DIOXIDE AND WATER CO-SOLVENT

Since the drying of organoclays is an extra processing step in the manufacturing of PLS nanocomposites, one which incurs additional operational costs for the material, it was desirable to see if the water present in clay could be used to improve the influence of $scCO_2$ rather than removing it. The work in this chapter represents a short study to examine this aspect.

5.1 Hydration, pH and organic content

Table 5.1.1 shows the hydration content, pH values and organic content of C20A before and after $scCO_2$ treatment with the presence of water as co-solvent. In order to display the effect of water co-solvent, results of the previous $scCO_2$-treated samples under the same conditions were added to the table. The organic content of the sample treated with $scCO_2$ /H_2O at 50°C was much higher than the others, indicating that temperature and water co-solvent may have a synergistic effect on the surfactant in C20A. The increased organic content may be attributed to two aspects: i) higher CO_2 concentration remaining after processing due to active Lewis acid/base sites in the clay, and ii) higher structural water content which can not be removed by standard drying procedures, brought into the interior by the $scCO_2$ under the conditions of 9.7 MPa, 50°C and 0.2 MPa/s. Temperature was a key factor to the influence of the hydrated moisture during the

$scCO_2$ treatment. At 50°C, the hydrated moisture would have remained in the clay even under the $scCO_2$ environment; however, the water would seem to be removed from the sample when exposed to the $scCO_2$ environment at 200°C. In Table 5.1.1, we can see that the organic content of the hydrated sample treated at 9.7 MPa, 200°C and 0.2 MP/s was as same as that treated without the co-solvent for the same conditions. It may also be due to the moisture accommodated in the $scCO_2/H_2O$ treated sample under 50°C that the hydration content after CO_2 treatment of this sample was significantly lower than the others. This is confirmed by the same pH values of the two hydrated samples. Interestingly, pH values of $scCO_2/H_2O$ treated C20A samples were lower than those of the untreated sample and $scCO_2$ treated samples. This could signify the generation of carbonic acid during the $scCO_2$ treatment. Unfortunately, our experiences with FTIR have not shown it to be a sufficiently sensitive technique to help resolve such chemical matters at the moment.

Table 5.1.1 Organic content, hydration content and pH of C20A before and after $scCO_2$ treatment

Sample description	**Organic content wt % ***	**Hydration content wt % †**	**pH**
Original	38.5	6.3	7.1 ± 0.0
Water co-solvent 9.7 MPa, 50°C, 0.2 MPa/s	42.1	2.9	6.4 ± 0.1
Water co-solvent 9.7 MPa, 200°C, 0.2 MPa/s	38.9	4.5	6.6 ± 0.2
No co-solvent 9.7 MPa, 50°C, 0.2 MPa/s	39.3	3.8	7.2 ± 0.0
No co-solvent 9.7 MPa, 200°C, 0.2 MPa/s	39.0	4.9	7.2 ± 0.1

* Maximum error for the organic content measurement was ± 1.0 wt %.

† Maximum error for the hydration content measurement was ± 0.3 wt %.

Results of hydration uptake, pH value and organic content for SCPX 2934 before and after $scCO_2$ treatment are shown in Table 5.1.2. Similar to C20A, the hydration content of SCPX 2934 after $scCO_2$ treatment decreased under both conditions, and yet higher organic content and lower hydration amount were found for the sample with treated with $scCO_2/H_2O$ at 50°C compared to at 200°C. Different from C20A, however, all pH values of SCPX 2934 samples were basically identical.

Table 5.1.2 Organic content, hydration ability and pH of SCPX 2934 before and after $scCO_2$ treatment

Sample description	**Organic content wt % ***	**Hydration content wt % †**	**pH**
Original	44.2	6.6	6.3 ± 0.1
Water co-solvent 9.7 MPa, 50°C, 0.2 MPa/s	45.8	2.6	6.0 ± 0.0
Water co-solvent 9.7 MPa, 200°C, 0.2 MPa/s	44.4	3.0	6.6 ± 0.1
No co-solvent 9.7 MPa, 50°C, 0.2 MPa/s	44.1	3.0	6.8 ± 0.0
No co-solvent 9.7 MPa, 200°C, 0.2 MPa/s	44.6	3.8	6.6 ± 0.0

* Maximum error for the organic content measurement was ± 1.0 wt %.

† Maximum error for the hydration content measurement was ± 0.3 wt %.

5.2 Basal spacing

Swelling of $scCO_2/H_2O$ treated C20A particles was characterized by XRD and TEM methods. The XRD results are shown in Figures 5.2.1 and 5.2.2. Under the same treatment conditions, compared to the species without water co-solvent, 2θ angle of (001) diffraction peak for the $scCO_2/H_2O$ treated C20A shifted to lower value, clearly indicating that water promoted greater clay expansion under $scCO_2$ environment. This is

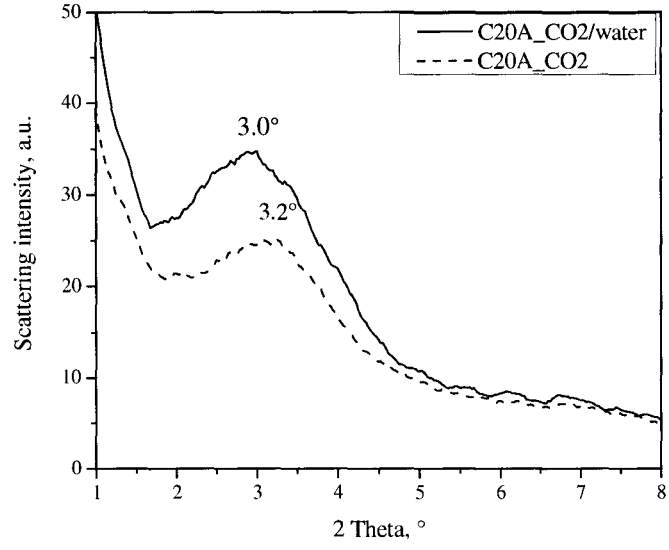

Figure 5.2.1 Comparison of XRD patterns of C20A treated with $scCO_2$ with and without presence of water co-solvent under 9.7 MP, 200°C and 0.2 MPa/s

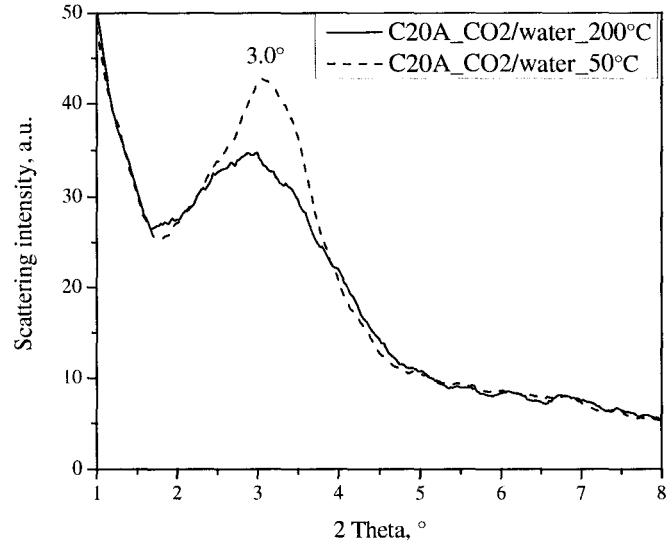

Figure 5.2.2 Comparison of XRD patterns of hydrated C20A treated with $scCO_2$ under different temperatures of 200°C and 50°C

an interesting result. TGA analysis in the following section may help us understand the phenomena. Figure 5.2.2 shows the difference in XRD patterns of the hydrated C20A treated with $scCO_2$ at 200°C and 50°C. Though positions of the (001) diffraction peak for the two case were identical, peak intensity for 50°C was significantly higher than that for 200°C, indicating that high temperature led to more heterogeneity in microstructure of the clay.

Observations of the powder particles for the $scCO_2/H_2O$ treated C20A by TEM confirmed the XRD results. Figure 5.2.3 gives the TEM micrographs for C20A treated with $scCO_2/H_2O$ at both conditions of 200°C and 50°C. In comparison with Figure 4.6.1 showing C20A treated with only $scCO_2$ at 9.7 MPa, 200°C and 0.2 MPa/s, we note that the co-solvent treated particles exhibited a looser packing of tactoids within the viewable exterior region of the particle. In fact, for the 50°C condition, some tactoids had been replaced with ordered exfoliated structures while none were evident at 200°C.

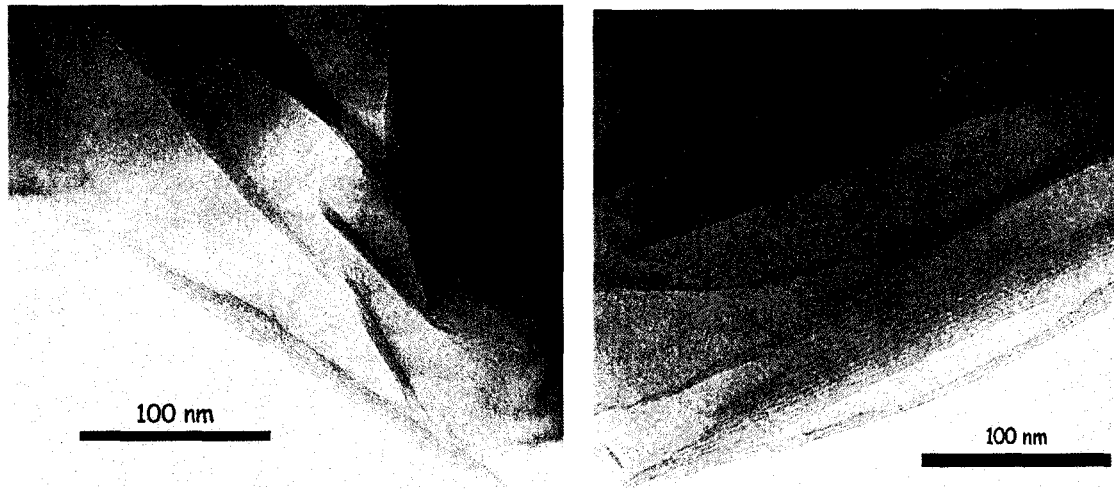

(a) (b)

Figure 5.2.3 TEM images of C20A processed with $scCO_2/H_2O$ at (a) 9.7 MPa, 200°C and 0.2 MPa/s and (b) 9.7 MPa, 50°C and 0.2 MPa/s

XRD results of SCPX 2934 treated with $scCO_2$ in the presence of water co-solvent are shown in Figure 5.2.4. In order to illustrate the effect of water co-solvent, SCPX 2934 treated without water co-solvent at 9.7 MPa, 200°C and 0.2 MPa/s was included in this figure. We note that the X-ray diffraction curve of (001) crystalline plane for the hydrated clay treated with $scCO_2$ under 200°C superposed over that for the un-hydrated sample treated under the same conditions, indicating that water co-solvent had no effect on the expansion of this clay treated under 200°C, consistent with previous observations in last chapter where swelling of SCPX 2934 never occurred after $scCO_2$ treatment under varied conditions. However, the diffraction peak for the hydrated SCPX 2934 treated with $scCO_2$ at 50°C was slightly shifted to a lower 2θ angle indicating that minor expansion of the clay occurred. It may be assumed that the expansion was simply induced by the water accommodated in the clay and was not related to the $scCO_2$ treatment. XRD analysis of the hydrated SCPX 2934 before its $scCO_2$ treatment may help confirm this. Unfortunately,

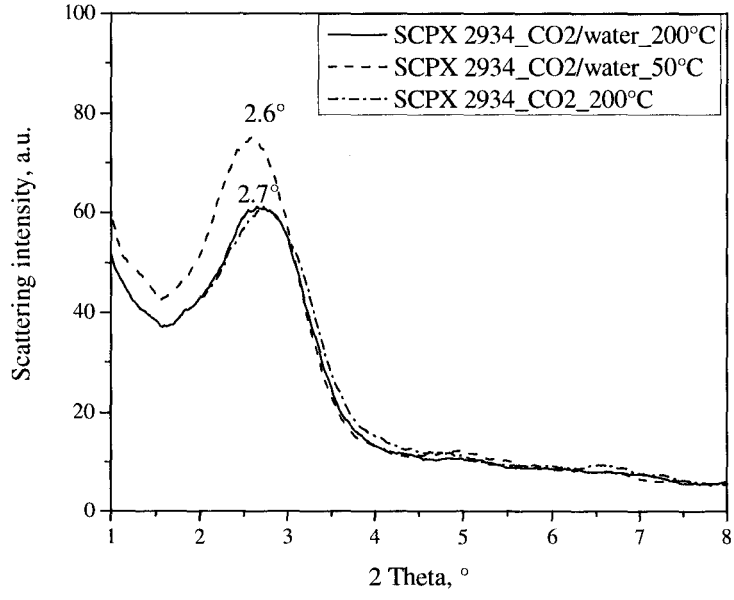

Figure 5.2.4 XRD patterns of SCPX 2934 treated with $scCO_2$ with the presence of water cosolvent at 9.7 MPa, 200°C and 0.2 MPa/s and 9.7 MPa, 50°C and 0.2 MPa/s

the measurement was not performed in consideration of moisture loss of the hydrated sample. As mentioned in last section, hydrated water may stay in the clay after $scCO_2$ treatment at 50°C. Morphologies of $scCO_2/H_2O$ treated SCPX 2934 processed at the two temperatures obtained by the TEM were shown in Figure 5.2.5. Similar to the micrographs of the $scCO_2$ treated clay shown in Figure 4.6.3, the tactoid structure of SCPX 2934 was unaltered by the treatment with the co-solvent, in agreement with the XRD observations.

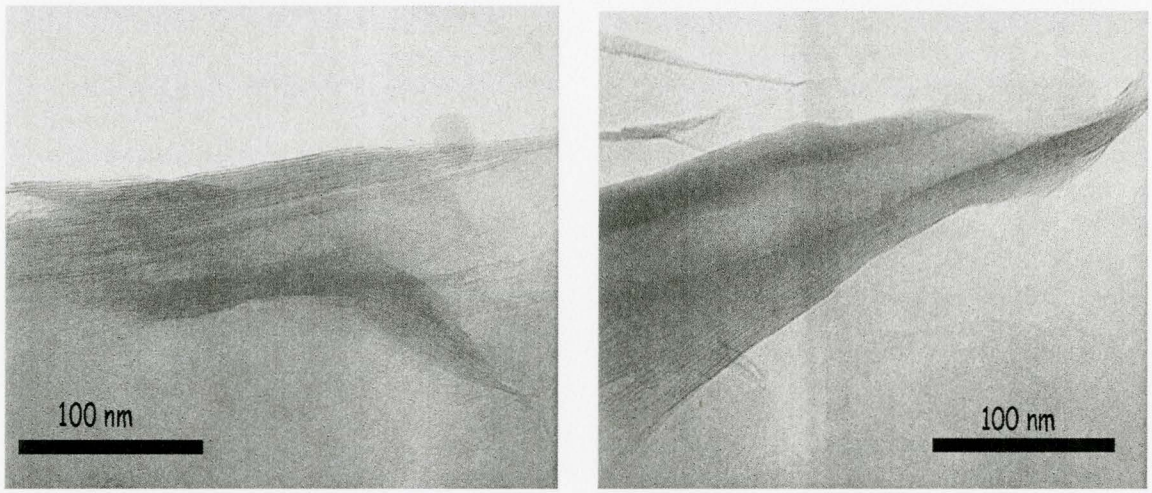

(a) (b)

Figure 5.2.5 TEM images of SCPX 2934 processed with $scCO_2$ and with water as cosolvent at (a) 9.7MPa, 200°C and 0.2MPa/s and (b) 9.7MPa, 50°C and 0.2MPa/s

5.3 Thermogravimetric analysis

The TGA results of C20A processed with $scCO_2$ with and without water as co-solvent under same conditions (9.7 MPa, 200°C and 0.2 MPa/s) are shown in Figure 5.3.1. The TGA thermogram for C20A in its original state was included to demonstrate the change of surfactant arrangement as a result of the $scCO_2$ treatment. We can see from the

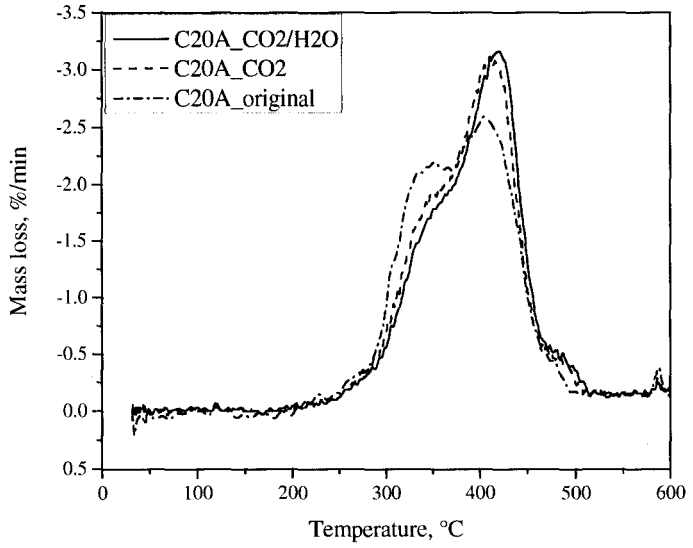

Figure 5.3.1 Comparison of TGA results between Cloisite 20A treated by $scCO_2$ with and without the presence of water co-solvent under 9.7 MPa, 200°C and 0.2 MPa/s

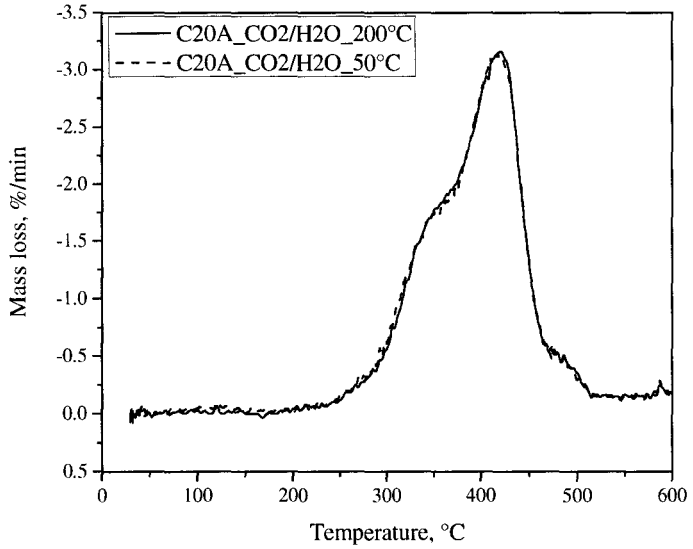

Figure 5.3.2 Comparison of TGA results between C20A treated with $scCO_2$ with water as cosolvent under 9.7 MPa, 200°C and 0.2 MPa/s and 9.7 MP, 50°C and 0.2 MPa/s

figure that an increase in the intensity of the peak at ~ 420°C and a corresponding decrease in the shoulder peak at ~330°C occurred indicating that the water co-solvent assisted some of the tail-to-tail bound surfactant molecules to transfer to the end-tethered species probably via further cation-exchange with the residual sodium ions. As discussed in Section 4.4.2, the increased end-tethered surfactant may lead to a higher tilt angle of the surfactant molecules arranged in the monolayer paraffin-type structure within the clay galleries, and therefore resulted in the increase in basal spacing observed by XRD analysis. The differential mass loss peak for the end-tethered shifted to higher temperature value indicating that the $scCO_2$ treatment with water as co-solvent improved thermal stability of the surfactant.

The TGA results of C20A treated with $scCO_2/H_2O$ under different temperatures are shown in Figure 5.3.2. It can be seen from the figure that the two curves can be superimposed over one another indicating that there was no difference in the surfactant arrangement between 200°C and 50°C, which is consistent with the observation by the XRD analysis.

As shown in Figure 5.3.3, all measured TGA curves for SCPX 2934, no matter what state it was, i.e. in its original state, treated states with a single solvent of $scCO_2$ or with water as co-solvent under different conditions, there was no difference among them. These results were consistent with the observations by XRD analysis, indicating that there were no changes in the surfactant packing. The minor expansion of SCPX 2934 treated with $scCO_2/H_2O$ under 9.7 MPa, 50°C and 0.2 MPa/s shown in Figure 5.2.4 was thought to be attributed to the water accommodated in the clay. TGA result of the sample confirmed this assumption.

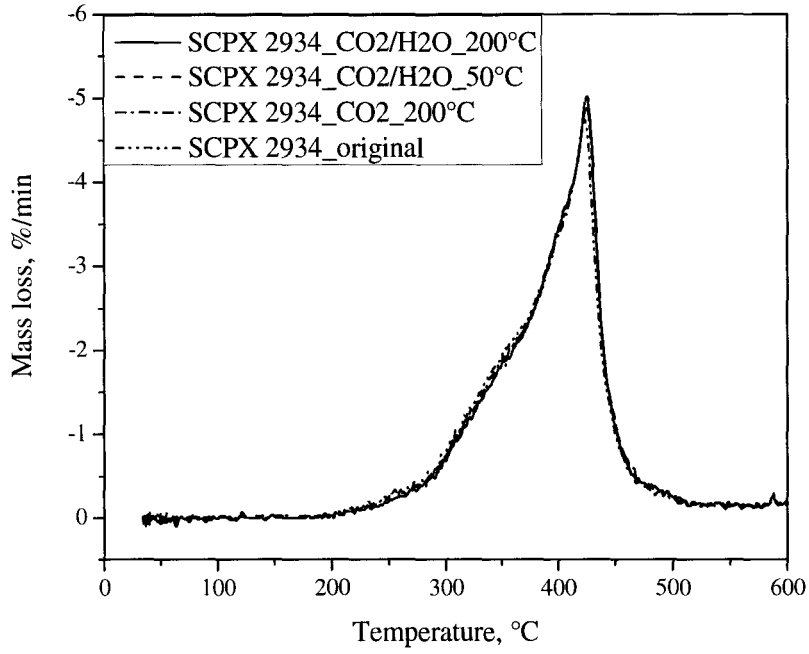

Figure 5.3.3 Differential mass loss plots determined by TGA for SCPX 2934: treated with $scCO_2$ and with water as cosolvent under 9.7 MPa, 200°C and 0.2 MPa/s and 9.7 MPa, 50°C and 0.2 MPa/s, treated with only $scCO_2$ at 9.7 MPa, 200°C and 0.2 MPa/s, and in its original state

5.4 Surface energy

As shown in Figure 5.4.1 and Figure 5.4.2, the $scCO_2/H_2O$ treated C20A and SCPX 2934 exhibited the same trend in that the surface energy increased after the treatment yet there were no difference in surface energy values between with and without water as a cosolvent. For C20A, the treated clay exhibited a greater dispersive component than the clay in its original state while the polar component did not change. For SCPX 2934, the polar component of the treated species decreased significantly compared to the original clay, but the dispersive component increased much more, and therefore the total

surface energy for the treated clays appeared to significant increase in comparison to the untreated clay. Based on the differences seen in the TGA particularly, we can see that the surface energy measurement was not sensitive to interior changes in the clay structure.

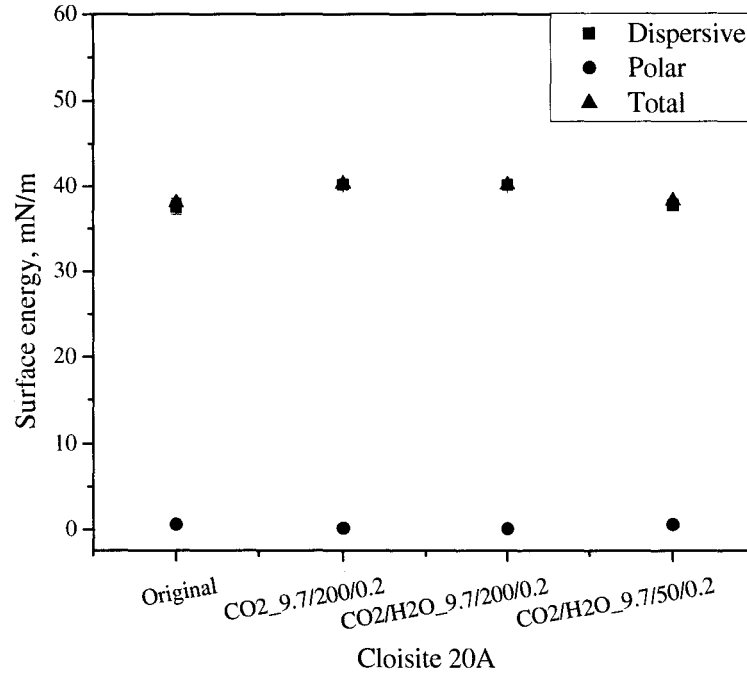

Figure 5.4.1 Surface energy of C20A in its original state, treated with CO_2 or with CO_2/H_2O. X-axis labels refer to the CO2 pressure (MPa)/vessel temperature (^{o}C)/pressure release rate (MPa/s)

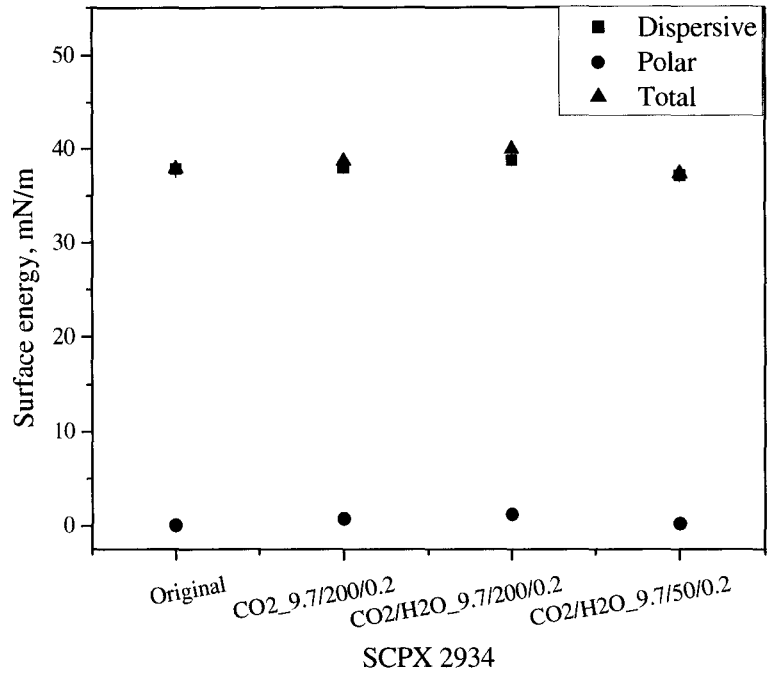

Figure 5.4.2 Surface energy of SCPX 2934 in its original state, treated with CO_2 or with CO_2/H_2O. X-axis labels refer to the CO2 pressure (MPa)/vessel temperature (^{o}C)/pressure release rate (MPa/s)

5.6 Conclusions

The effect of the water co-solvent on the microstructure of an organoclays depends on the clay species. For C20A, the effect was significant. With help of the moisture accommodated in the C20A, the surfactant redistribution proceeded more readily, allowing more surfactant to be transferred to ionically bound species on the silicate surface. This transition led to a more loosely packed tactoid structure and even some ordered exfoliated structures. Lower processing temperatures were important to preserve the off-line properties of these clays, though it is not known yet whether this

criterion extends to in-situ. Use of the water co-solvent with SCPX 2934 had little effect on the microstructure, but no less so than the $scCO_2$-processed samples.

CHAPTER 6 CONCLUSIONS AND RECOMMENDATIONS

6.1 Conclusions

This thesis has discussed changes to microstructures of organoclays produced by treatment with supercritical carbon dioxide, with and without water as a co-solvent, under varied conditions. The surfactant arrangements of the as-received organoclays examined were determined as a lateral monolayer for SCPX 2971 and SCPX 2972, a lateral bilayer for SCPX 1137, a paraffin-type monolayer with tilt angle less than 90° for Cloisite 20A, and a paraffin-type monolayer with tilt angle of ~90° for SCPX 2934. The surfactant arrangement between silicate sheets and the surfactant's structure itself determined whether change of an organoclay occurred for the microstructure by $scCO_2$ treatment. Only Cloisite 20A, the organoclay with two long alkyl chain surfactant and paraffin-type monolayer structure with a tilt angle less than 90°, exhibited basal expansion after $scCO_2$ treatment. Only SCPX 2971, the clay with aromatic surfactant and lateral monolayer structure, remained completely unchanged under any trial condition. The interlayers of SCPX 1137, SCPX 2972 and SCPX 2934 either remained unchanged or collapsed slightly after the $scCO_2$ treatment, depending upon the treatment conditions. Under almost all conditions and for all clays, the treatment with $scCO_2$ had no major effect on the exterior chemistry that would change the interfacial properties. The majority of change by scCO2 was in the interior of the clays.

Expansion of Cloisite 20A was attributed to surfactant rearrangement and an increase in the tilt angle of surfactant due to the $scCO_2$ treatment. High temperatures and high pressure release rate promoted the clay expansion. High temperatures led to melting of the surfactant crystals and increased surfactant mobility. Explosive depressurization may produce a force inside galleries of the clay particles sufficient to push out the silicate sheets.

The high melting point of the aromatic surfactant for SCPX 2971 may have been responsible for its unchanged microstructure under $scCO_2$ because the solid-like surfactant confined in clay galleries was difficult to move even under the supercritical fluid environment. In addition, lateral monolayer surfactant arrangements are more difficult to turn to other structures through surfactant rearrangement or even concentration changes.

The lateral bilayer structure and higher melting point of confined surfactant in SCPX 1137 galleries were the reasons for the morphology stability of this clay in the $scCO_2$ processing. Only under high temperature and high pressure, did the morphology of this clay exhibited even minor changes due to increased mobility of the surfactant and increased solubility of $scCO_2$.

In spite of low melting point and ready removal of the surfactant in SCPX 2934, the erect paraffin-type structure constrained further increases in its gallery spacing. Conversely, the surfactant mobility under the $scCO_2$ environment may result in denser surfactant packing and therefore, a minor collapse occurred under most conditions examined.

Interaction of the $scCO_2$ with an organoclay took place primarily by its plasticization on surfactant of the clay. No chemical reaction occurred during the $scCO_2$ processing, though in the presence of the water co-solvent Lewis acid/base reactions were

thought to alter the silicate chemistry, resisting further hydration. Use of water as a co-solvent was found to help expand Cloisite 20A and even partially exfoliate it in some extent, but the water had no discernable effect on the morphology of SCPX 2934.

Considering swelling behavior in the $scCO_2$ treatment and surface energy, Cloisite 20A and SCPX 2934 were thought the ideal candidates for next stage of the project.

6.2 Recommendations

Studies on the interaction of $scCO_2$ with organoclays in this thesis were off-line. An in-situ XRD study [Thompson et al. 2008] showed that pressure had a stronger effect on basal spacing than temperature, and that higher pressures were favored, different from the off-line study in this thesis. Considering an alternative route for preparing PLS nanocomposites, an organoclay may need to maintain suspension state in $scCO_2$ solvent, some in-situ analyses, for instance, FT-IR and TGA, may be needed. The in-situ analysis may help us better understand the interaction between $scCO_2$ and an organoclay and microstructure of an organoclay suspended in $scCO_2$ solvent.

Water as a co-solvent proved to favor expansion of Cloisite 20A. It may also be a helpful co-sovent in following step in preparation of PLS nanocomposites. In such a case SCPX 2971 might be revisited as a viable organoclay since it exhibited full exfoliation after washing with mixture of water and ethanol. Currently it has been excluded from the list of ideal candidates due to its high surface energy and rigid surfactant structure and there remain fears of its possible agglomeration in TPO nanocomposites due to its high hydrophilicity. However, it could be fully exfoliated by the water co-solvent/scCO2 system before compounding with a polymer melt, it may still be an interesting species for our system.

LIST OF REFERENCES

Alexandre, M. and Dubois, P. Polymer-layered silicate nanocomposites: preparation, properties and uses of a new class of materials, Mater. Sci. Eng. 2000, 28: 1-63

Bachx P, Goldman S, J. Phys. Chem. 85 (1981), 2975

Barry JJA, Gidda HS, Scotchford CA, Howdle SM. Porous methacrylated scaffolds: supercritical fluid fabrication and in vitro chondrocyte responses, Biometerials 25 (2004), 3559-3568

Bertini F, Canetti M, Audisio G, Costa G, Falqui L, Characterization and thermal degradation of polypropylene-montmorillonite nanocomposites, Polymer Degradation and Stability 91 (2006), 600-605

Bonczek JL, Harris WG, Nkedi-Kizza P, Monolayer to bilayer transitional arrangements of hexadecyltrimethylammonium cations on Na-montmorillonite, Clays Clay Miner., 50 (2002), 11-17

Bongiovanni R, Mazza D, Ronchetti S, Turcato EA, The finfluence of water on the intercalation of epoxy monomers in Na-montmorillonite, J. Coll. Interf. Sci. 296 (2006), 515-519

Braida I, Mattea M, Cardarelli D. Extraction-adsorption-desorption process under supercritical condition as a method to concentrate antioxidants from natural sources, J. Supercritical Fluids, *In Press*, 2007

Chatterjee A, Iwasaki T. Ebina T, Miyamoto A, A DFT study on clay-cation-water interaction in montmorillonite and beidellite, Computational Materials Science 14 (1999), 119-124

Chernyak Y, Henon F, Harris RB, Gould RD, Franklin RK, Edwards FR, DeSimone JM, Carbonell RG. Formation of Perfluoropolyether coatings by the rapid expansion of supercritical solutions (PESS) process, Part 1: Experimental Results. Ind. Eng. Chem. Res. 40 (2001), 6118-6126

Clark K, Lee S, Removal of ungrafted monomer from polypropylene-graft-maleic anhydride via supercritical carbon dixide extraction, Polym. Eng. Sci., 44(9) (2004), 1636-1641

De Rosa C, Auriemmna F, Capitani D, Caporaso L, Talarico G, Solid state ^{13}C NMR analysis of syndiotactic copolymers of propene with 1-butene, Polymer 41 (2000), 2141-2148

De Simone JM, Paisner SN. Methods of forming porous polymeric structures using carbon dioxide and polymeric structures formed thereby, USA patent, US: 2003180522, 2003

Deng Y, Dixon JB, White GN, Intercalation and surface modification of smectite by two non-ionic surfactants, Clays and Clay Materials 51 (2003), 150-161

Dennis HR, Hunter DL, Chang D, Kim S, White JL, Cho JW, Paul DR. Effect of melt processing conditions on the extent of exfoliation in organoclay-based nanocomposites. Polymer 2001, 42, 9513-9522

Dong Z, Liu Z, Han B, Pei X, Liu L, Yang G. Modification of isotactic polypropylene films by grafing of methyl acrylate using supercritical CO_2 as a swelling agent. J Supercrit Fluids, 32 (2004) 67-74

Durmus A, Kasgoz A, Macosko CW, Linear low density polyethylene (LLDPE)/clay nanocomposites. Part I: Structural characterization and quantifying clay dispersion by melt rheology, Polymer 48 (2007)4492-4502

Eleektorowicz M, El-Sadi H, Lin J, Ayadat T. Effect of supercritical fluid extraction parameters and clay properties on the efficiency of phenanthrene extraction, J. Colloid Inerface Sci. 309 (2007), 445-452

Elkovitch MD, Lee LJ, Tomasko DL. Effect of supercritical carbon dioxide on morphology development during blending. Polym. Eng. Sci. 40 (2000), 1850-1861

Erman B, Mark JE, Science and Technology of Rubber, Elsevier Academic Press, 2005

Favre H, Lagaly G, Clay Miner. 26 (1991), 19

Fornes TD, Yoon PJ, Hunter DL, Keskkula H, Paul DR. Effect of organoclay structure on nylon 6 nanocomposite morphology and properties. Polymer 43 (2002), 5915-5933

Frost RL, Zhou Q, He H, Xi Y, An infrared study of adsorption of para-nitrophenol on mono-, di- and tri-alkyl surfactant intercalated organoclays, Spectrochimica Acta Part A, 69 (2008), 239-244

Fujiwara T, Yamaoka, Kimura Y, Wynne KJ. Poly(lactide) swelling and melting behavior in supercritical carbon dioxide and post-venting porous material, Biomacromolecules, 6 (2005), 2370-2373

García-López D, Gobernado-Mitre I, Merino JC, Pastor JM, Effect of the amount and funtionalization grade of PPgMA compatibilization agent in polypropylene/clay nanocomposites, Polymer Bulletin 59 (2007), 667-676

Giannelis EP, Krishnamoorti R, Manias R, Polymer-silica nanocomposites: model systems for confined polymers and polymer brushes, Adv. Polym. Sci. 1999; 118: 108-147

Glebov EM, Krishtopa LG, Stepanov V, Krasnoperov LN, Kinetics of a Diels-Alder reaction of maleic anhydride and isoprene in supercritical CO_2, J. Phys. Chem. A, 105 (2001), 9427-9435

Gokel GW, Dean's Handbook of Organic Chemistry, Second Edition, *McGraw-Hill*, 2004

Hao J, Whitaker MJ, Serhatkulu G, Shakesheff KM, Howdle SM. Supercritical fluid assisted melting of poly(ethylene glycol): a new solvent-free route to micro particles, J. Mater. Chem. 15 (2005), 1148-1152

Hasegawa N, Okamoto H, Kato M, Usuki A, Sato N, Nylon 6/Na-montmorillonite nanocomposites prepared by compounding Nylon 6 with Na-montmorillonite slurry, Polymer 44 (2003), 2933-2937

He H, Frost RL, Bostrom T, Yuan P, Duong L, Yang D, Xi Y, Kloprogge JT, Changes in the morphology of organoclays with $HDTMA^+$ surfactant loading, Appli. Clay Sci. 31 (2006), 262-271

He H, Duchet J, Galy J, Gerard JF, Influence of cationic surfactant removal on the thermal stability of organoclays, J. Coll. Interf. Sci. 2006; 295: 202-208

Hong, C. H., Lee, Y. B., Bae, J. W., Jho J. Y., Nam B. U., Hwang, T. W., Molecular Weight Effect of Compatibilizer on Mechanical Properties in Polypropylene/Clay Nanocomposites, J. Ind. Eng. Chem. 2005, 11, 293-329

Horsch S, Serhatkulu G, Gulari E, Kannan RM, Supercritical CO_2 dispersion of nano-clays and clay/polymer nanocomposites, Polymer 47 (2006), 7485-7496

Horsch S, Serhatkulu G, Gulari E, Kannan RM, Supercritical CO_2 intercalation of layered silicates, J. Supercrit. Fluids 39 (2006), 264-270

Huang X, Margulis CJ, Li Y, Berne BJ, Why is the partial molar volume of CO_2 so small when dissolved in a room temperature ionic liquid? Structure and dynamics of CO_2 dissolved in [Bmim+][PF6-], J. Am. Chem. Soc. 127 (2005), 17842-17851

Ishii R, Wada H, Ooi K. A comparison of supercritical carbon dioxide and organic solvents for the intercalation of 4-phenylazoaniline into a pillared clay mineral, J. Colloid Interface Sci. 254 (2002), 250-256

Iveson S, Litster JD, Hapgood K, Ennis BJ, Nucleation, growth and breakage phenomena in agitated wet granulation processes: a review, Powder Technology, 117 (2001), 3-39

Jordan JW, Organophilic bentonites, I. Swelling in organic liquids, J. Phys. Colloid Chem. 1949; 53:294-306

Kato M, Usuki A, Okada A. Synthesis of Polypropylene Oligomer-Clay interaction Compounds. J. Appl. Polym. Sci. 1997, 66, 1781-1785

Kawasumi M, Hasegawa N, Kato M, Usuki A, Okada A. Preparation and Mechanical Properties of Polypropylene-Clay Hybrids. Macromolecules 1997, 30, 6333-6338

Kavahara Y, Yoshioka T, Sugiura K, Ogawa S, Kikutani T. Dyeing behavior of high-speed spun poly(ethylene terephthalate) fibers in supercritical carbon dioxide, J. Macromol. Sci. B: Phys. 40(2) (2001), 189-197

Kazarian SG, Brantley NH, Eckert CA. Dyeing to be clean: Use supercritical carbon dioxide, CHEMTECH, July 1999, 36-41

Kazarian SG, Polymers and Supercritical Fluids: Opportunities for Vibrational Spectroscopy, Macromol. Symp. 184 (2002), 215-228

Kazarian S, Briscoe BJ, Welton T, Combining ionic liquids and supercritical fluids: in situ ATR-IR study of CO_2 dissolved in two ionic liquids at high pressure, Chem. Commun. 2000, 2047-2048

Kemmere MF, Meyer T. Supercritical carbon dioxide in polymer reaction engineering, Wiley-Vch Verlag GmbH & Co. kGaA, Winheim, Germany, 2005

Kim S, Kim Y-S, Lee S-B. Phase behaviors and fractionation of polymer solutions in supercritical carbon dioxide, J. Supercrit. Fluids, 13 (1998), 99-106

Kim DH, Fasulo PD, Rodgers WR, Paul DR, Effect of the ratio of maleated polypropylene to organoclay on the structure and properties of TPO-based nanocomposites. Part I: Morphology and mechanical properties, Polymer, 48 (2007), 5960-595978

Koh S-M, Dixon JB, Preparation and application of organo-minerals as sorbents of phenol, benzene and toluene, Appl. Clay Sci. 18 (2001), 111-122

Kojima Y, Usuki A, Kawasumi M, Okada A, Fukushima Y, Kurauchi T, Kamigaito O. Mechanical properties of nylon 6-clay hybrid. J Mater Res 1993; 8: 1185–1189

Kojima Y, Fukumori K, Usuki A, Kawasumi M, Okada A, Kurauchi T, Kamigaito O. Gas permeabilities in rubber-clay hybrid. J Mater Sci Letters 1993; 12: 889–890

Kojima Y, Usuki A, Kawasumi M, Okada A, Kurauchi T, Kamigaito O. Sorption of Water in Nylon 6-Clay Hybrid. J Appl Polym Sci 1993; 49: 1259–1264

Lagaly G, Layer charge determination by alkylammonium ions, In Clay Minerals Society Workshop Lectures 6, Layer Charge Characteristics of 2:1 Silicate Clay Minerals, A.R. Mermut (Ed.), Boulder, Colorado, 1994

Lagaly G, Interaction of alkylamines with different types of layered compounds, Solid State Ionics 22 (1986), 43-51
Lagaly G, Layer charge heterogeneity in vermiculites, Clays and Clay Minerals 30 (1982), 215-222

Lagaly G, Gonzalez MF, Weiss A, Problems in layer-charge determination of montmorillonites, Clay Minerals 11 (1976), 173-187

Lee SY, Kim SJ, Transmission electron microscopy of hexadecyltrimethylammonium-exchanged smectite, Clay Miner. 37 (2002), 465-471

Lertwimolnun W., Vergnes B., Influence of Compatibilizer and Processing Conditions on the Dispersion of Nanoclay in a Polypropylene Matrix, Polymer, 2005, 46: 3462-3471

Li D, Han B, Liu Z. Grafting of 2-hydroxyethyl methacrylate onto isotactic polypropylene using supercritical CO_2 as a solvent and swelling agent. Macromol. Chem. Phys. 202 (2001), 2187-2194

Lim ST, Choi HJ, Jhon MS, Dispersion quality and rheological property of polymer/clay nanocomposites: Ultrasonification effect, J. Ind. Eng. Chem. 2003, 9:51-57

Litchfield D, Nguyen Q, Baird Donald. Super-critical carbon dioxide assisted melt intercalation of polymer layered silicate nanocomposites, ANTEC 2007, 72-75

Liu H-C, Shih H-H, Tsai C-C, Uw C-T, Liu W-B. Manufacturing polymeric foam using supercritical fluids, USA Patent, US: 2003057197, 2003

Liu T, Hu G-H, Tong G-S, Zhao L, Cao G-P, Yuan W-K. Supercritical carbon dioxide assisted solid-state grafting of maleic anhydride onto polypropylene, Ind. Eng. Chem. Res. 44 (2005), 4292-4299

Liu Z, Song L, Dai X, Yang G, Han B, Xu J. Grafting of methylacrylate onto isotactic polypropylene film using supercritical CO_2 as a swelling agent, Polymer 43 (2002), 1183-1188

Lu W, Loerner H, Vaia R, Effect of electric field on exfoliation of nanoplates, Appl. Phys. Lett. 2006, 89: Art. No. 223118

Ma J, Bilotti E, Peijs T, Darr JA, Preparation of polypropylene/sepiolite nanocomposites using supercritical CO_2 assisted mixing, European Polymer Journal 43 (2007), 4931-4939

Manke CW, Gulari E, Mielewski DF, Lee EC-c, System and method of delaminating a layered silicate material by supercritical fluid treatment, US Patent 6,469,073 (2002)

McHugh MA, Krukonis VJ. Supercritical Fluid Extraction, Butterworth-Heinemann, Stoneham, MA, 2nd edition, 1994

Maiti P, Nam PH, Okamoto M, Kotaka T, Hasegawa N, Usuki A, The effect of crystallization on the structure and morphology of polypropylene/clay nanocomposites, Polym. Eng. Sci. 42 (2002), 1864-1871

Mendes MF, Coelho GLV. Desorption processes: Supercritical fluid regeneration of modified clays, Adsorption, 11 (2005), 139-146

Mielewski DF, Lee EC-c, Manke CW, Gulari E, System and method of preparing a reinforced polymer by supercritical fluid treatment, US Patent 6,753,360 (2004)

Nalawade SP, Picchioni F, Marsman JH, Janssen LPBM, The FT-IR studies of the interactions of CO_2 and polymers having different chain groups, J. Supercritical Fluids, 36 (2006), 236-244

Nguyen QT, Baird DG. An improved technique for exfoliating and dispersion nanoclay particles into polymer matrices using supercritical carbon dioxide, Polymer 48 (2007), 6923-6933

Oriakhi, C. Nano sandwiches, Chemistry in Britain 1998, 34: 59-62

Osman MA, Ploetze M, Suter UW, Surface treatment of clay minerals – thermal stability, basal-plane spacing and surface coverage J. Mat. Chem 13 (2003), 2359-2366

Osman MA, Seyfang G, Suter UW, Two-dimensional melting of alkane monolayers ionically bonded to mica, J. Phys Chem B 104 (2000), 4433-4439

Owens D, Wendt RC, Estimation of the Surface Free Energy of Polymers, *J. Appli. Polym. Sci.* 13 (1969), 1741–1747

Pinnavaia, T.J., G.W. Beall, Polymer-Clay Nanocomposites, New York, Wiley, 2000

Polubesova T, Rytwo G, Nir S, Serban C, Margulies L, Adsorption of benzyltrimethyl ammonium and benzyltriethyl ammonium on montmorillonite: Experimental studies and model calculations, Clays Clay Miner. 45 (1997), 834-841

Ravishanker G, et al. J. Am. Chem. Soc., 106 (1984), 4102-4108

Reutergardh LB, Parkpian P, Chaiyaraksa C. Supercritical fluid extraction of planar and mono-ortho PCB in selected tropical soils, Chemosphere 36(7) (1998), 1565-1573

Runt JP, "Crystallinity Determination", Encyclopedia of Polymer Science and Engineering, 2nd ed., Vol.4, Wiley and Sons, N.Y. (1986)

Schmidt D., Shah D. Giannelis E.P., New advances in polymer/layered silicate nanocomposites, Current Opinion in Solid State and Materials Science, 2002, 6: 205-212

Shal RK, Paul DR. Organoclay degradation in melt processed polyethylene nanocomposites. Polymer 47 (2006), 4075-4084

Shi D, Yang J, Yao Z, Wang Y, Huang H, Jing W, Yin J, and Gosta G. Functionalization of Isotactic Polypropylene with Maleic Anhydride by Reactive extrusion: mechanism of melt grafting. Polymer 2001, 42: 5549-5557

Simon L, private communications, 2006

Song R, Wang Z, Meng X, Zhang B, Tang T, Influences of catalysis and dispersion of organically modified montmorillonite on flame retardancy of polypropylene nanocomposites, J. Appl. Polym. Sci., 106 (2007), 3488-3494

Soares VL, Nascimento RSV, Menezes VJ, Bastista L, TG characterization of organically modified montmorillonite, J. Therm. Anal. Calor. 75 (2004), 671-676

Taylor LT. Supercritical Fluid Extraction, Wiley, New York, 1996

Thompson, MR, Yeung KK, Recyclability of a Layered Silicate-Thermoplastic Olefin Elastomer Nanocomposite, Polymer Degradation and Stability, 2006, 91:2396-2407

Thompson MR, Tzoganakis C, Rempel GL, A Parametric Study of the Terminal Maleation of Polypropylene through an Alder Ene Reaction, J. Polym. Sci.: Part A: Polymer Chemistry, 36 (1998), 2371-2380

Thompson MR, Tzoganakis C, Rempel GL, Terminal functionalization of polypropylene via the Alder Ene reaction, Polymer 39 (1998), 327-334

Thompson MR, Balogh MP, Speers R, Fasulo PD, Rodgers WR, In-situ X-ray diffraction studies of alkyl quaternary ammonium montmorillonite in a CO_2 environment, J. Chem. Phys. 2008, *submitted*

Tomasko DL, Li H, Kiu D, Han X, Wingert MJ, Lee LJ, Koelling KW, A Review of CO_2 Applications in the Processing of Polymers, Ind. Eng. Chem. Res. 42 (2003), 6431-6456

Touillaux R, Salvador P, Vandermeersche C, Fripiat JJ, Study of water layers absorbed on Na- and Ca-montmorillonite by the pulsed nuclear magnetic resonance technique, Isr. J. Chem 1068; 6: 337-348

Treece MA, Oberhauser JP, Processing of polypropylene–clay nanocomposites: Single-screw extrusion with in-line supercritical carbon dioxide feed versus twin-screw extrusion, J. Appl. Polym. Sci. 103 (2007) 884-891

Usuki A, Kojima Y, Kawasumi M, Okada A, Fukushima Y, Kurauchi T, Kamigaito O. Synthesis of nylon 6-clay hybrid. J Mater Res 1993; 8: 1179–1184

Vaia RA, Teukolsky RK, Giannelis EP, Interlayer Structure and Molecular Environment of Alkylammonium Layered Silicates, Chem. Mater. 6 (1994), 1017-1022

Vaia RA, Jandt KD, Kramer EJ, Giannelis EP. Kinetics of Polymer Melt Intercalation. Macromolecules 1995, 28, 8080-8085

Vaia RA, Jandt KD, Kramer EJ, Giannelis EP. Microstructural Evolution of Melt Intercalated Polymer-Organically Modified Layered Silicates Nanocomposites. Chem. Mater. 1996, 8, 2628-2635

Vaia R.A., E.P. Giannelis, Lattice of polymer melt intercalation in organically-modified layered silicates, Macromolecules 30 (1997), 7990-7999

van Oss CJ, Giese RF, Surface modification of clays and related minerals, J. Disp. Sci. Technol., 24 (2003), 363-376

Walter P, Mäder D, Reichert P, Mülhaupt R, Novel polypropylene materials, J. Macromol. Sci. A: 36 (1999), 1613-1639

Wang L-Q, Liu J, Exarhos GJ, Flangan KY, Bordia R, Conformation Heterogeneity and Mobility of Surfactant Molecules in Intercalated Clay Minerals Studied by Solid-State NMR, J. Phys. Chem. B, 104 (2000), 2810-2816

Wang W, Li L, Xi S, A fourier transform infrared study of the coagel to micelle transition of cetyltrimethylammonium bromide, J. Colloid Interface Sci. 155 (1993), 369-373

Wang H., Zeng C., Svoboda P., James Lee L. Preparation and Properties of Polypropylene Nanocomposites, 59 th ANTEC Proceedings, Dallas, 2001, 2203-2207

Wang Y, Chen F-B, Li Y-C, Wu K-C, Melt Processing of Polypropylene/Clay Nanocomposites modified with Maleated Polypropylene Compatibilizers, Composites: Part B 2004, 35: 111-124

Wang Y, Chen F-B, Wu K-C, Wang J-C, Shear Rheology and Melt Compounding of Compatibilized-Polypropylene Nanocomposites: Effect of Compatibilizer Molecular Weight, Polym. Eng. Sci. 2006, 46: 289-302

Wang Y-C, Feng-B - W, Kai-C-Wang, Jiahn-C, Clay dispersion and physical properties of melt-blended PP/organoclay nanocomposites: effect of interfacial interaction, Composite Interfaces 13 (2006), 831-852

West BL, Kazarian SG, Vincent MF, Brantley NH, Echert CA. Supercritical fluid dyeing of PMMA films with azo-dyes, J. Appl. Polym. Sci. 69 (1998), 911-919

Xi Y, Frost RL, He H, Modification of the surfaces of Wyoming montmorillonite by the cationic surfactants alkyl trimethyl, dialkyl dimethyl, and trialkyl methyl ammonium bromide, J. Coll. Interf. Sci. 305 (2007), 1150-158

Xi Y, Ding Z, He H, Frost RL, Structure of organoclays – an X-ray diffraction and thermogravimetric analysis study, J Coll Interf Sci 2004; 277; 116 – 120

Xie W, Gao Z, Pan W-P, Hunter D, Singh A, Vaia R. Thermal Degradation Chemistry of Alkyl Quaternary Ammonium Montmorillonite, Chem. Mater. 13 (2001), 2979-2990

Xu Y, Brittain WJ, Vaia RA, Price G, Improving the physical properties of PEA/PMMA blends by the uniform dispersion of clay platelets, Polymer 47 (2006), 4564-4570

Yang K, Ozisik R. Effects of processing parameters on the preparation of nylon 6 nanocomposites, Polymer 47 (2006), 2849-2855

Yariv S, Michaelian KH, Structure and Surface Acidity of Clay Minerals, In: Organo-clay compleses and interactions, Marcell Dekker, NY, 2002

Yariv S, Staining of clay minerals and visible absorption spectroscopy of dye-clay complexes, In: Organo-clay complexes and interactions, Marcell Dekker, NY, 2002

Yariv S, The effect of tetrahedral substitution of Si by Al on the surface acidity of the oxygen plane of clay minerals, Int. Rev. Phys. Chem. 1992; 11: 345-375

Zhang Y-Q, Lee J-H, Jiang H-J, Nah C-W, Preparing PP/clay nanocomposites using a swelling agent, Composites. Part B: Engineering, 35 (2004), 133-138

Zhao Y, Huang H-X. Dynamic rheology and microstructure of polypropylene/clay nanocomposites prepared under sc-CO_2 by melt compounding, Polymer Testing 27 (2008), 129-134

APPENDICES

Appendix A HPC for in-situ XRD measurement

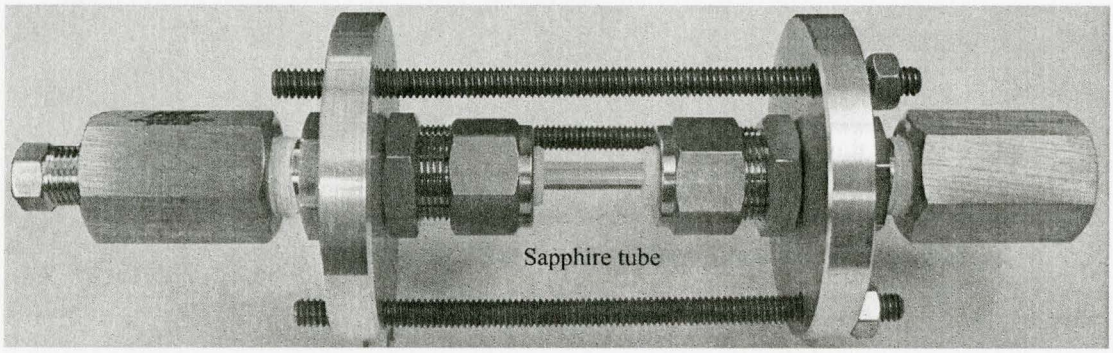

Appendix B Full factorial design of effect of $scCO_2$ on organoclays

Sample No.	Surfactant	Pressure psi	Temp. °C	Time hrs	Pressure drop MPa/s
34	Cloisite 20A	1400	50	6	4.8
35	SCPX 1137	1400	50	6	4.8
36	SCPX 2934	1400	50	6	4.8
37	SCPX 2971	1400	50	6	4.8
38	SCPX 2972	1400	50	6	4.8
39	Cloisite 20A	1400	200	3	0.2
40	SCPX 1137	1400	200	3	0.2
41	SCPX 2934	1400	200	3	0.2
42	SCPX 2971	1400	200	3	0.2
43	SCPX 2972	1400	200	3	0.2
44	Cloisite 20A	1400	50	6	0.2
45	SCPX 1137	1400	50	6	0.2
46	SCPX 2934	1400	50	6	0.2
47	SCPX 2971	1400	50	6	0.2
48	SCPX 2972	1400	50	6	0.2
49	Cloisite 20A	1100	200	3	0.2
50	SCPX 1137	1100	200	3	0.2
51	SCPX 2934	1100	200	3	0.2
52	SCPX 2971	1100	200	3	0.2
53	SCPX 2972	1100	200	3	0.2

Appendix B Full factorial design of effect of $scCO_2$ on organoclays (continued)

Sample No.	Surfactant	Pressure psi	Temp. °C	Time hrs	Pressure drop MPa/s
54	Cloisite 20A	1100	50	6	4.8
55	SCPX 1137	1100	50	6	4.8
56	SCPX 2934	1100	50	6	4.8
57	SCPX 2971	1100	50	6	4.8
58	SCPX 2972	1100	50	6	4.8
24	Cloisite 20A	1400	200	3	4.8
25	SCPX 1137	1400	200	3	4.8
26	SCPX 2934	1400	200	3	4.8
28	SCPX 2971	1400	200	3	4.8
27	SCPX 2972	1400	200	3	4.8
59	Cloisite 20A	1100	50	6	0.2
60	SCPX 1137	1100	50	6	0.2
61	SCPX 2934	1100	50	6	0.2
62	SCPX 2971	1100	50	6	0.2
63	SCPX 2972	1100	50	6	0.2
29	Cloisite 20A	1100	200	3	4.8
30	SCPX 1137	1100	200	3	4.8
32	SCPX 2934	1100	200	3	4.8
64	SCPX 2971	1100	200	3	4.8
31	SCPX 2972	1100	200	3	4.8

Appendix C Moisture uptake of the $scCO_2$ treated organoclays

Processing conditions	Cloisite 20A	SCPX 2934	SCPX 1137	SCPX 2972	SCPX 2971
50°C, 7.6 MPa, 0.2 MP/s	4.1	3.2	5.1	6.1	10.2
200°C, 7.6 MPa, 0.2 MP/s	4.2	3.5	5.4	5.6	12.3
50°C, 9.7 MPa, 0.2 MP/s	4.9	3.8	5.8	5.7	10.5
200°C, 9.7 MPa, 0.2 MP/s	3.7	3.0	4.9	5.1	11.8
50°C, 7.6 MPa, 4.8 MP/s	3.9	3.2	5.1	5.7	10.3
200°C, 7.6 MPa, 4.8 MP/s	5.7	3.8	4.1	7.1	11.2
50°C, 9.7 MPa, 4.8 MP/s	3.2	2.3	4.3	5.4	10.4
200°C, 9.7 MPa, 4.8 MP/s	5.3	6.4	6.2	9.7	17.4